Nanoporous carbon materials: modern production methods and applications

Vladimir V. Pavlenko,[a,b,c]* 🟢   **Alexander Yu. Zakharov,**[a] 🟢   **Zhanibek E. Ayaganov,**[a] 🟢
**Zulkhair A. Mansurov**[a,c] 🟢

[a] *Institute of Combustion Problems, Almaty, Kazakhstan*
[b] *Department of Electrical and Computer Engineering, Nazarbayev University, Astana, Kazakhstan*
[c] *Al-Farabi Kazakh National University, Almaty, Kazakhstan*

The review presents data on the nomenclature and production methods of the most intensively investigated classes of nanoporous carbon materials, which are increasingly used in science, medicine, and various fields of economy. The traditional activated carbons, which are produced by conventional biomass and fossil hydrocarbon processing methods, are compared with nanoporous carbon materials obtained using modern synthetic methods. Recommendations are given on the use of template synthesis to obtain carbon materials with a controlled nanoporosity. Self-template synthesis, in which environmentally benign and readily available organic salts can be used as precursors, is considered as a promising avenue of research. This approach markedly reduces the cost of template synthesis of nanoporous carbons and allows for the preparation of carbon materials with specific particle morphology from organometallic precursors. Methods for the preparation of functional materials with ordered architectures of micro- and mesopores are considered, including modern functionalization and doping approaches. A part of the review is devoted to advanced applications of nanoporous carbon materials such as water treatment, energy and hydrogen storage, separation of gas mixtures, development of catalysts and sensors, and solution of other significant problems. The conclusion summarizes the experience of application of various methods for the preparation of nanoporous carbon materials, identifies the most problematic issues of the development and practical use of these materials, and presents the authors' view on further development of this area of materials science.
The bibliography includes 353 references.

Keywords: carbon materials, nanoporous materials, activated carbons, micropores, mesopores, macropores, template synthesis, soft templates, hard templates, self-templates, zeolites, silica oxide, xerogels, silica gels, metal-organic frameworks.
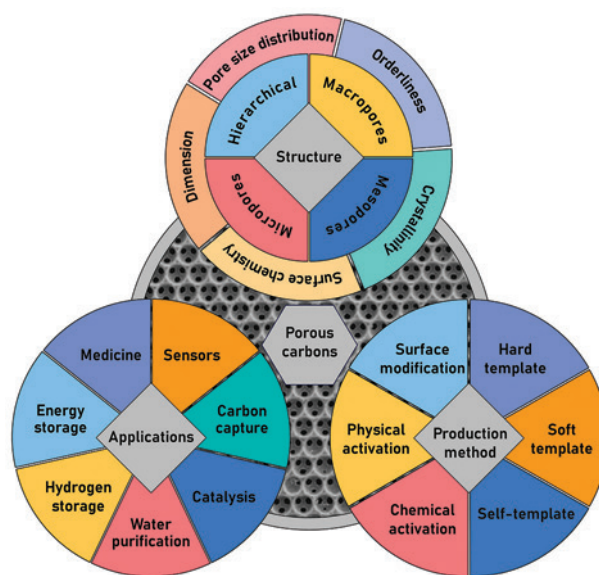
V.V.Pavlenko. PhD, Head of Laboratory of Functional Nanomaterials at the Institute of Combustion Problems, Associate Professor at Al-Farabi Kazakh National University.
E-mail: vladimir.Pavlenko@kaznu.edu.kz
Current research interests: Energy conversion and storage systems, water purification and rare metals extraction systems, methods of preparation of adsorbents and functional nanoporous materials, petrochemistry.
A.Yu.Zakharov. Specialist (Magister), Researcher at the Laboratory of Functional Nanomaterials of the Institute of Combustion Problems.
E-mail: alexan.zakharov@ya.ru
Current research interests: systems of capacitive deionization of water, electrochemical supercapacitors, development of methods of carbon adsorbents production.

Z.E.Ayaganov. Researcher at the Laboratory of Functional Nanomaterials of the Institute of Combustion Problems, PhD candidate at the al-Farabi Kazakh National University.
E-mail: zhanibek13@gmail.com
Current research interests: systems of capacitive deionization of water, electrochemical supercapacitors, carbon nanomaterials, thin films.
Z.A.Mansurov. Councilor of General Director of the Institute of Combustion Problems, Laureate of the State Prize of the Republic of Kazakhstan, Doctor of Chemical Sciences, Professor at Al-Farabi Kazakh National University.
E-mail: zmansurov@kaznu.kz
Current research interests: kinetics and mechanisms of hydrocarbon combustion and structures of cold and sooty flames, synthesis and research of carbon nanomaterials for various functional purposes.
Translation: Z.P.Svitanko

2 of 42

V.V.Pavlenko, A.Yu.Zakharov, Z.E.Ayaganov, Z.A.Mansurov
Russ. Chem. Rev., 2024, **93** (9) RCR5122

Contents

1. Introduction

Porous materials have been known since ancient times; however, before the industrial revolution era, their application was limited to the filtration of water. Due to the rapid expansion of production capacities, industry was faced with the need to purify gases and waste water, which initiated a focused research on carbon materials as sorbents. In 1915, wide use of chemical weapons in World War I and the accumulated experience in the development of carbon sorbents resulted in the design of the first gas mask based on activated carbon.[1] The appearance of the Brunauer–Emmett–Teller (BET) mathematical model for the description of gas sorption in 1938 allowed insight into the fine porous structure of various materials. Further development of synthetic methods, advancement of analytical techniques, and the development of promising applications such as nanoporous catalysts,[2] energy storage systems,[3] and other resulted in appearance of inorganic porous materials the porosity characteristics of which can be precisely varied during their preparation by using inorganic templates representing inverse replicas of a specified porous structure that do not decompose during the synthesis. The first structurally ordered porous carbon materials were prepared using silica as a hard template.[4] The studies of zeolites, carried out in parallel, soon made it possible to switch from microporous materials with 10 Å channels[5] to mesoporous ones with pore size of more than 10 nm[6,7] and 20 nm;[8] this markedly expanded the range of potential applications of these materials. Currently, porous carbon materials can be obtained both by etching of a homogeneous matrix and by using template synthesis techniques. The possible precursors for the preparation of porous carbon materials include a variety of carbon-containing products, ranging from fossil coals to specially prepared polymer compositions or metal-organic frameworks (MOFs).

There are numerous reviews devoted to sodium-ion batteries,[9] supercapacitors (SCs),[10,11] water treatment systems,[12,13] *etc*., which address carbon materials for particular applications, or consider not only carbon materials, but also other classes of compounds potentially suitable for these applications. Review publications of another type summarize data on carbon materials derived from a particular feedstock: fossil coals,[14] cross-linked polymers,[15] agro-industrial waste,[16] *etc*. There are also reviews addressing particular methods for the preparation of carbons: conventional methods of chemical and physical activation[17,18] and relatively new methods using soft[19] and hard[20] templates. It is noteworthy that the most advanced methods of synthesis using combined templates or self-templates[†] are rarely found in

review publications. Little attention is given to comparison of characteristics of the porous carbon materials obtained by template synthesis and biocarbon activation methods. There is also a problem that the theoretical grounds lag behind the development of practical methods for the preparation of carbons. A typical problem is the absence of a common nomenclature for these materials, which leads to confusions: for example, the term 'graphene' is used to denote virtually any two-dimensional carbon materials.[21]

The present review, first, considers various approaches to systematization of carbon materials (Section 2); second, integrates methods for the production of carbon materials, including both conventional physical and chemical activation methods, which are described in detail in Section 3, and template synthesis (Section 4); third, describes the advanced methods that include the use of combined templates and self-templates, in particular a promising method in which inexpensive organic precursors serve as self-templates. Section 5 is devoted to the current applications of the porous carbon materials, including recent achievements in biomedicine (nanopore DNA sequencing), microwave absorption (stealth technology), energy storage (design of supercapacitors based on solid electrolytes) and so on. The review also provides a summary of standard methods for characterization of carbon materials and the relationships between the structure or chemical composition of a carbon material and particular applications.

2. Nomenclature and characterization methods

Development of the nomenclature of carbon materials is an integrated task that requires unified approaches for various stages of the carbon preparation ranging from the selection of the precursor to the understanding of structural features and properties of the material to be produced. In this Section, we present various approaches to classification of carbon materials and briefly survey typical methods used for characterization of their structure and properties (Table 1).

2.1. Classification of carbon materials

Over several decades of investigation of carbon materials, the main principles of the structure–property relationships of these materials have been elucidated;[22] however, no unified concept that would combine the principles of formation and structural properties for carbon materials have been elaborated as yet. This is largely associated with the difficulty of constructing a real

---

[†] Self-templates are templates formed during the synthesis upon decomposition of the carbon precursor (in most cases, oxides).

V.V.Pavlenko, A.Yu.Zakharov, Z.E.Ayaganov, Z.A.Mansurov
Russ. Chem. Rev., 2024, **93** (9) RCR5122

3 of 42

Table 1. Main methods used for characterization of porous carbon materials.

Method	Information provided by this method
Gas sorption	Specific surface area (SSA), type of porosity, total pore volume, pore size distribution
Scanning electron microscopy (SEM)	Surface and particle morphology
Transmission electron microscopy (TEM)	Porous structure morphology and defects, visualization of the porous structure
X-ray diffraction (XRD)	Degree of graphitization, phase composition of crystalline impurities
Raman spectroscopy	Degree of graphitization
Energy dispersive spectroscopy (EDX)	Quantitative elemental composition of the surface (elements heavier than Na)
X-Ray photoelectron spectroscopy (XPS)	Semi-quantitative elemental composition of the surface, determination of carbon hybridization and interatomic bonds
Fourier transform infrared spectroscopy (FTIR)	Qualitative composition of functional groups on the surface
Thermal decomposition	Contents of H, N, C, O, and S elements in the material bulk
Ash content	Total weight fraction of inorganic impurities (the ash can be additionally characterized by EDX and XRD to establish the qualitative and quantitative composition)
Cyclic voltammetry (CV)	Specific capacitance, cycling efficiency, durability
Galvanostatic charge/discharge (GCD)	Specific capacitance, power density, energy density, cycling efficiency, durability
Electrochemical impedance spectroscopy (EIS)	Impedance, contributions of diffusion resistance, charge transfer resistance, *etc*.

model for disordered carbons and studying the exact mechanisms of formation of ordered structures in them, which are often referred to in the literature as self-assembly. Nevertheless, a few concepts for classification of carbon materials have been proposed, the most comprehensive of which are discussed below.

Heimann *et al*.[23] proposed a classification based on the type of carbon hybridization. This concept can be depicted as a ternary diagram (Fig. 1), the vertices of which are occupied by basic carbon structures with sp (carbyne), sp^2 (graphite), and sp^3 (diamond) hybridizations, respectively. The transition forms of carbon in which atoms occur in different hybridization states, depending on the ratio, are located at the edges or inside the
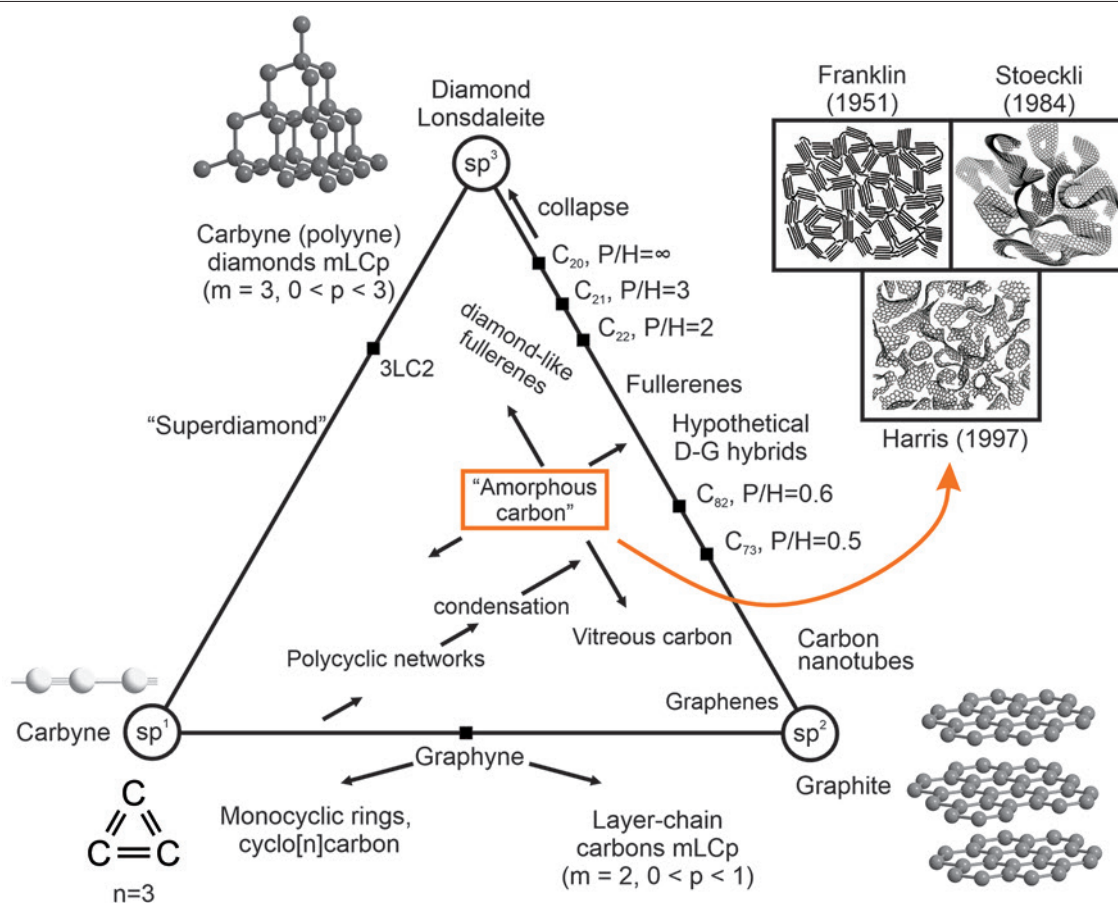

Figure 1. Ternary diagram (Csp^3, Csp^2, Csp) of solid carbon allotropes and main structural models of disordered carbon materials. P/H is the pentagon to hexagon ratio in the material. D-G are diamond–graphite hybrids. *m*LC*p* are carbons with *m* layers and structural parameter *p*. The Figure was created by the authors using published data.[23–26]

triangle (see Fig. 1). The structures of disordered amorphous carbon materials, such as activated carbon, carbon black, carbon fibres, *etc*., which have carbon atoms in all three hybridization states, can be described by several models (see Fig. 1). The simplest model was proposed by Franklin and Randall in 1951 and implies alternation of graphene stacks and amorphous parts of the structure.[24] Later, in 1984, Stoeckli and Kraehenbuehl proposed an alternative model describing a carbon structure as one wrinkled graphene ribbon.[25] Currently, the structural model proposed by Harris in 1997 is considered to be most accurate.[26] This model describes the structure of porous carbon as randomly packed fragments of defective graphene sheets and fullerenes with possible inclusion of various heteroatoms.[25] Irrespective of the type of model, it is implied that the structure of disordered carbon materials includes alternating amorphous and crystalline domains.[27] Depending on the orientation of domains relative to one another, materials behave differently during high-temperature pyrolysis. If the domains are highly ordered, on heating to 1500–3000 °C, they form a graphite structure; these materials are designated as soft, or graphitizing carbons. When the arrangement of graphene layers in the material is highly disordered, transition to graphite does not take place even at temperatures above 3000 °C; these materials are known as hard or non-graphitizable.

Ordered carbons mainly contain atoms in two hybridization states (sp^2 and sp^3). These materials can be classified, according to their dimensionality, into three-dimensional (3D), two-dimensional (2D), one-dimensional (1D) and zero-dimensional (0D), with each dimensionality being characterized by a particular morphology (Fig. 2). The 3D carbon materials include graphite with two allotropes differing in the layer packing in the structure, graphite derivatives (intercalated derivatives, oxidized graphite, *etc*.), carbon nanotube (CNT) networks, *etc*. Two-dimensional materials include single- and multilayer graphenes,
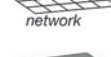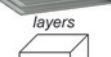
graphene nano- and microsheets, nanofilms and other similar structures, first classified in 2013 by Bianco *et al*;[21] and 1D materials are represented by CNTs.[28, 29] Various types of ordered carbon materials were considered by Terrones *et al*.[30]

Esser and Dronskowski[31] extended and specified the Heimann's approach using modern quantum chemical simulation methods: degrees of orbital mixing were calculated using density functional theory (DFT) with the generalized gradient approximation (GGA) and the Perdew–Burke–Enzerhof exchange correlation potential. This approach made it possible to switch from the ratios of sp-, sp^2-, and sp^3-hybridized atoms to the mean hybridization sp^n, where $1 < n < 3$. A more precise diagram including key allotropes and molecular forms of carbon such as carbyne, diamond, graphite, graphene, various types of CNTs, *etc*. is presented in Fig. 3. More specific consideration demonstrates that some carbons (*e.g*., diamond and fullerenes) have a more complex orbital structure and are located more closely to the triangle centre than in the Heimann's study. Also, more precise consideration made it possible to subdivide allotropes of one form of carbon [diamond (Fd3m), lonsdaleite ($P6_3$/mmc)]. Nevertheless, even the specified diagram inherits some features due to which the classification cannot be considered complete. First, both diagrams are ambiguous regarding interpretation of the structural features of materials: whereas in some forms and allotropes, carbon atoms have different, but strictly specified hybridizations, in some other allotropes, they acquire sp^n type hybridization. Second, although both diagrams are called 'diagrams of carbon allotropes' in the original publications, they actually combine both the allotropes (*e.g*., graphite and diamond) and various forms of carbon (*e.g*., fullerene and CNTs). Third, even after the introduction of more precise data of Esser and Dronskowski,[31] some forms of the same allotrope still occupy different positions (graphite and graphene), although they are structurally identical. These discrepancies force researchers to develop classifications based on other criteria.

To describe structural characteristics of ordered carbons, Belenkov and Greshnyakov[32] proposed classification into those having only covalent bonds and those containing both covalent and van der Waals bonds. The carbons with covalent bonds are described in terms of two parameters: N_a, which reflects the number of covalent bonds of a carbon atom (0 to 4), and nD_c, defining the crystallographic dimensionality of the structure (0 to 3); these values allow one to define 12 sorts of ordered structures with covalent bonds between the atoms, of which only nine structures are basic and can sustainably exist; the other three groups ([$0D_c$, 4], [$1D_c$, 4] and [$2D_c$, 4]) correspond to model structures. The authors note that the above groups include not only ideal structures, but also various polymorphs.[32]

The structure of materials with mixed van der Waals and covalent bonds is described using the primary structural blocks given above. The structural types formed from identical blocks are summarized in Table 2, while other phases are described by combining various structural blocks. It was proposed to consider amorphous carbon materials as derivatives of ordered ones with various structural defects.[33] The proposed approach may be convenient for solving problems related to modelling of various structures; however, it proves to be poorly applicable for description of disordered carbon materials.

Recently, Monthioux[34] proposed to separate molecular and allotropic forms of carbon. According to the definition they proposed, only ordered carbon structures (mainly crystalline ones) can be classified as allotropes. A number of molecular forms can also be allotropic if their elements are arranged in an

Dimension	Material	Structure	Morphology
0D	Fullerene		ellipse sphere
1D	CNTs		tube
	nanoribbons		ribbon
	helices		helix
2D	graphene		
	Haeckelite		sheet
	2D networks		network
3D	graphite		layers
	diamond		кубическая
	amorphous carbon		chaotic porous

Figure 2. Morphological features of the main carbon materials.

V.V.Pavlenko, A.Yu.Zakharov, Z.E.Ayaganov, Z.A.Mansurov
Russ. Chem. Rev., 2024, **93** (9) RCR5122

5 of 42

Figure 3. Ternary diagram including real and theoretical allotropes of carbon.[31]

Table 2. Classification of carbon phases and nanostructures with mixed type of bonds.[32]

Crystal dimensionality, nD_c	Number of covalent bonds formed by the carbon atom, N_a				
	0	1	2	3	4
$0D_c$	Chain, plane, or 3D distribution of single atoms	Chain, plane, or 3D distribution of atom pairs	Chain,* plane,* or 3D distribution* of nanorings	Chain and plane of fullerene-like clusters, fullerite	Chain, plane, or 3D distribution of framework clusters
$1D_c$	–	–	Plane or bundle of chains; plane* or bundle* of helices	Plane or bundle of CNTs, ribbons,* or helices*	Plane or bundle of CNTs, ribbons,* or helices*
$2D_c$	–	–	–	Graphite-like phases, interpenetrating graphene-like layers	Graphite-like phases, interpenetrating graphene-like layers
$3D_c$	–	–	–	Interpenetrating 3D graphites	Interpenetrating diamond-like phases

Note. * There are common and interpenetrating structural types.

ordered manner (*e.g.*, CNT bundles). In order to systematically describe various forms of carbon, the author proposed to consider molecular forms as single molecules and crystalline forms based on sp³-hybridization (most often, three-dimensional) as a set of various allotropes; the crystalline and mixed forms based on sp²-hybridized atoms were described using four criteria:[34] morphology (shape of particles), texture (relative orientation of graphene stacks), nanotexture (crystallite size and defects), and structure (crystallographic structure of crystallites). Presumably, this approach would provide, if not a complete classification of carbon materials by combining them into groups by identical criteria, at least unification of approaches to the description of carbon materials.

The above classifications are based on the features of the target carbon structures, without considering specific features of the carbon precursors used in the synthesis. This approach is

convenient when applied to materials obtained in laboratory, but when it comes to large-scale production of porous carbon materials (mainly activated carbons), it is necessary to identify the relationships between the properties of initial precursors and the properties of target products. Classification of fossil coals used in industry is based on their origin (genetic classifications) and technical details. Genetic classifications reflect the differences between the coals depending on the initial material, the origin, and transformation patterns. Actually, the influence of primary and secondary geological factors (source material, water cut, depth of immersion, *etc.*) determine the coal composition and quality in terms of consumer value. These classifications are based on elemental and type composition and the yields of thermal processing products. Technical classifications are meant for grouping of coals in accordance with the requirements imposed on raw materials by various

6 of 42

V.V.Pavlenko, A.Yu.Zakharov, Z.E.Ayaganov, Z.A.Mansurov
Russ. Chem. Rev., 2024, **93** (9) RCR5122

industries and do not reflect the natural characteristics of the coals.[35] It is important to note that the above classifications refer only to fossil coals, *i.e.*, the precursors for the production of porous materials. There are no published data on approved classifications that would relate the raw material characteristics to the properties of the resulting porous carbons. Nevertheless, since fossil coals are most often converted to highly porous carbon materials *via* chemical and physical activation, it can be assumed that the properties of the resulting carbons would depend, first of all, on the porosity and ash content, including the ash composition of the precursor. Since the main goal of activation is to increase the porosity, the use of precursors with more higher primary porosity results, in most cases, in carbon materials with larger specific surface area (SSA).[36] The presence of mineral components in the precursors can be either beneficial or harmful for the characteristics of the target carbon material;[37] this largely depends on the ash composition: some inorganic elements (such as K, Na, Ca) can be involved in self-activation or act as self-templates (*e.g.*, Si, Mg, *etc.*). These processes are discussed in more detail in Section 3.2 dealing with the chemical activation of carbon-containing precursors.

2.2. Morphology and structure

The morphology of porous carbon materials is analysed by scanning electron microscopy (SEM). A few dozens of morphological types of carbons can be distinguished;[38–40] the particle morphology is mainly determined by the method of synthesis and by the precursors: carbon materials obtained by carbonization of natural raw materials usually retain the precursor texture; hydrothermal synthesis usually produces perfect spherical particles; the use of self-templates affords more complex particle morphologies. Conversely, the porous structure virtually does not depend on the used precursors, but is determined by the type of template and the presence/absence of the activation stage: the use of hard templates results in a material that is a inverse replica of the template with an ordered porous structure and a narrow or bimodal pore size distribution; the use of self-templates and activation methods results, most often, in the formation of a microporous structure with a hierarchical pore size distribution; the use of soft templates may

provide various types of porous structure. The morphological features of carbon materials prepared by various methods are summarized in Table 3.

The textural characteristics of porous carbon materials are closely connected with SSA; for a long time, the value of $2650 \text{ m}^2 \text{ g}^{-1}$ corresponding to the maximum area of a graphene monolayer has been considered to be the limiting SSA value.[52] However, most of the currently used models assume that the real packing of the layers is chaotic and that graphene monolayers can be represented by small planar and distorted pieces and can have functional groups at the edges, *etc*. On the other hand, the modern computational capacities do not allow operation with an infinite number of atoms and interactions between them, which restricts the model to some averaged fragment that does not perfectly represent the real structure. In view of the above assumptions, modern theoretical models predict the possibility of obtaining disordered carbon materials with SSA of up to $6000 \text{ m}^2 \text{ g}^{-1}$.[53,54] The SSA values for real products still do not exceed $4000-4300 \text{ m}^2 \text{ g}^{-1}$ (Refs 55–57) and are well described under the assumption that the carbon structure consists of small graphene-like moieties. For example De Biase and Sarkisov[58,59] modelled the commercial Maxsorb MSC-30 carbon with SSA of $2500-3500 \text{ m}^2 \text{ g}^{-1}$ with a high accuracy (Fig. 4).

The structural characteristics and the total surface area of nanopores are usually investigated using gas sorption/desorption technique.[60] The gases used for this purpose include N_2, CO_2, He, *etc*.[61,62] Nitrogen, which is inert and has small molecules easily penetrating inside nano-sized pores (>0.7 nm), is used most often. Microporous structure can be studied using CO_2, the molecules of which have geometrical dimensions similar to those of N_2, but higher kinetic energy because the measurements are carried out at higher temperature (273 or 298 K). The drawbacks of the method include chemisorption of CO_2 on a surface with alkaline functional groups.[63] The most versatile solution is to use He, since this gas consists of perfectly spherical inert particles with a minimum size;[64] however extensive use of this method is restricted because it is necessary to carry out measurements at super low temperature of 4.2 K.

According to IUPAC classification accepted in 1985, he physical sorption/desorption of a gas is described by six types of isotherms (Fig. 5);[65–69] the features of porous materials
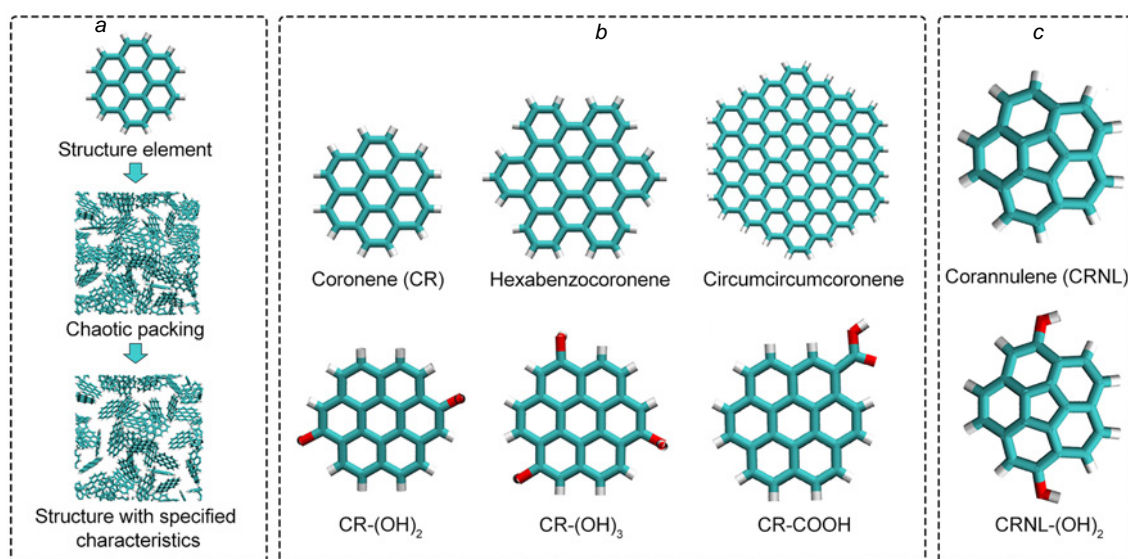

Figure 4. Principle of modelling of the carbon structure with a high surface area (*a*); planar (*b*) and distorted (*c*) blocks used to model the commercial Maxsorb MSC-30 carbon. Colours of the atoms: carbon is turquois, oxygen is red, hydrogen is grey.[58,59]

V.V.Pavlenko, A.Yu.Zakharov, Z.E.Ayaganov, Z.A.Mansurov
Russ. Chem. Rev., 2024, **93** (9) RCR5122

7 of 42

Table 3. Selected morphological types of carbon materials obtained by different methods.

Particle morphology	Pore morphology	Preparation method	Preparation procedure	Ref.
Spherical particles with a narrow size distribution (the maximum at 1.5 nm)	Disordered porous structure with a hierarchical pore size distribution; distribution maximum at 1.5 nm	Chemical activation (KOH)	Hydrothermal carbonization of glucose at 220 °C. Activation with KOH at 700 °C	40
Non-uniform	Disordered porous structure with a hierarchical pore size distribution; distribution maximum at 2.75 nm	Combined chemical activation (H_3PO_4 + KOH)	Hydrothermal activation of lignite with H_3PO_4 at 180 °C followed by activation with KOH at 700 °C	41
Non-uniform	Disordered porous structure with a hierarchical pore size distribution; distribution maximum at 3 nm	Self-catalytic activation	Self-catalytic activation of rotten potato waste	42
Non-uniform	Ordered porous structure with a bimodal pore size distribution (maxima at 0.9 and 8.7 nm)	Hard template synthesis (SiO_2)	Carbonization of a mixture of glucose and SiO_2 (hard template) at 900 °C. Leaching of the template with NaOH	43
Uniform three-dimensional interconnected foam morphology	Disordered porous structure with a hierarchical pore size distribution; distribution maximum at 3 nm	Hard template synthesis (MgO)	Bio-oil dissolution in $Mg(COOH)_2$. Carbonization at 800 °C; washing with HCl	44
Non-uniform	Ordered microporous structure, distribution maximum at 1 nm (inverse CaY)	Hard template synthesis (CaY zeolite)	Saturation of CaY zeolite (hard template) with precursor vapour. Carbonization at 900 °C. Template removal with HF	45
Inverse replica of the template	Ordered porous structure with a bimodal size distribution (meso- and macropores) (inverse replica of SiO_2)	Hard template synthesis (monolithic SiO_2)	Impregnation of a monolithic silica template with coal tar pitch (1 MPa pressure). Carbonization at 800 °C. Template removal with HF. Graphitization at 1800 or 3000 °C	46
Spherical particles of approximately 120–145 nm size with different porosity	Dendritic porous structure with a distribution maximum at 5, 13, 21, and 37 nm depending on the synthesis conditions	Soft template synthesis (F127)	Self-assembly of micelles from dopamine, trimethylbenzene, and F127 surfactant. Drying and carbonization at 800 °C	47
Nanofibres of 3 to 5 µm length and 200 to 300 nm width	Disordered microporous structure, distribution maximum at 1.6 nm	Soft template synthesis (polyvinylpyrrolidone)	$FeCl_3$-catalyzed naphthalene alkylation with α,α'-dichloro-*p*-xylene. Carbonization at 700 °C	48
Non-uniform	Disordered porous structure with a bimodal pore size distribution (0.9 and 3.5 nm)	Self-template synthesis (magnesium citrate as the template)	Carbonization at 900 °C. Template removal with HCl	43
Retention of the precursor fibrous structure	Disordered porous structure with a bimodal pore size distribution (37 and 239 nm)	Self-template synthesis (spongin-based 3D frameworks)	Treatment with HCl. Carbonization at 650 °C. Hydrothermal functionalization	49
CNT-decorated hollow rhombic dodecahedra	Disordered porous structure with a bimodal pore size distribution (1.5 and 10 nm)	Combined self-template synthesis (ZIF-67@ZIF-8)	Epitaxial growth of ZIF-67 on ZIF-8. Carbonization at 900 °C followed by washing with H_2SO_4. Oxidation at 350 °C, P doping using NaH_2PO_2 at 300 °C	50
Porous graphene-like nanosheets of 5–10 nm size	Disordered porous structure with hierarchical pore size distribution	Self-template synthesis (K-MOF)	Solvothermal synthesis of K-MOF rods from potassium nitrate and 1,3,5-tricarboxybenzene in *N,N*-dimethylformamide. Precarbonization of K-MOF at 450 °C. Carbonization at 800 °C. Washing with HCl	51

corresponding to each type of isotherm are summarized in Table 4. It is noteworthy that type IV and V isotherms are characterized by the presence of hysteresis caused by differences between the adsorption and desorption (see Fig. 5);[65,66] the type of hysteresis loop is related to the shape of pores,[70] and the relationship between the pore shape and type of hysteresis is briefly depicted in Fig. 5 and is addressed in detail in a recent review.[69]

The theoretical description of sorption isotherms is based on the BET theory. It is important to note that the BET theory is applied only in the range of partial pressures (P/P_0) from 0.05 to 0.35 for the isotherm branch corresponding to monolayer adsorption,[62] *i.e.*, for type II and IV isotherms. For type I isotherms, this range shifts to lower pressure of 0.005–0.1. An incorrect choice of points for type I isotherms leads to
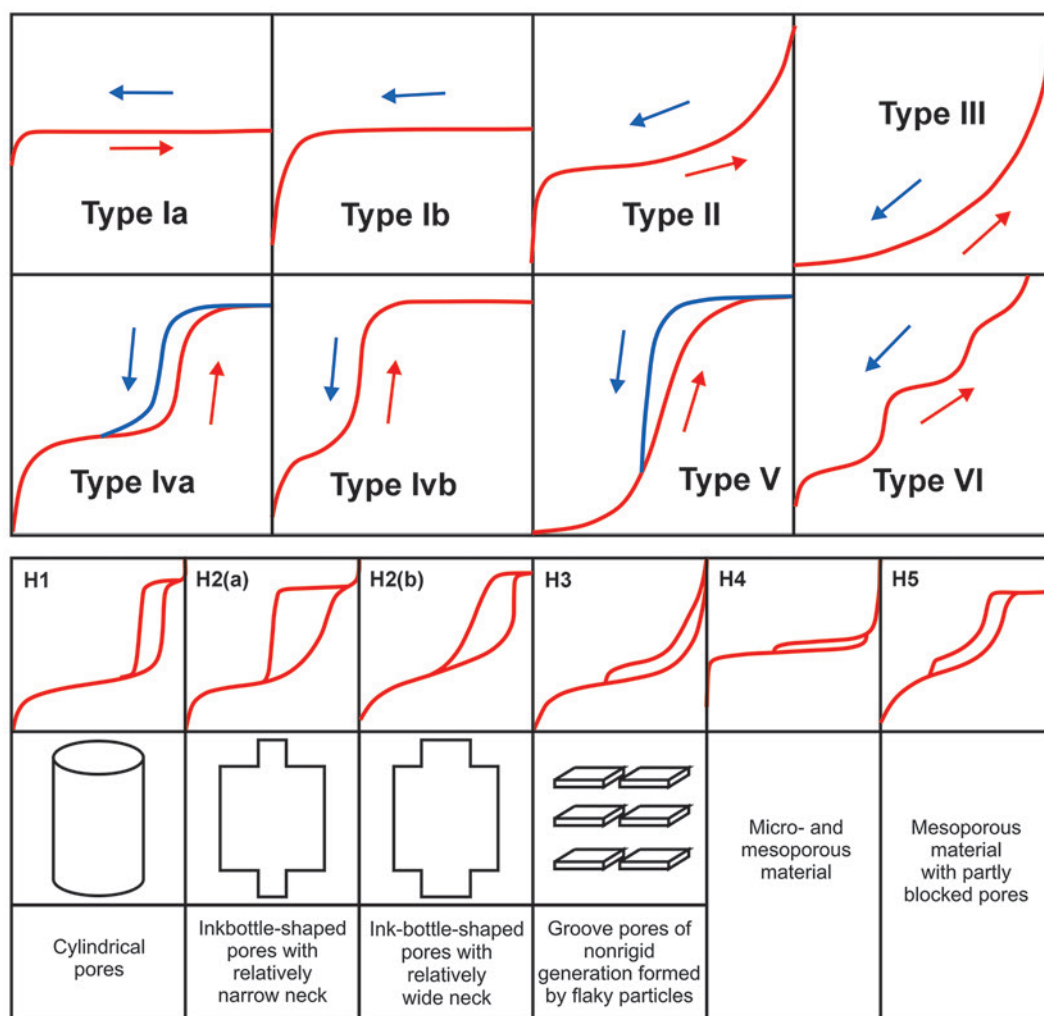
8 of 42

V.V.Pavlenko, A.Yu.Zakharov, Z.E.Ayaganov, Z.A.Mansurov
Russ. Chem. Rev., 2024, **93** (9) RCR5122

Figure 5. Types of sorption/desorption isotherms, different hysteresis loops and corresponding porosity types according to the IUPAC classification.[65–69]

Table 4. Relationship between the type of isotherm and key characteristics of porous materials.[65–69]

Type of isotherm	Structural features of materials
Ia	Microporous materials, greater part of the accessible surface is inside micropores, pore diameter <0.7 nm
Ib	Microporous materials, greater part of the accessible surface is inside micropores, pore diameter <2.5 nm
II	Macroporous and non-porous materials, mono-/multilayer sorption
III	Macroporous and non-porous systems with weak sorbate–sorbent interactions (special case of type II isotherms)
IVa	Mesoporous materials with pore size of 1.5–100 nm, hysteresis is due to capillary condensation in pores larger than 4 nm (at 77 K and 87 K for N_2 and Ar, respectively)
IVb	Mesoporous materials with pore size of 1.5–4 nm; no hysteresis as all pores smaller than the critical value (4 nm for N_2 and Ar at 77 K and 87 K, respectively)
V	Mesoporous materials, mono-/multilayer sorption
VI	Homogeneous nonporous systems with layer-by-layer adsorption

underestimation of SSA. The pore size distribution for macro- and mesoporous structures was estimated using the Barrett–Joiner–Halenda (BJH) method;[63] for microporous structures, Dubinin–Radushkevich, Dubinin–Astakhov and Dubinin–Stoeckli equations were used.[71] The most versatile approach is the use of density functional theory (DFT), which is highly flexible and can take into account various structural details. A modified DFT method, non-local density functional theory (NLDFT) for liquids, is often used; this method takes into account weak interactions between the adsorbate particles and provides a fairly accurate description for the adsorption isotherms of both micro- and mesoporous materials.[72] The main drawback of NLDFT is that the pore surface is assumed to be perfectly smooth, which leads to artefacts in the description of materials with pore size less than 1.5 nm. A few approaches have been proposed to eliminate this drawback, including the reverse Monte Carlo statistical modelling, mixed geometry model and other.[73] The quenched solid density functional theory (QSDFT) method, a DFT modification proposed in 2012, was the most successful of them.[74] In this approach, the surface is simulated using a roughness parameter rather than a uniform field. The development of two-dimensional NLDFT models (2D-NLDFT) also markedly improved the accuracy of modelling of the porous structure for carbon materials.[75] This approach models a pore by a slit between parallel disk-shaped graphene

V.V.Pavlenko, A.Yu.Zakharov, Z.E.Ayaganov, Z.A.Mansurov
Russ. Chem. Rev., 2024, **93** (9) RCR5122

9 of 42

Table 5. Methods for processing the data obtained by gas sorption/desorption and parameters derived from these data

Method	Theoretical grounds	Determined parameters
Brunauer–Emmett–Teller method	BET theory	Total specific surface area and pore volume
Density functional theory method	DFT	Pore size distribution
Barrett–Joiner–Halenda method	Kelvin equation	Mesopore size distribution
Dubinin–Radushkevich method	Potential theory of Polanyi and assumption of Gaussian pore size distribution	Micropore volume
Horvath–Kawazoe method	Potential theory of Polanyi, model of slit-like pores	Micropore size distribution
Cheng–Yang method	Potential theory of Polanyi, model of spherical pores	
Saito Foley method	Potential theory of Polanyi, model of cylindrical pores	

sheets and, due to the circular symmetry, can be considered in only two dimensions. The model may additionally include corrections taking account of the energy heterogeneity and geometric surface corrugation. These and other theoretical models for the calculation of porous structure parameters from adsorption isotherms are described in detail in recent papers.[66, 69] The methods for processing the data obtained by gas sorption/desorption and the parameters derived from these data are summarized in Table 5.

When it is impossible to carry out comprehensive studies of the porous structure of a material using gas adsorption, it is possible to use adsorption of iodine (determination of iodine number) or methylene blue. The main drawbacks are the impossibility of taking into account the microporous structure, because of the size of the iodine molecule (10 Å), and high reactivity of iodine towards functional groups on the surface of the carbon material, which may result in overestimation of the target characteristics.[76] The size of the methylene blue molecule is approximately $17.0 \times 7.6 \times 3.3$ Å;[77] it is mainly used to estimate the adsorption of small organic molecules and the cation exchange capacity of meso- and macroporous functionalized carbon materials.[78]

The porous structure can be characterized by TEM, which allows detailed investigation of the microstructure of a material, including the external porosity between the carbon grains.[79] It is important that microscopic examinations of this type cover only local sites, and to gain complete information, it is necessary to carry out a series of measurements for data averaging.

The ordered parts of carbon materials are studied using X-ray diffraction methods. In order to detect a short-range order of carbon atoms along a and c crystallographic directions, it is necessary to detect positions of (002) and (100) reflections located in the range $2\theta = 22 - 24°$ and $43 - 44°$ ($\lambda_{CuK\alpha} = 1.54$ Å), which are related to the distances between the crystallographic planes of graphite by the Bragg equation:

$$n\lambda = 2d \cdot \sin\theta$$

(where n is the order of diffraction, λ is the X-ray radiation wavelength, d is the interplanar spacing, θ is the diffraction angle).[80] The average interplanar spacing in the graphite-like domains of most carbon materials is in the range of $0.347 - 0.443$ nm.[9] The degree of graphitization of a carbon material is estimated by comparing the integral intensities of the (002) and (100) reflections of the reference graphite and the sample.[81] X-ray diffraction is also used to identify crystalline impurities.

Since crystalline graphite-like domains in disordered carbon materials have nanometre sizes, X-ray diffraction reflections collected using standard diffraction methods are markedly broadened, which complicates analysis of the structure.[9] More accurate analysis of the local microstructure can be performed

by small-angle X-ray scattering (SAXS). After processing of the results experimentally obtained by SAXS, it is possible to plot the pair distribution function G(r), in which the distances between peaks reflect the interatomic distances between a conventional central atom and surrounding atoms (Fig. 6).[82] The intensity of each peak corresponds to the relative contribution of atoms located at particular distances.

A more precise method for determination of the degree of graphitization is Raman spectroscopy. Typical spectra include two major peaks: G peak ($\sim 1580 - 1600$ cm^{-1}), caused by vibrations of the sp^2-hybridized carbon atoms in graphite-like domains, and 1D peak ($\sim 1300 - 1350$ cm^{-1}), caused by the presence of structural disorder; in some cases, second-order 2D peak can also be manifested (~ 2700 cm^{-1}) as an overtone of the 1D peak.[83] The degree of graphitization is determined by calculating the ratio of absolute or integral areas of the 1D and G peaks, which are most often described by the Lorenz function and asymmetric Breit–Wigner–Fano function, respectively.[80]

2.3. Chemical composition

The chemical composition of the surface is among the most important characteristics of carbon materials. The major heteroatoms present in a carbon material are O and N; in the case of doping or surface modification by functional groups, S, B, and P may appear.[84–86] The chemical composition of the surface is studied by EDX, XPS, and IR spectroscopy. The bulk of the material is analyzed using thermal decomposition methods with quantitative analysis of the released gases [CHNS(O) analysis].

Energy dispersive spectroscopy is used to analyze the local surface composition, making it possible to determine the composition at a particular site or construct the 2D distribution maps for particular elements. When internal standards are used, EDX provides quantitative analysis with an accuracy of $1 - 5\%$. The main drawback is the difficulty to perform accurate analysis of light atoms (for most instruments, elements lighter than Na).[87] An alternative method is the characteristic electron energy loss spectroscopy (EELS), which provides information on the atom hybridization and valence bonds.[80]

X-ray photoelectron spectroscopy (XPS) makes it possible to identify atoms in the surface layer and the presence and types of bonds between the atoms. The standard spectrum includes C1s ($280 - 292$ eV), N1s ($396 - 408$ eV), and O1s ($530 - 536$ eV) peaks, each can be deconvoluted into a number of components corresponding to C–C, C–O, C=O, C–N, N–O, *etc.* bonds and their combinations corresponding to different functional groups: C–OH, –COOH, –C–NH$_2$, C–NO$_2$, and other.[88, 89] Similarly, it is possible to detect dopants and determine their environment.[90]

Qualitative analysis of the surface functional groups is performed using mid-IR spectroscopy ($4000 - 400$ cm^{-1}). This wavenumber range covers most of the lines corresponding to the
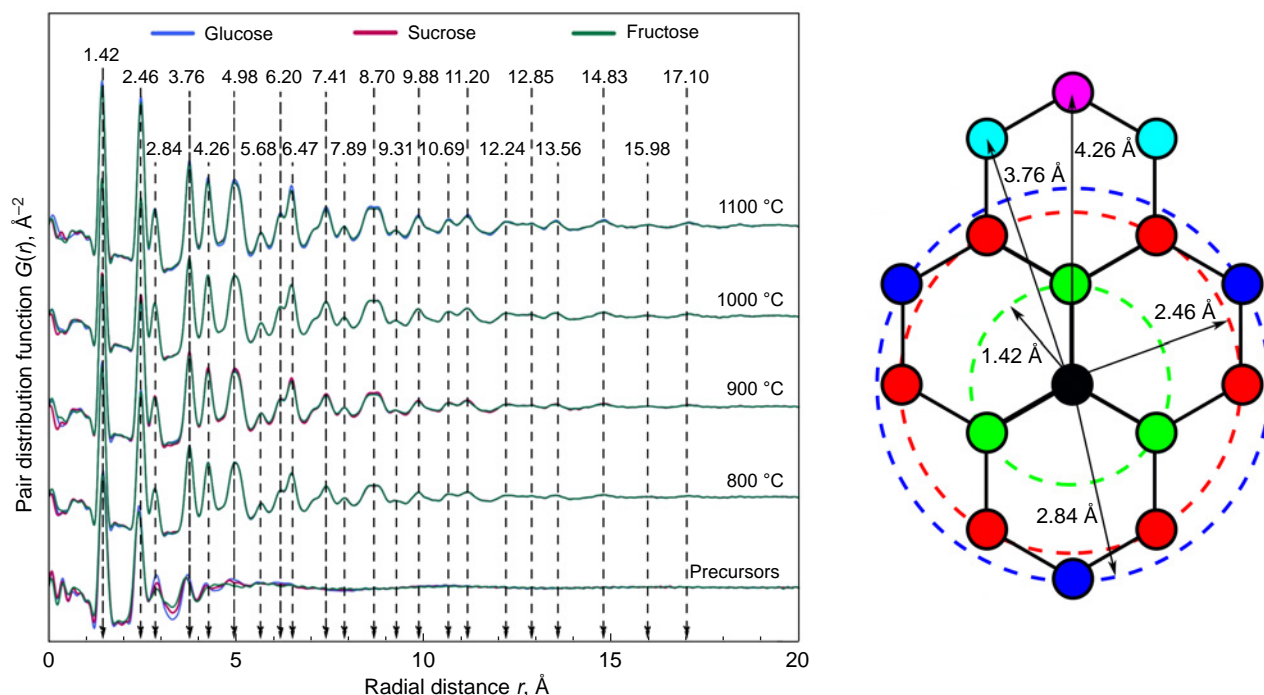
Figure 6. Correspondence of the coordination spheres of the carbon atom in the graphene layer and peaks of the pair distribution function.[82]

vibrational-rotational structure[91] of common functional groups such as carboxyl, lactone, phenol, quinone, *etc*.[88,89] The spectra are analyzed by comparison with the spectra of standards.

The composition of the sample bulk is analyzed by thermal decomposition techniques. On heating the sample in an inert atmosphere, selective decomposition of oxygen-containing functional groups with predominant evolution of CO_2 or CO takes place (Fig. 7).[88] When analysis is carried out in an oxygen environment, CO_2, H_2O, NO_2, and SO_2 can be formed depending on the sample composition. Separate analysis of these gases makes it possible to quantify the corresponding atoms in the sample.[92]

These studies serve for monitoring the changes in the composition and structure at various stages of production of a carbon material.[93] Using EDX, Yagmur *et al*.[94] showed that carbons obtained from various parts of oleaster (flesh, peel, seed) by an optimized procedure using various activating agents have similar contents of carbon (82–86%) and different

Figure 7. Temperature ranges corresponding to the release of CO_2 (*a*) and CO (*b*) upon decomposition of different types of oxygen functional groups: SCA — strong carboxylic acids, WCA — weak carboxylic acids, CAn — carboxylic anhydrides, L — lactones, Ph — phenols, CQ — carbonyl quinones.[88,89]

contents of oxygen (8 to 16%, depending on the activating agent used).[94]

2.4. Electrochemical properties

Energy density and power density are the key electrochemical characteristics of any energy storage system. In the case of supercapacitors, the energy density is determined by capacitance C and the operating voltage V according to the formula

$$E = {}^1\!/_2 C \cdot V^2 \tag{2}$$

The operating voltage is mainly determined by the electrolyte composition, while the capacitance C is proportional to SSA. Hence, large surface area is a key requirement to electrode materials.[95] On the other hand, the power density depends on the equivalent series resistance of the system, one of the contributions to which is diffusion resistance, generated by the motion of electrolyte ions in the porous structure of the carbon material. To attain a high energy density, appropriate design of the porous structure is necessary, as small pore size and complex topology increase the diffusion resistance. The factors that have beneficial effect on the final characteristics of the system are summarized in Fig. 8.

Typical methods for investigation of the electrochemical performance of carbon materials include CV, GSD, and EIS. All of the above methods are used to measure three basic parameters – voltage, current, and time; they can be used to determine other parameters including capacitance, equivalent series resistance, operating voltage, time constant, and other energy characteristics of supercapacitors. It is noteworthy that for presentation of test results, it is necessary to distinguish between the properties of the whole cell and its active material. The principles of determination of the indicated values for supercapacitors are described in detail in a fundamental review by Zhang and Pan;[96] the details and mechanisms of processes that take place in batteries and methods for calculation of electrochemical characteristics are described in a recent review
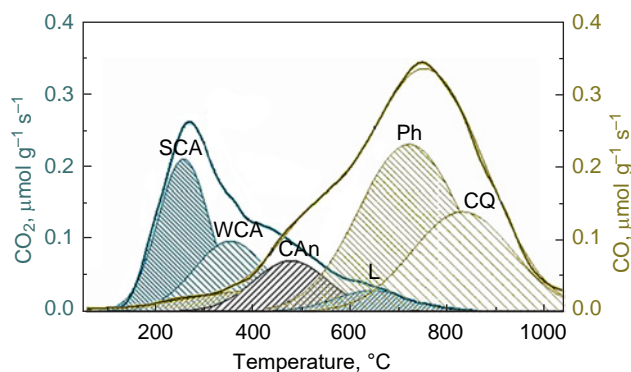
V.V.Pavlenko, A.Yu.Zakharov, Z.E.Ayaganov, Z.A.Mansurov
Russ. Chem. Rev., 2024, **93** (9) RCR5122
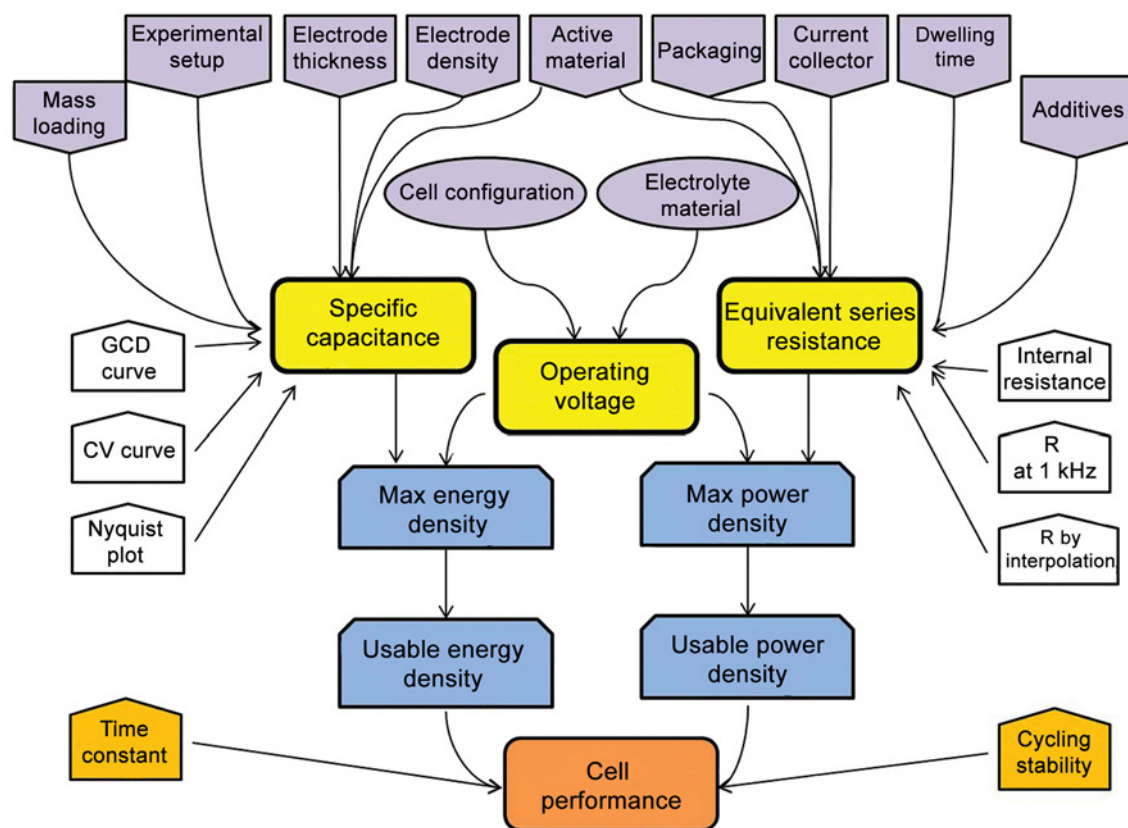
11 of 42

Figure 8. Relationships of the key performance characteristics, testing methods and other factors for evaluation of supercapacitors.[96] Copyright WILEY 2014.

by Abramova *et al.*[9] The optimization principles of the porous structure to achieve the desired performance of the target device are discussed in detail in Section 5.2.

3. Production of activated carbons

Activated carbons are a class of meso- and microporous materials obtained by chemical or physical activation of carbon precursors. Using activation, it is possible to obtain carbons with either equal pore size or hierarchical pore size distribution.[97] Typical precursors for the production of activated carbons are carbonized lignocellulosic biomass, mineral raw materials (coals, pitches, coke, *etc.*), and synthetic carbon materials (*e.g.*, carbonized xerogel).

The precursors are obtained by pyrolysis of organic raw materials in oxygen-free atmosphere at temperatures of 300–900 °C. The process includes several stages: dehydration (up to 200 °C), active pyrolysis (200–450 °C), and passive pyrolysis (above 450 °C).[98] At temperatures higher than 150 °C, demethylation, decarboxylation, and other reactions start,[80] resulting in the evolution of considerable amounts of gaseous products (mainly CO, CO_2, and CH_4).[99] The active pyrolysis stage is accompanied by decomposition of lignin with breaking of C–C and C–O bonds;[100] on further temperature rise, the lignin decomposition products undergo polymerization, removal of functional groups, rearrangements, *etc*. The processes involved in the carbonization of lignocellulosic materials are depicted in Fig. 9 and are described in detail in the literature.[98, 101]

The product obtained by pyrolysis is subjected to physical or chemical activation (Fig. 10)[18, 102–107] accompanied by changes in the porous structure: expansion of the pores formed during carbonization *via* thermal, chemical and/or physical etching; and formation of new pores *via* chemical/physical etching and opening of isolated cavities previously not connected to the surface. In the limiting case, a microporous structure can be converted to a mesoporous one (*e.g.*, due to burning-out of walls between neighbouring pores) and a mesoporous structure can be converted to microporous one (for example, because of the formation of new micropores in a mesopore wall during chemical etching). The most popular chemical activating agents are KOH, H_3PO_4, and $ZnCl_2$; physical activation is usually performed using steam or CO_2.

3.1. Physical activation

Physical activation is the major method for the industrial production of activated carbons, with steam or CO_2 being used as activators. This method is considered to be the most environmentally benign,[108] as it gives no by-products resulting from the activating agents with impurities present in the carbonized material.

It is believed that physical activation with steam is based on various oxidation processes.[109] One of the described mechanisms (see Fig. 10) implies that carbon reacts with active oxygen released as a result of thermal decomposition of water molecules adsorbed on the carbon surface.[110] The CO_2 activation proceeds more slowly, which allows better control over the process. The CO_2 activation results in the predominant formation of mesopores, while steam activation gives microporous carbons, which is attributable to the formation of different inhibitors.[111] Despite high energy consumption and moderate SSA values (mainly from 70 to 1500 m^2 g^{-1}), the use of physical activation is economically feasible.[112] In addition, recent studies show that in some cases, carbons with SSA > 3000 m^2 g^{-1} can be obtained by this method.[113]

12 of 42

V.V.Pavlenko, A.Yu.Zakharov, Z.E.Ayaganov, Z.A.Mansurov
Russ. Chem. Rev., 2024, **93** (9) RCR5122
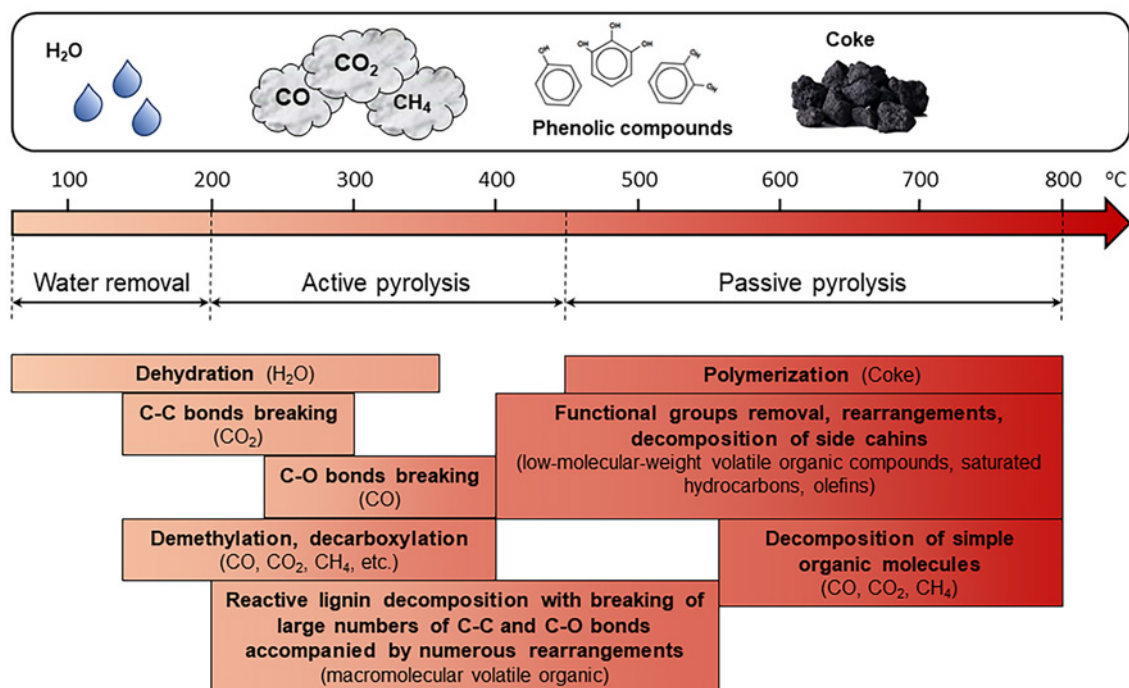
Figure 9. Main processes taking place during pyrolysis of lignocellulosic precursors. The major products of thermolysis are given in parentheses.
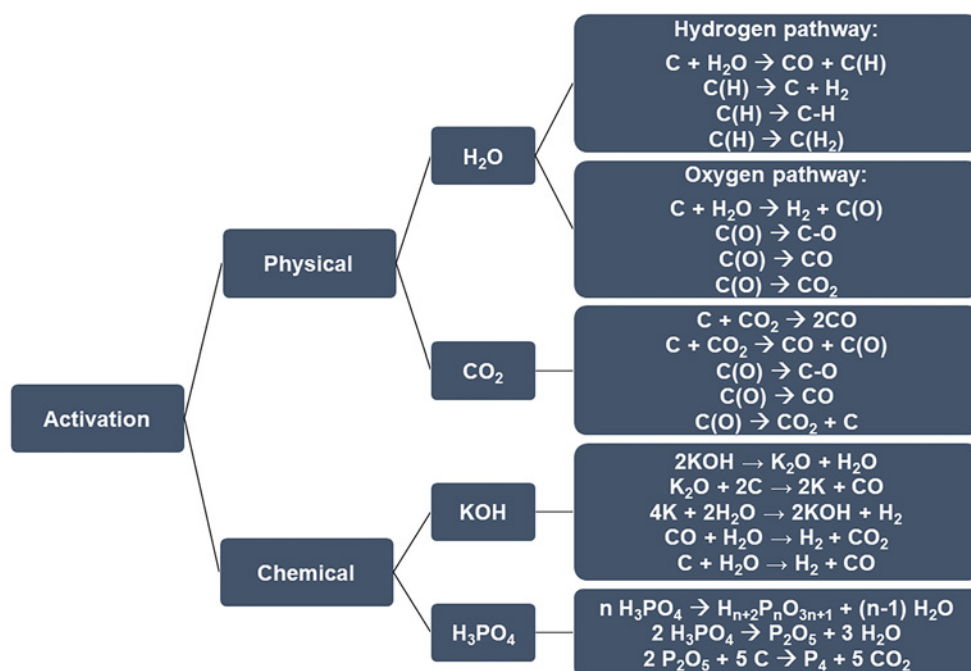
Figure 10. Key methods of activation of carbon materials and induced reactions. $C(H)$ and $C(O)$ are hydrogen and oxygen complexes on the surface of a carbon material, $C-H$ and $C-O$ are hydrogen and oxygen atoms bound to the surface carbon by covalent bonds, $C(H_2)$ is hydrogen adsorbed on the surface of a carbon material. The Figure was created by the authors using published data.[18, 102–107]

3.2. Chemical activation

Chemical activation is the most effective method for the production of activated carbons with high SSA. This process includes several stages. First, the initial carbonized material is saturated with chemical oxidants by mechanical stirring or keeping in a saturated solution of the activator,[18] and then the mixture is dried. Then activation is carried out at a temperature from 400 to 900 °C depending on the type of activator (700–900 °C for alkaline activators and about 450–500 °C for H_3PO_4 and $ZnCl_2$) and the precursor.[114] The parameters affecting characteristics of the resulting carbon include the heating rate, activation temperature, as well as the nature, type, and weight ratio of the activator and the carbon precursor.

The reagents used as chemical activators (KOH, H_3PO_4, K_2CO_3, $ZnCl_2$, $CaCl_2$, *etc.*) act as dehydrating agents affecting the pyrolytic decomposition and preventing the formation of resins, which increases the yield of the activated carbon. The chemical activation may proceed simultaneously with carbonization,[18] which is a common practice in the case of using H_3PO_4, but in other cases, this is, most often, a separate stage in the activated carbon production.

V.V.Pavlenko, A.Yu.Zakharov, Z.E.Ayaganov, Z.A.Mansurov
Russ. Chem. Rev., 2024, **93** (9) RCR5122

13 of 42

The use of carbonized products as carbon-containing precursors for H_3PO_4 activation is inefficient; the synthesis is usually performed in one stage.[115] In the phosphoric acid activation, the acid concentration is the key parameter.[116] The main processes are depolymerization of the starting raw material, dehydration, and redistribution of biopolymers in the material (see Fig. 10).[107] Also, most of impurity mineral elements are washed away, the number of acid groups on the surface of the material increases, and phosphoric-acid residues generate a network structure, which provides additional ordering of the carbon material.[107] An excessive amount of acid markedly inhibits the activation due to the formation of an insulating layer on the surface.[117]

Specific features of activation with $ZnCl_2$ is the catalytic activity of zinc chloride towards condensation of aromatic compounds and the formation of predominantly mesoporous structure.[118] Meanwhile, $ZnCl_2$ does not directly react with the carbon surface, which makes it most environmentally benign among all of the used chemical activators.[119] One of the mechanisms implies the reaction with water vapour to give hydroxy dichlorozincic acid ($ZnCl_2 + H_2O \rightarrow H[ZnCl_2(OH)]$), which acts as an etching agent.[119] Simultaneously, $ZnCl_2$ catalyzes the removal of large numbers of H and O atoms from the surface of the carbon material as H_2O, instead of converting them into hydrocarbons or oxygen-saturated organic compounds,

which leads to higher yield of the resulting carbon.[120] The occurrence of these processes is also indicated by decreasing contents of the phenolic and carboxyl groups on the surface simultaneously with increasing content of lactone groups.[121] This method can be used for single-stage activation of lignocellulosic materials that have not been pre-carbonized.

Currently, the activation with KOH provides the best results and affords carbons with SSA > 3500 m^2 g^{-1}.[113] The so high values are attained due to the transformation of some mesopores into micropores and formation of new micropores.[122] The results of NaOH activation are poorer, which is apparently related to lower melting point of potassium hydroxide providing better penetration of potassium into pores compared to sodium.[123]

The mechanism of $FeCl_3$ activation consists of numerous steps: at temperatures of 200 to 300 °C, ferric chloride cleaves the glycosidic bonds of cellulose, which results in H_2O release to give amorphous FeOOH. In the second step of pyrolysis at temperatures between 330 and 700 °C, FeOOH decomposes to give Fe_2O_3, which may act as a Lewis acid catalyzing cross-linking reactions or be reduced with the surface carbon atoms to give Fe_3O_4 and CO, which results in the generation of a microporous structure (Fig. 11).[124, 125] Oxide particles can be retained on the surface, leading to the formation of a mesoporosity during acid post-treatment.[126] If the carbon material is pre-
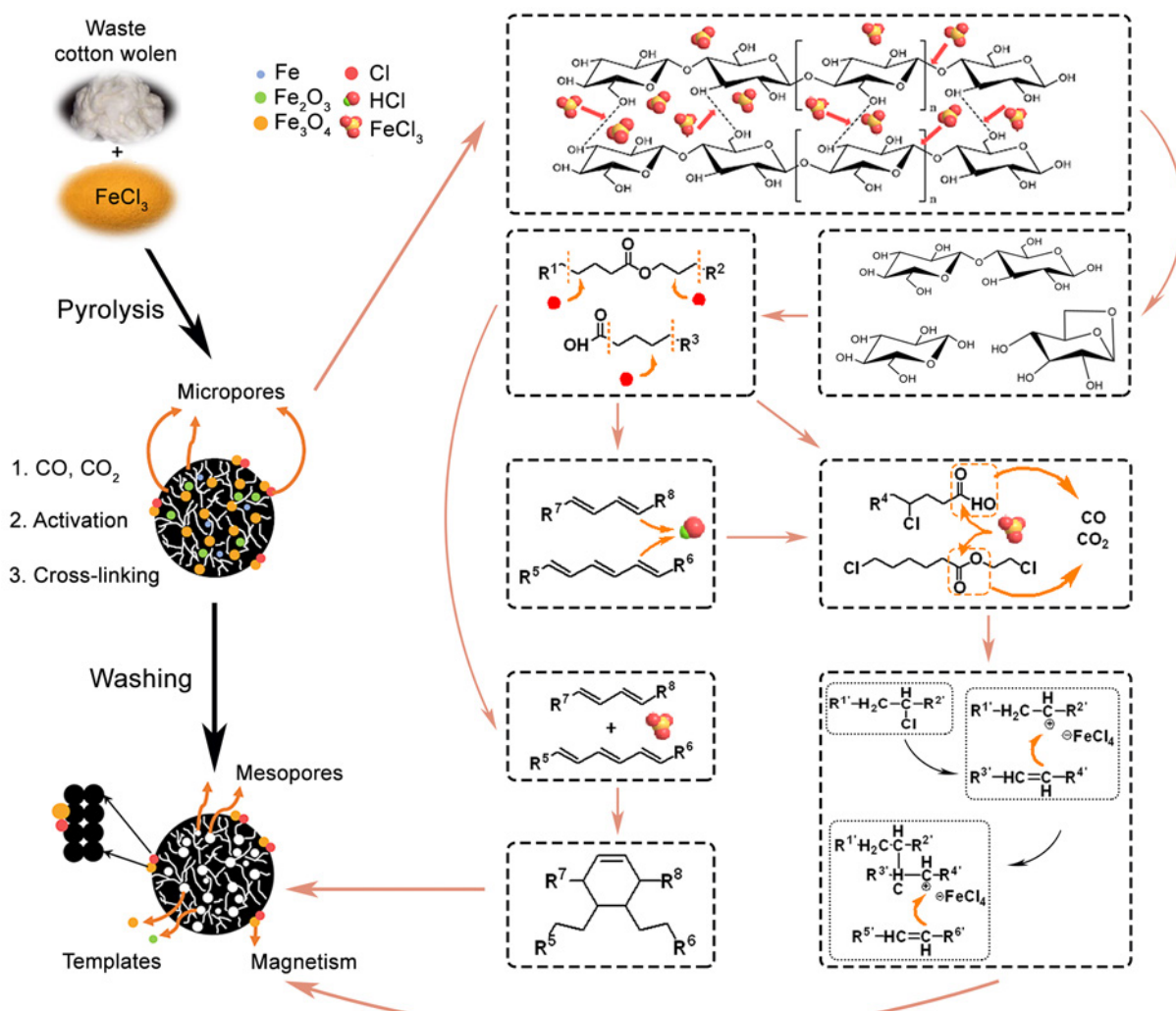

Figure 11. Schematic diagram of catalytic activation of a carbon material with $FeCl_3$.[124]

Table 6. Advantages and drawbacks of activation methods.

Activation type	Activating agent	Advantages of the method	Drawbacks of the method
Physical	H_2O	Most environmentally benign; easy to use (in particular, in industry); purity of the resulting carbons is sufficient for the food and pharmaceutical industries; one-stage carbonization–activation process	High power consumption; low efficiency; long process duration
	CO_2	Easy to use (in particular, in industry); purity of the resulting carbons sufficient for the food and pharmaceutical industries; one-stage carbonization–activation process	High power consumption; low efficiency; long process duration
Chemical	KOH	Best efficiency, two-stage carbonization–activation process	corrosive reagent; lowest yield
	H_3PO_4	One-stage carbonization–activation process; the lowest process temperature among chemical activators	Corrosive reagent
	$ZnCl_2$	One-stage carbonization–activation process	Corrosive and toxic reagent

impregnated with ferric chloride, the capture of iron particles by the surface occurs before activation. During the subsequent annealing in a CO_2 atmosphere, these particles catalyze reactions giving off CO and CO_2 and serve as templates for the formation of mesoporous structure.[127]

The use of iron particles is not the only example of catalytic activation; similar properties are inherent in Al and Mn chlorides.[128] There are known examples of self-catalytic activation by K, Na, and Ca: annealing of tobacco leaves in an inert atmosphere at 800 °C yields a carbon material with a surface area of 1749 $m^2\,g^{-1}$ and a narrow pore size distribution with maximum at 1.2 nm.[129] A small amount of K_2CO_3 (approximately 2 mass%) can also be used as a catalytic additive and can be regenerated in a CO_2 atmosphere.[130]

Wang *et al.*[42] described a procedure for the preparation of a porous carbon material with SSA of 2200 $m^2\,g^{-1}$ from potato waste without using additional reagents. The starting material was placed into a reactor, which was evacuated and heated to 800–1000 °C; water present in the feed acted as an activator. A control experiment carried out in a nitrogen atmosphere did not show appearance of a porous surface.[42]

Thus, chemical activation methods provide carbons with a greater SSA (up to 4000 $m^2\,g^{-1}$) than physical activation methods.[131] However, the use of relatively expensive corrosive activators and the need for additional treatment of waste wash water increase the cost of chemical activation techniques and hinder its application in industry.[132] In addition, the use of this method inevitably gives rise to new (mainly oxygen-containing) groups on the surface, which is not always beneficial for the properties of the target material.[133] One of the simplest ways for the removal of undesirable functional groups from the surface is the introduction of an additional stage of annealing at 700–900 °C,[43] which is accompanied by degradation of most of oxygen-containing functional groups (see Fig. 6). The relationship between the precursor composition, annealing conditions, and formation of various functional groups is described in detail in a few recent reviews.[11, 18, 133, 134]

Despite the limitations inherent in the chemical activation method, it is used to produce carbons with high surface area for special applications (Maxsorb, YEC, *etc.* brands). The choice of particular method depends on the purpose: the maximum surface area is attained using chemical activation with KOH; if cost is the crucial factor, physical activation is used. A trade-off solution is H_3PO_4 activation, which provides carbons with relatively high surface area, with the production cost being

moderate. Characteristic features of various activation methods are summarized in Table 6.

3.3. Use of carbonized biomass

The activated carbons obtained from carbonized biomass are distinguished by high SSA (with average values of 500–3500 $m^2\,g^{-1}$, Table 7)[131, 135–145] and high adsorption capacity and electrical capacitance;[146] therefore, they can be used as electrodes for SCs,[147] batteries,[148] water and gas treatment systems,[135] *etc.* Virtually any carbon-containing plant and animal raw materials are applicable as precursors for carbonization;[149,150] however, plant-based lignocellulosic materials are used most often, including walnut and peanut shells,[115, 151] wood and tree bark,[152] rice husk,[153] wheat straw,[154] *etc.* Porous carbons can also be obtained from a variety of domestic and industrial wastes.[155] Among the benefits of the method, mention should be made of both raw material diversity, ready availability, and renewability and the simplicity of generation of doped carbons containing N, P, O, and S atoms without additional surface modification procedures.[156]

An increase in SSA *via* the formation of additional microporosity can be attained using activation of carbon cloth and materials obtained by template synthesis. The production of these materials is considered in the corresponding Sections devoted to the synthesis using soft and hard templates.

3.4. Carbon cloth

Carbon cloth, which is widely used in energy storage systems[157] and in capacitive water deionization (CDI) cells,[158] is formed by spinning of polyacrylonitrile fibres (PAN) and the subsequent carbonization. The overall flow diagram of the process includes several stages and is depicted in Fig. 12. The surface area of the carbon cloth can be increased by both conventional physical or chemical activation methods and advanced electrochemical oxidation and plasma modification methods, which simultaneously develop the porous structure and modify the surface of the material. Since carbon cloth has virtually no porosity, as opposed to carbonized biomass, it can be effectively activated by mere annealing in air. For example, Gu *et al.*[159] showed that annealing of carbon cloth in air at 450 °C for 3 h increases SSA from <1 $m^2\,g^{-1}$ to 751.2 $m^2\,g^{-1}$. The electrochemical activation is carried out in an HNO_3/H_2SO_4 solution at a

V.V.Pavlenko, A.Yu.Zakharov, Z.E.Ayaganov, Z.A.Mansurov
Russ. Chem. Rev., 2024, **93** (9) RCR5122

15 of 42

Table 7. Specific surface area and specific electrical capacitance of EDLs for selected porous carbons obtained from carbonized materials

Type of activation	Activator	Raw material	BET specific surface area (SSA), $m^2\,g^{-1}$	Specific capacitance, $F\,g^{-1}$	Carbonization (1) and activation (2) conditions [carbon:activator mass ratio]	Ref.
Chemical	KOH	Lotus seedpods	4048	419 (0.5 A g^{-1}, 6 M KOH)	500 °C, 60 min, N_2; 400 °C, N_2, [1:4]	131
		Rice husk	2755	106 (1 mV s^{-1}, 1 M NaCl)	450 °C, 60 min, N_2; (2) 800 °C, N_2, [1:4]	135
		Oyster mushrooms (*Pleurotus ostreatus*)	2913	122 (1 A g^{-1}, 6 M KOH)	500 °C, 120 min, N_2; 850 °C, N_2, [1:8]	136
	H_3PO_4	Hazelnut shells	1363	248 (0.2 A g^{-1}, 6 M KOH)	600 °C, 90 min, N_2; 600 °C, 90 min, N_2, [1:1]	137
	H_3PO_4 + KOH	Hazelnut shells	3469	338 (0.2 A g^{-1}, 6 M KOH)	None; H_3PO_4, 600 °C, 90 min, N_2, [1:1]; NaOH, 850 °C, 120 min, N_2, [1:4]	137
	NaOH	Mangosteen peel	2623	357 (1 A g^{-1}, 6 M KOH)	600 °C, 120 min, N_2; 700 °C, 120 min, N_2, [1:3.5]	138
	$ZnCl_2$	Cotton biomass	1990	240 (1 A g^{-1}, 6 M KOH)	None; 800 °C, N_2, [1:3]	139
	$CuCl_2$	Lotus	1722	390 (1 A g^{-1}, 6 M KOH)	800 °C, 120 min, N_2; 800 °C, 120 min, N_2, [1:5]	140
Physical	H_2O	Kelp	1140	279 (0.5 A g^{-1}, 6 M KOH)	None; 850 °C, 60 min	141
		Pine nut shell	956	128 (0.5 A g^{-1}, 6 M KOH)	500 °C, 15 min; 850 °C, 60 min	142
		Sulfonated polymer nanotubes	852	276 (1 A g^{-1}, 6 M KOH)	None; 800 °C, 120 min	143
	CO_2	Bamboo	1496	–	800 °C, 240 min, N_2; 850 °C, 240 min	144
		Willow biomass	738	81 (0.1 A g^{-1}, 6 M KOH)	<700 °C (CO_2), then >700 °C, (N_2); 800 °C, 60 min	145
		Lignocellulosic biomass	751	93 (0.1 A g^{-1}, 6 M KOH)	450 °C, 30 min, N_2; 800 °C, 60 min	145
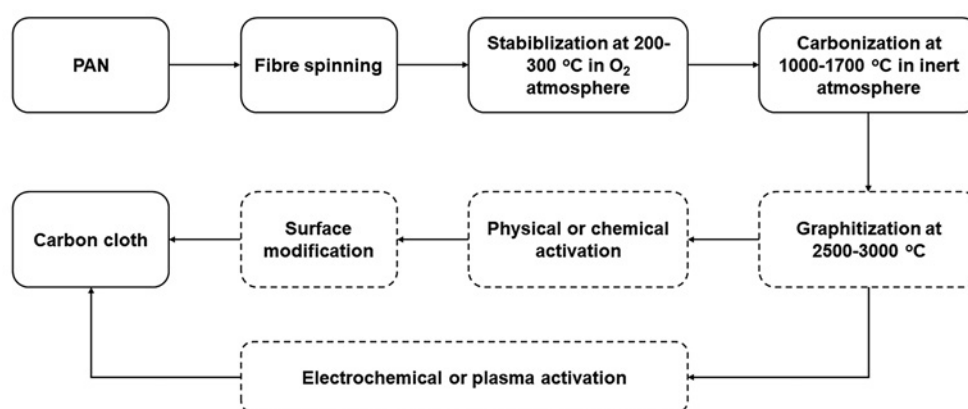
Figure 12. General flow diagram for the production of a carbon cloth.

potential of about 3 V for a limited period of time (~ 10 min); new pores are formed *via* controlled oxidation of the material surface.[157] As a drawback of the electrochemical activation, note the moderate depth of the generated pores, which is not more than 50 nm, while the diameter of a typical carbon fiber is approximately $5-10$ μm.[160]

As a modified electrochemical activation process, Han *et al.*[161] proposed a strategy that included the stage of formation of a primary meso- and macroporous structure prior to the proper electrochemical activation (Fig. 13). For this purpose, the initial cloth (6.5 $m^2\,g^{-1}$) was modified with NiOOH nanoflakes; after annealing in the oxygen atmosphere and

treatment with HF, they formed up to 150 nm deep pores; SSA of the resulting material was 25.7 $m^2\,g^{-1}$. After the development of microporous structure upon electrochemical activation, SSA increased to 201.3 201.3 $m^2\,g^{-1}$.[161]

The carbon cloth activation with nitrogen plasma was described by Chodankar *et al.*[162] Although no data on the low-temperature nitrogen sorption/desorption were given in that paper, indirect studies such as atomic force microscopy and electrochemical measurements confirm the increase in the surface area and the formation of extensive porosity. Apart from the development of porous structure, intercalation of nitrogen

16 of 42

V.V.Pavlenko, A.Yu.Zakharov, Z.E.Ayaganov, Z.A.Mansurov
Russ. Chem. Rev., 2024, **93** (9) RCR5122

Figure 13. Strategy of generation of the primary porous structure in carbon cloth fibres before electrochemical activation.[161] Copyright WILEY 2018.
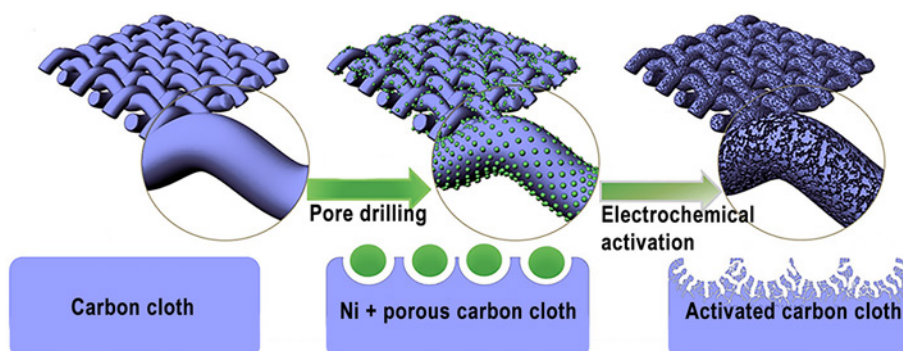
atoms into the carbon structure occurs during plasma treatment, which is confirmed by the XPS data.

3.5. Fossil coals

A considerable part of industrial manufacture of activated carbon is based on various fossil raw materials and their processing products as precursors, including peat, hard coal, anthracite, coke, oil pitch, *etc.*[163] Peat has a large number of internal defects and carbon content less than 60%; hence, pores are easily formed in peat. The carbon content in brown coal is 65–70%; bituminous coal contains 75–85% carbon; and the carbon content in anthracite is up to 95% with a high degree of ordering of molecular structure.[164] Since the compositions of the raw materials are different, the processing methods are also different. Due to the high content of volatile components, peat-based biomass is usually subjected to pyrolysis at 400 °C under limited access of oxygen before activation.[165,166] Bituminous coals with a high content of tar and volatile components may sinter or swell during heating; therefore, they require additional pretreatment.[167,168] Anthracite can be activated immediately under appropriate conditions.[169] Brown coals contain large amounts of volatile compounds, which increases the yield of gas and oil fractions formed during pyrolysis. Brown coal is initially dried and then activated with acids.[41] Another specific feature of brown coal is relatively high content of sulphur (mainly

sulfides), which requires an additional desulfurization stage after the formation of activated carbon.[170,171]

Since the manufacture of carbons from fossil raw materials is the subject of a number of recent reviews,[12,14,37,172,173] we will not concentrate on this issue. Methods for obtaining porous materials from mineral feedstock and characteristics of their porous structure are summarized in Table 8.

4. Template synthesis

Since the activation processes used to produce porous carbon materials do not provide an ordered porous structure in the vast majority of cases, materials with controlled porosity are obtained using special methods generally called template synthesis.[183] In this synthesis, one or several precursors (or products of their interaction) form a porous structure template. The resulting carbon material is an imprint of the template; thus it is possible to control its porous structure with high accuracy, obtain nanopores with identical morphology, and to attain a narrow or hierarchical pore size distribution. This method is widely used to obtain micro-, meso-, and macroporous carbon materials and CNTs.[184] Depending on the principles of interaction between the precursors and the template, different types of template synthesis are distinguished (Fig. 14).

The templates that are not destroyed during the synthesis and do not interact with carbon-containing precursors are commonly designated as hard templates.[186] Usually, these are specially
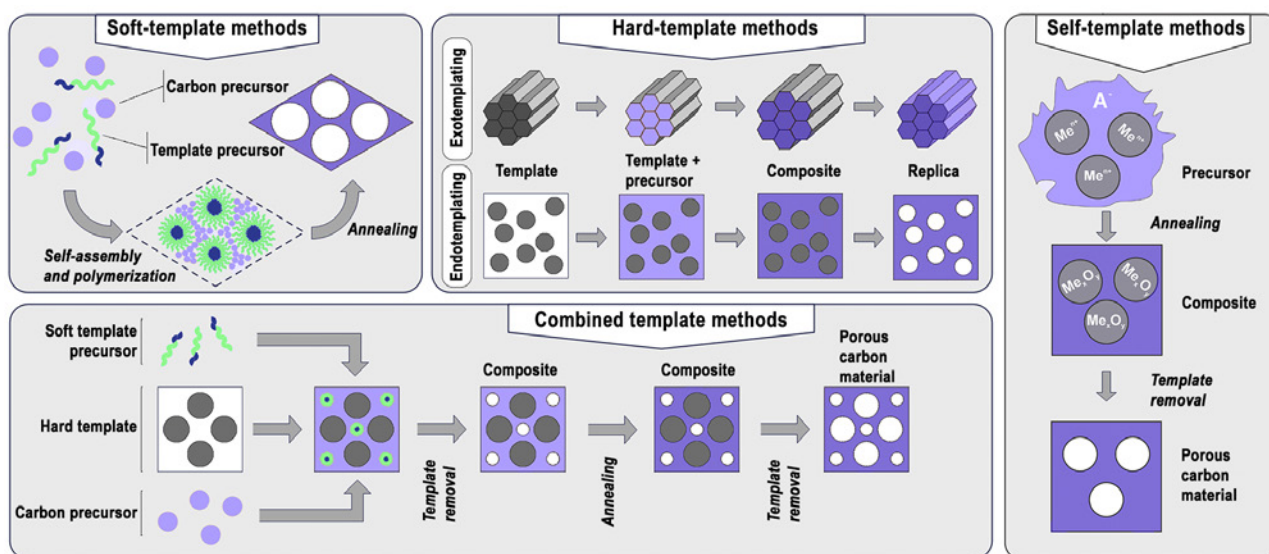

Figure 14. Classification of template synthesis methods according to the types of templates used. Me^{n+} is metal cation, A^{m-} is the anionic template matrix (*e.g.*, organic salt anions).[185]

V.V.Pavlenko, A.Yu.Zakharov, Z.E.Ayaganov, Z.A.Mansurov
Russ. Chem. Rev., 2024, **93** (9) RCR5122

17 of 42

Table 8. Production methods and selected characteristics of some carbons derived from mineral raw materials

Raw material	Elemental composition of the raw material (mass%)					Processing method (mass ratios are given)	BET specific surface area (SSA), $m^2\,g^{-1}$	Pore volume, $cm^3\,g^{-1}$		Pore diameter (D_{av}), nm	Ref.
	C	H	N	O	S			V_{Σ}	V_{mic}		
Hard coal	73.7	4.4	1.4	–	0.2	The starting material was impregnated with KOH in 1:1 ratio, then preactivated at 450 °C for 30 min and activated at 900 °C for 45 min. All processes were carried out in an inert atmosphere.	1192	0.63	0.50	2.12	167
	72.6	4.9	1.7	19.9	0.9	The starting material was impregnated with KOH in 1:5.1 ratio, then activated at 760 °C for 120 min in an inert atmosphere.	2380	1.07	0.89	1.80	168
Brown coal	54.0	–	1.1	40.4	–	The starting material was impregnated with 5 M HCl at 55 °C for 2 h, then dried and impregnated with 10 M H_2O_2 at 55 °C for 2 h. The material was placed into a Teflon reactor, 10 M H_3PO_4 was added, and the mixture was kept for 180 °C for 3 h. Then the material was collected, washed, mixed with dry KOH in 1:3 ratio, and activated at 700 °C for 120 min in an inert atmosphere	2852	1.39	1.17	1.95	41
	65.1	6.6	-	24.8	–	The starting material was treated with 25% H_2O_2 in an ultrasonic bath for 6 h, then the sample was washed, mixed with dry KOH in 1:2 ratio, and activated at 800 °C for 60 min under inert atmosphere	1021	0.52	0.40	–	174
Semi-coke	76.7	1.2	0.7	–	0.5	The starting material was kept in a gas mixture ($NO:NH_3:SO_2:H_2O:N_2 = 0.1:0.05:0.05:5:94.8$ mol.%) at 150 °C for 90 min and then at 400 °C for 40 min. The heating rate was 5 °C/min	88.4	0.07	0.04	1.27	175
	81.5	3.0	0.8	14.2	0.4	The starting material was treated with 6 M HCl (70 °C, 120 min), then with HF (70 °C, 240 min), and with 6 M HCl (70 °C, 120 min). The washed and dried material was activated at 700 °C for 70 min in a steam atmosphere	590	0.29	0.24	0.55	176
Coke	72.9	1.1	0.9	0.3	0.6	The starting material was impregnated with 1 M HCl for 12 h, and then activated at 1000 °C for 120 min in a CO_2 atmosphere	637	0.36	0.20	2.28	177
	96.2	2.9	0.5	0.2	0.2	The starting material was activated at 850 °C for 240 min in a steam atmosphere	643	0.34	0.23	2.11	178
Peat	–	–	–	–	–	The starting material was impregnated with K_2SO_4 and then preactivated at 700 °C and activated at 800 °C for 60 min. The repeated activation was carried out at 900 °C for 45 min in a steam atmosphere	1334	0.70	0.60	0.63	179
Anthracite	87.3	2.4	1.0	7.5	0.9	The starting material was mixed with dry KOH in 1:4 ratio and activated at 850 °C for 60 min under inert atmosphere	1200	0.50	0.47	–	169
Petroleum pitch	93.1	4.6	–	2.3	–	The starting material was mixed with dry KOH in 1:4 ratio and then activated at 800 °C for 60 min under inert atmosphere	3230	1.56	1.47	1.80	180
	92.9	6.3	–	–	–	The starting material was mixed with dry KOH in 1:1 ratio and then activated at 850 °C for 60 min under inert atmosphere	1855	0.77	0.72	–	181
Rubber	50.8	–	–	44.4	–	The starting material was impregnated in a KOH solution in 1:2 ratio (in terms of pure alkali) and then activated at 700 °C for 120 min under inert atmosphere	1130	0.41	0.13	3.50	182

prepared porous inorganic materials such as mesoporous silica and microporous zeolites. As opposed to the use of hard templates, the use of soft templates implies that the template binds to the polymeric carbon precursor and, after matrix stabilization, is removed prior to carbonization or destroyed during pyrolysis. Soft templates are flexible organic molecules that refer to the classes of surfactants or block copolymers [183] that can self-assemble into ordered structures. The interaction of these templates with precursors occurs *via* weak van der Waals or electrostatic interactions.[186] In the self-template synthesis, various organic compounds containing an inorganic residue serve as precursors for the preparation of porous carbon materials. In this case, one of the template components is extracted during the synthesis, and the voids that arise form a porous structure.

4.1. Hard templates

The manufacture of porous carbon material using hard templates includes several stages: template fabrication, introduction of a carbon precursor into the template, pyrolysis, and etching of the template from the porous structure of the final product.[10] The commonly used hard templates are inorganic frameworks such as zeolites,[45] porous silica,[46] MgO,[148] ZnO (Ref. 187) and so on.

The most popular silica templates possessing an ordered mesoporous structure are MCM-41, SBA-15, and KIT-6, which are used to manufacture mesoporous carbons CMK-1, CMK-3, and CMK-8, respectively (Fig. 15). The resulting porous structure of carbon materials depends not only on the template, but also on the method used to remove it: Duraisamy *et al.*[188] showed that the removal of KIT-6 template by treatment with NaOH gives rise to a disordered porous structure with a hierarchical size distribution of pores, whereas the use of HF or polyvinylidene fluoride preserves the ordered porosity. It is also important that the synthesis of porous carbon materials with SiO_2-based templates not always provides a correlation between the pore size in the final carbon material and the template size. This can be attributed to several factors. First, conditions of synthesis such as temperature and time can considerably influence the size and shape of pores, even when the same template is used.[189] Second, the thermal decomposition of the carbon precursor generates additional micropores, which increases the total SSA of the carbon material and changes the pore size distribution.[190] Third, the removal of the silica template

Figure 15. Selected hard templates with an ordered porous structure and carbon materials based on them.

may be accompanied by partial clogging of the pores, which also affects their final pore size.[191] Finally, due to the lower structural support of larger pores, they are more likely to be deformed and/or compressed than smaller pores.[190] It is also noted in the publications that for samples with larger mesopores, the pore diameter determined as the peak of the size distribution function (10.4 nm for the STC-20-1 sample) is much smaller than the diameter of silica particles (20 nm) used as the template, which attests to considerable change in the structure of pores during the pyrolysis.[190]

The synthesis of nanoporous carbon materials using a colloidal solution of SiO_2 as a hard template was described by Béguin *et al.*[43] A commercially available colloidal solution HS-40 was mixed with glucose, which functioned as a carbon precursor, the mixture was pyrolyzed at 900 °C, and then the hard template was leached within 24 h. The resulting carbon material had an SSA of 1162 $m^2\ g^{-1}$ and a monomodal pore size distribution with a maximum around 12 nm. Similarly, Yu *et al.*[192] fabricated nitrogen-doped carbon materials with a hierarchical pore size distribution from a mixture of gelatine and nano-sized ZnO. During pyrolysis of the composite, zinc oxide acts as both the template and the activator, which was confirmed by using two carbonization procedures (Fig. 16): in one case, high-temperature pyrolysis of the carbon material with the template was carried out. Alternatively, low-temperature pyrolysis was performed and then the template was leached, and the carbon material was subjected to an additional carbonization stage at high temperature. The specific surface area of the activated carbon was 2464 $m^2\ g^{-1}$, while in the latter case, this value was much lower and amounted to 737 $m^2\ g^{-1}$.

A classical application of zeolites was described by Kyotani *et al.*[193] The authors synthesized microporous carbon materials using USY zeolite with a pore size of about 0.74 nm as a hard template. Polyacrylonitrile and polyfurfuryl alcohol were used as carbon-containing precursors. After deposition of organic precursor vapour in the zeolite pores, fabrication of the polymer composite, and annealing, the template was dissolved in a mixture of HF and HCl. The preparation of USY-based carbon material using propylene as a carbon-containing precursor was reported. The obtained material had a high SSA of 3600 $m^2\ g^{-1}$.[194]

The use of a composite based on HZSM-5 zeolite and SBA-15B silica as a mixed hard template was reported by Sobrinho *et al.*[195] The composite templates based on these components were fabricated by grinding the zeolite and silica in various mass ratios (25:75, 50:50 and 75:25). The resulting matrix was impregnated with palm oil acting as a source of carbon and subjected to high-temperature annealing under inert atmosphere. The resulting materials had a surface area from 492 to 690 $m^2\ g^{-1}$ and a pore volume of 0.233 to 0.862 $cm^3\ g^{-1}$ depending on the template used.

Wang *et al.*[196] obtained a bimodal porous carbon using a soft/hard dual template based on F-127/SiO_2 and resole as the carbon precursor (Fig. 17). The resulting carbon material had SSA of 1647 $m^2\ g^{-1}$ and a bimodal pore size distribution with peaks at about 2 and 5 nm.

The number of stages involved in the synthesis of carbon materials can be decreased by using the *in situ* etching of templates in which the agent used to remove the template is present from the very beginning in the precursor mixture; this eliminates the need for the additional stage of template removal. For example, a hard template of Fe_2O_3 nanoparticles (acting also as the source for iron doping) and citric acid as both a carbon source and an etching agent can be used to obtain Fe–N-doped three-dimensional porous carbon materials with a hierarchical
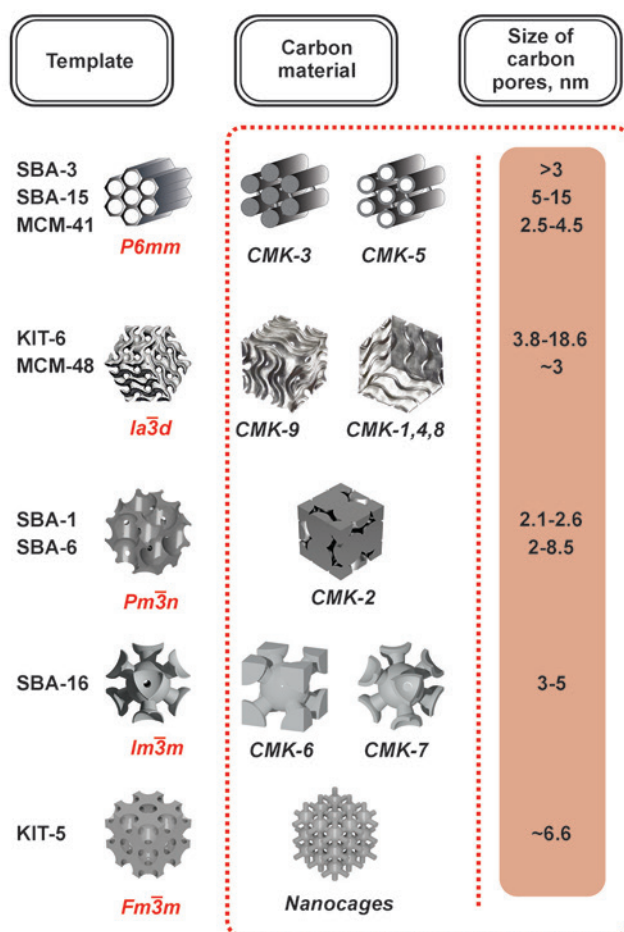
V.V.Pavlenko, A.Yu.Zakharov, Z.E.Ayaganov, Z.A.Mansurov
Russ. Chem. Rev., 2024, **93** (9) RCR5122
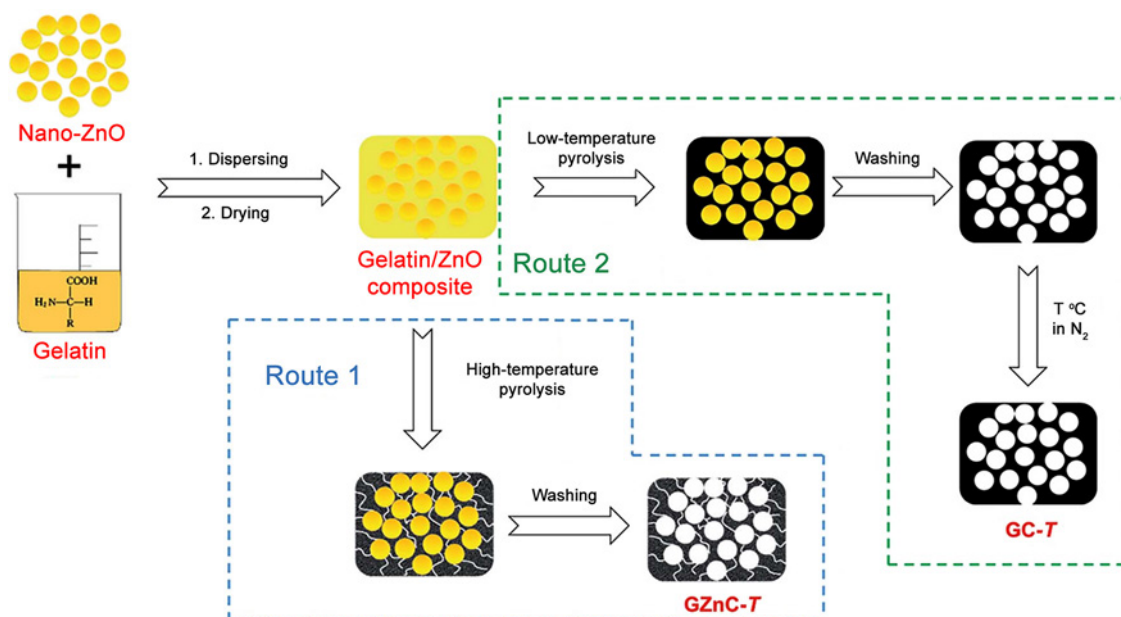
19 of 42

Figure 16. Schematic illustration of the synthesis of porous carbon with ZnO template. Synthetic route 1 implies a dual role of ZnO: as a structuring template and as an activator, whereas synthetic route 2 implies the use of ZnO only as a hard template.[192] Copyright the Royal Society of Chemistry.

pore size distribution. The resulting material had uniform iron and nitrogen distributions and possessed a porous structure with a hierarchical size distribution and high SSA (1644 $m^2 g^{-1}$).[197]

Despite the fact that SiO_2 nanoparticles, zeolites, and other materials are widely used to produce carbons with highly ordered porous structure, their relatively high cost and difficulty of regeneration prevents the widespread practical application of hard templates.

4.2. Soft templates

The synthesis of porous carbon materials using soft templates includes several stages, similarly to the synthesis of mesoporous silicas and zeolites by the same method. In the first stage, soft template micelles arrange the carbon precursor molecules into a uniform structure. Then this framework is stabilized *via* polymerization of the carbon precursor; then the template is removed, and the porous polymer is annealed. Using micelles of amphiphilic block copolymers as templates, it is easy to control the morphology and size of the mesopores (Fig. 18) by adjusting, for example, the size, composition, and concentration of the template polymers or the composition and degree of precursor polymerization. Furthermore, approaches related to the application of soft templates can be extended to the preparation of carbon materials with hierarchical meso- and macroporosity. Peng *et al.*[47] used this approach to obtain carbon nanoparticles
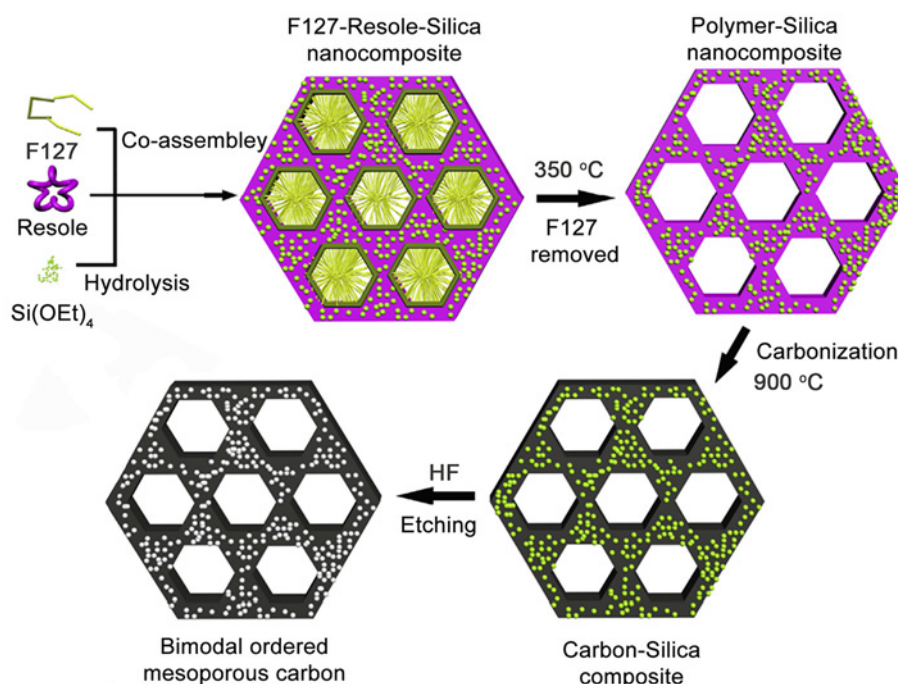

Figure 17. Fabrication of ordered micro-mesoporous carbon using the F-127/SiO_2 dual template.[196] Copyright Elsevier 2016.
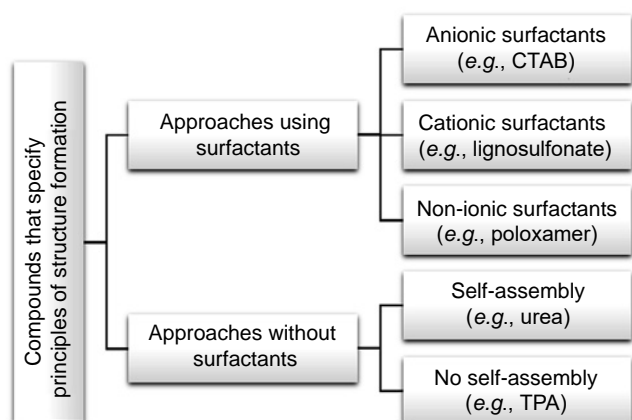
Figure 18. Schematic diagram of various types of soft templates. CTAB is cetyltrimethylammonium bromide, TPA is tris(4-bromophenyl)amine. The Figure was created by the authors using published data in the Ref 198.

of different morphology (Fig. 19). Dopamine was used as a carbon precursor and the F127 surfactant served as the micelle-forming agent; the variation of morphology was attained by adding different amounts of 1,3,5-trimethylbenzene. In combination, this provided 128 nm particles with large pores of 37 nm diameter.

An alternative approach implies the use of methods not involving micelle-forming agents; instead, structure organization occurs *via* self-assembly, cross-linking of polymers, and so on. It is noteworthy that in this approach, the soft templates are not removed from the polymer composition before carbonization, but are wholly carbonized together with the main precursor of the carbon material.[10]

The main shortcomings of the method are less precise control over the pore size compared to hard template processes and

relatively low SSA values. Other typical examples of using soft templates include pyrolysis of xerogels,[199–202] polymer hydrogels,[203] polymer fibres obtained by electrospinning,[204] *etc*.

The carbonization of dried xerogels affords meso- and macroporous carbon materials with a small contribution of micropores, independent of the parameters of the initial gel.[199] If more extensive surface is needed, it is possible to add activators either in the primary annealing stage or as a separate stage.[200] Using chemical activation, Gorska *et al*.[201] obtained a predominantly microporous carbon xerogel with SSA = 2350 m^2 g^{-1} and micropore/mesopore volume ratio of 1.1. A mesoporous carbon xerogel obtained by a similar procedure without chemical activation had SSA = 637 m^2 g^{-1}.[202]

Polymer hydrogels are formed similarly to xerogels *via* polymerization and cross-linking of organic precursors; however, this does not require complex processes of drying before carbonization. Recently, Barzegar *et al*.[203] synthesized a polymer hydrogel from polyvinyl alcohol and polyvinyl-pyrrolidone by the hydrothermal method using microwave radiation to accelerate the reaction (Fig. 20). The resulting hydrogel was carbonized and chemically activated with KOH, which afforded a porous carbon material with SSA = 1846 m^2 g^{-1}. The introduction of graphene into a mixture of precursors made it possible to increase SSA to 3107 m^2 g^{-1}.

Yu *et al*.[205] used polystyrene cryogel as the template and a fluorine-containing polyamic acid as the major source of carbon. The cryogel-based template was fabricated by freeze drying from a polystyrene solution in 1,4-dioxane; then the template was impregnated with the main source of carbon and the resulting composite was annealed at 1000 °C. The obtained carbon material had SSA = 2443 m^2 g^{-1} and a micropore volume of 0.9 cm^3 g^{-1}.

The use of hyper-cross-linked polymers as precursors to obtain porous carbon materials was described in recent reviews.[15, 206] In this case, the porosity is formed during polymerization due to cross-linking, which prevents the chains
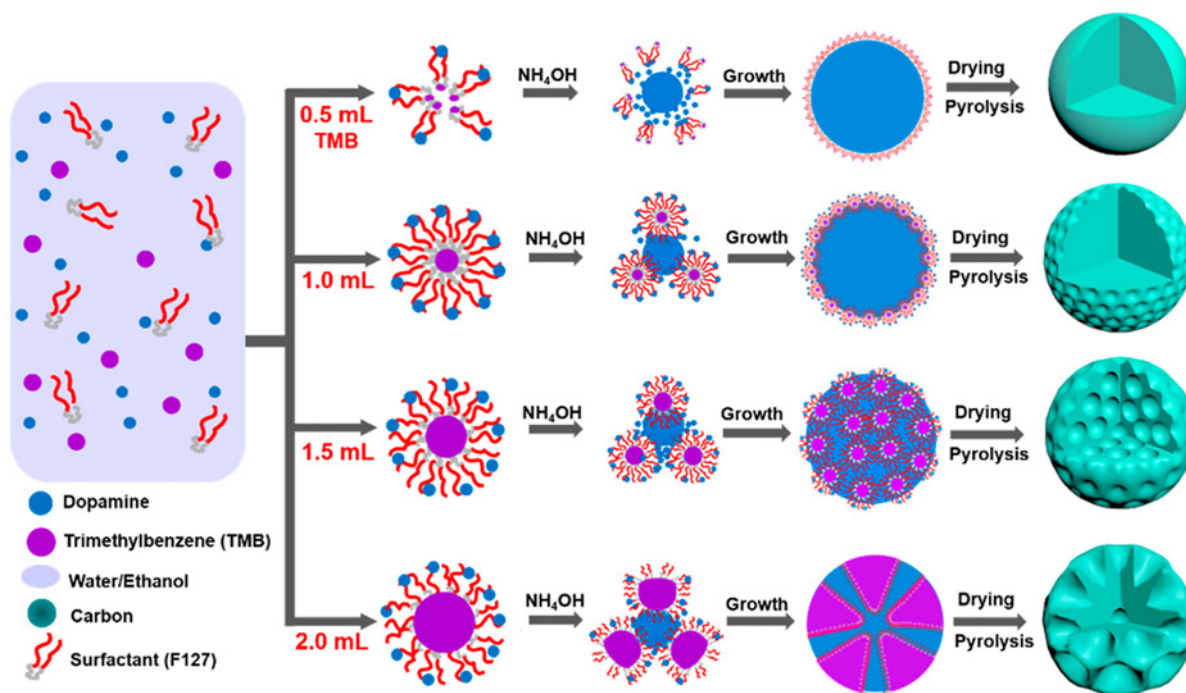

Figure 19. Schematic illustration of the formation of N-doped mesoporous carbon nanospheres with various morphologies of particles obtained by the versatile nanoemulsion assembly approach.[47] Copyright American Chemical Society 2019.

V.V.Pavlenko, A.Yu.Zakharov, Z.E.Ayaganov, Z.A.Mansurov
Russ. Chem. Rev., 2024, **93** (9) RCR5122
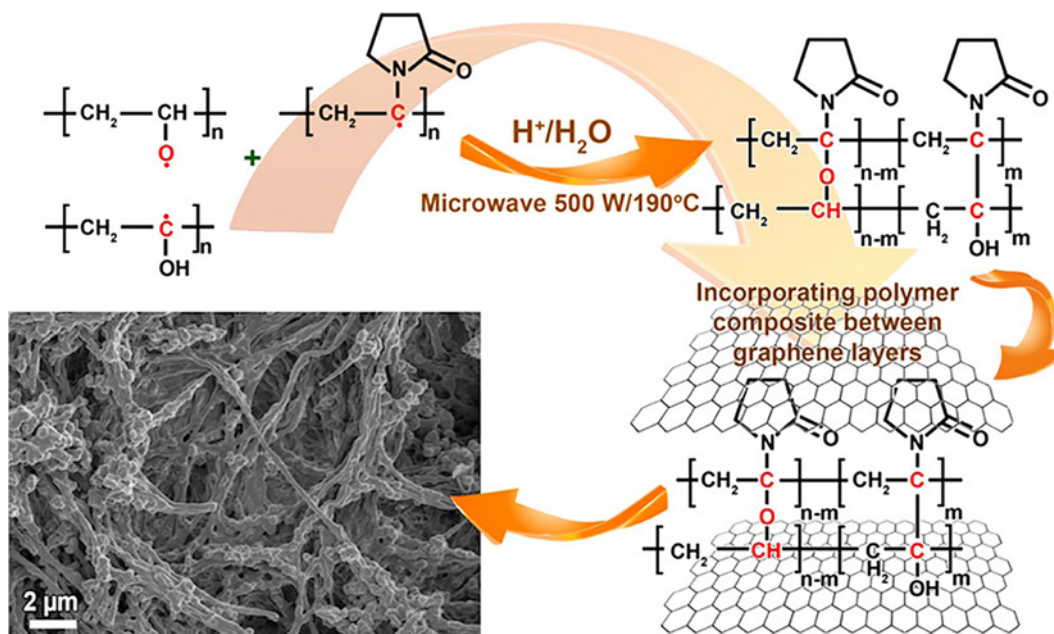
21 of 42

Figure 20. Reaction between polyvinylpyrrolidone and polyvinyl alcohol assisted by microwave radiation to give polymer hydrogel with addition of graphene. The addition of graphene favours preservation of the porous structure and prevents the structural collapse of the interlayer spacing.[203] Published in accordance with the CC BY license.

from folding into a dense non-porous structure.[207] The method is based on the use of one-step Friedel–Crafts reaction; methylal is often used as the cross-linking agent; and a wide range of aromatic compounds are suitable as monomers.[15] The porous structure characteristics in the synthesized carbon materials and the presence of heteroatoms and functional groups can be controlled by selecting aromatic monomers and by changing the stoichiometry of polymerization and incorporation of functionalized copolymers. For example, Babu *et al*.[48] used this protocol to manufacture a porous nanofibre for SC applications. The synthesis was performed for 24 h from naphthalene and

1,2-dichloroethane to which the Friedel–Crafts catalyst and α,α'-dichloro-*p*-xylene were added. The resulting material was carbonized at 700 °C for 6 h under inert atmosphere.

Electrospinning is also used to obtain polymer compositions for the subsequent carbonization. This method is employed to draw micro- and nanoscale fibres from polymer solutions using an electric field. A typical precursor for the preparation of nanofibres by this method is PAN, which is often combined with poly(methyl methacrylate) (PMMA). During pyrolysis of the mixture, PMMA template is completely burned out at temperatures below 400 °C, whereas carbonization of PAN to

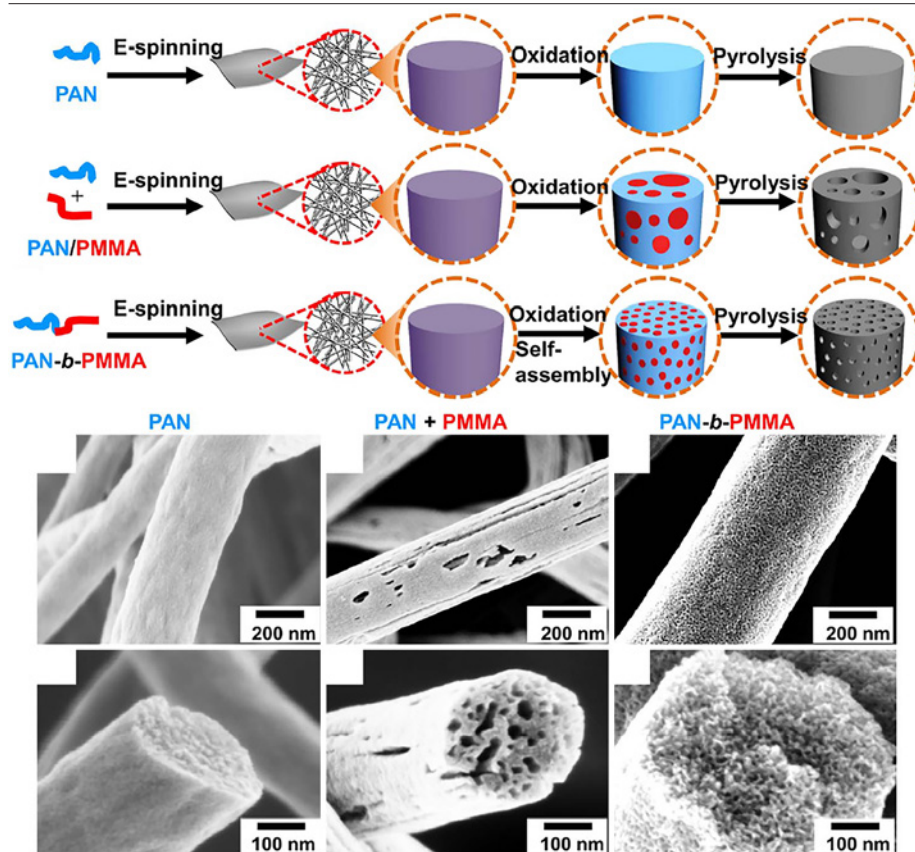**Figure 21.** Schematic illustration of the preparation of carbon materials using electrospinning from various precursors: PAN (*a*), PAN+PMMA mixture (*b*), and poly(acrylonitrile-*block*-methyl methacrylate) (*c*). SEM images of carbon fibres derived from PAN (*d*, *e*), PAN+PMMA (*f*, *g*), and poly(acrylonitrile-*block*-methyl methacrylate) (*h*, *i*).[208] Published in accordance with the CC BY license.

give a porous structure occurs at higher temperature. Zhou *et al.*[208] showed that the use of poly(acrylonitrile-*block*-methyl methacrylate) (Fig. 21), instead of the classical PAN+PMMA mixture, results in a more than twofold increase of SSA of the obtained carbon material (from 245 to 503 $m^2 g^{-1}$). The carbon material obtained from the block copolymer has a bimodal pore size distribution with peaks at 0.5 and 10 nm, whereas the porous carbon from PAN+PMMA is characterized by a broad distribution of pore sizes from 5 to 100 nm.[208] Irrespective of the precursor used, the electrospun carbon material can be subjected to chemical or physical activation, which makes it possible to increase SSA up to more than 2500 $m^2 g^{-1}$.[204]

An unusual implementation of the soft template method was reported by Xin *et al.*[209] A sewage sludge was used as a carbon precursor, and various flocculants (cationic and anionic polyacrylamides and chitosan) were used as templates. In this case, the flocculant functions as a nucleating agent, that is, it is responsible for the pore formation and surface modification. The obtained materials had SSA = $102-137$ $m^2 g^{-1}$ and a pore volume from 0.149 to 0.183 cm^3.

Chen *et al.*[210] used lignosulfonate as a soft template, which was formed from urea. Actually, restructuring of urea to lignosulfonate took place at low temperature; lignosulfonate was transformed into nitrogen- and sulfur-doped ordered porous carbon material.

4.3. Self-templates

Self-templates contain both an organic part, which serves as a source of carbon during pyrolysis, and mineral components, which are removed afterwards to form a porous structure. Unlike the methods described above, the self-template method does not require the use of additional precursors to generate the porous structure, which naturally arises during the pyrolysis. The pyrolysis of self-templates involves decomposition of the organic part; simultaneously, the inorganic part acts as the template for the formation of porous structure; the particles thus formed aggregate and diffuse towards the surface, forming a hierarchical distribution of pore sizes. After pyrolysis, the template is leached upon treatment with acid or alkali.[183] For example, the thermal decomposition of Prussian blue ($Fe_4[Fe(CN)_6]_3$) affords iron oxide nanoparticles, which act as a hard template. As a result of the above-mentioned diffusion and aggregation processes, these particles move to the surface of the carbon material and leave voids, which form the final material porosity. Prussian blue can be used both independently of other compounds and in combination with organic precursors of carbon.[211] The template synthesis method was first proposed in the early 1980s when Knox *et al.*[4] used spherical solid gel particles as the template and a phenol/1-aminohexane mixture as the carbon source. The carbon material obtained after removal of the template had a specific surface area of $460-600$ $m^2 g^{-1}$. Various organic salts are also suitable as self-templates. Tian *et al.*[212] used zinc gluconate as the precursor mixed with NH$_4$Cl (1:1 mass ratio) for nitrogen doping of the target carbon. The resulting carbon material had a specific surface area of 1162 $m^2 g^{-1}$, pore size of 3.33 nm, and nitrogen content of 4.57 at.%.

A classical example of using the self-template method is carbonization of natural raw materials. In this case, inorganic elements present in the initial raw material act as templating agents that form the primary porosity, which further develops during the activation. For example, during the rice husk carbonization, silicon present in large amounts in the raw

material acts as the self-template. Special leaching of silicon is not performed, since this precursor is activated in an excess of alkali.[135]

The self-template method is also used to introduce elements such as nitrogen or phosphorus into the carbon material in order to increase the electrochemical activity. For example, using the self-template method, Wang *et al.*[213] prepared a highly porous carbon material with hierarchical pore size distribution and a surface area of 2160 $m^2 g^{-1}$. They used saccharose as a source of carbon, while disodium zinc ethylenediaminetetraacetate served as the nitrogen donor and self-template.[213] The ZnO and Na$_2$CO$_3$ nanoparticles formed upon thermal treatment of EDTANa$_2$Zn/ saccharose composites are uniformly distributed in the nitrogen-doped carbon, which helps to generate a mesoporous structure. In addition, ZnO nanoparticles promote high-temperature etching of carbon as an activating agent.

Metal-organic frameworks[214-216] and zeolitic imidazolate frameworks (ZIFs)[217-219] are also suitable as precursors for the self-template method. During the pyrolysis of these compounds, the organic part decomposes to form carbon, while the metal clusters play the role of a templating agent. For example, direct carbonization of rod-like MOF-74 (Fig. 22 *a*) gave rise to carbon nanorods (SSA = 1559 $m^2 g^{-1}$), which were converted to graphene nanoribbons with SSA = 1492 $m^2 g^{-1}$ *via* the subsequent treatment with KOH.[215] The variation of the porosity of carbon materials obtained from ZIF-8 by post-activation of the material and framework pre-etching (Fig. 22 *b*) was described by Jeoung *et al.*[219]

The introduction of heteroatoms and control of their ratio in the target carbon structures can be accomplished by replacing bridging ligands or by using secondary carbon precursors.[217, 220] The appropriate selection of precursors, control of the pyrolysis temperature, and application of various post-treatment methods altogether make it possible to obtain carbon materials with specified porosity characteristics. The structure morphology can be changed not only by replacing metals in the original precursors, but also by using additional reagents. For example, recently, Liu *et al.*[221] demonstrated that coating of the ZIF-8 precursor with a thin SiO$_2$ layer (>40 nm) prior to pyrolysis gives rise to hollow cube-like carbon structures, whereas pyrolysis of pristine (or coated with a thinner SiO$_2$ layer) precursor is accompanied by structure collapse, and the resulting materials do not have inner voids. An inverse strategy can also be used to produce hollow carbon particles. Feng and Zhang[222] grew ZIFs-Co$_x$Zn$_{1-x}$ nanocrystals on the surface of spherical SiO$_2$ particles; then the resulting composite was subjected to pyrolysis and silicon leaching. It was shown that depending on the Co/Zn ratio, either hollow spherical Co/NHC particles (for $x > 0.75$) or nanotube-decorated CNT-Co/NHC particles (for $x < 0.75$) are formed.

In recent years, methods for the synthesis of CNT-decorated core–shell porous structures[218,223,224] using MOFs or covalent organic frameworks as both the core and the shell have been actively developed. In this case, the primary precursor is usually carbonized to give an ordered carbon material with active sites, in which controlled growth of the secondary carbon precursor is subsequently performed; the secondary carbonization affords the target carbon structure (Fig. 23). Apart from MOFs, organic salts such as magnesium, zinc, sodium, potassium, and calcium citrates and gluconates and other salts are widely used as precursors for self-template synthesis; this may give porous carbon materials with SSA of approximately 2000 $m^2 g^{-1}$.[43,109]

While comparing the carbon materials obtained using different synthetic strategies, the following regularities should
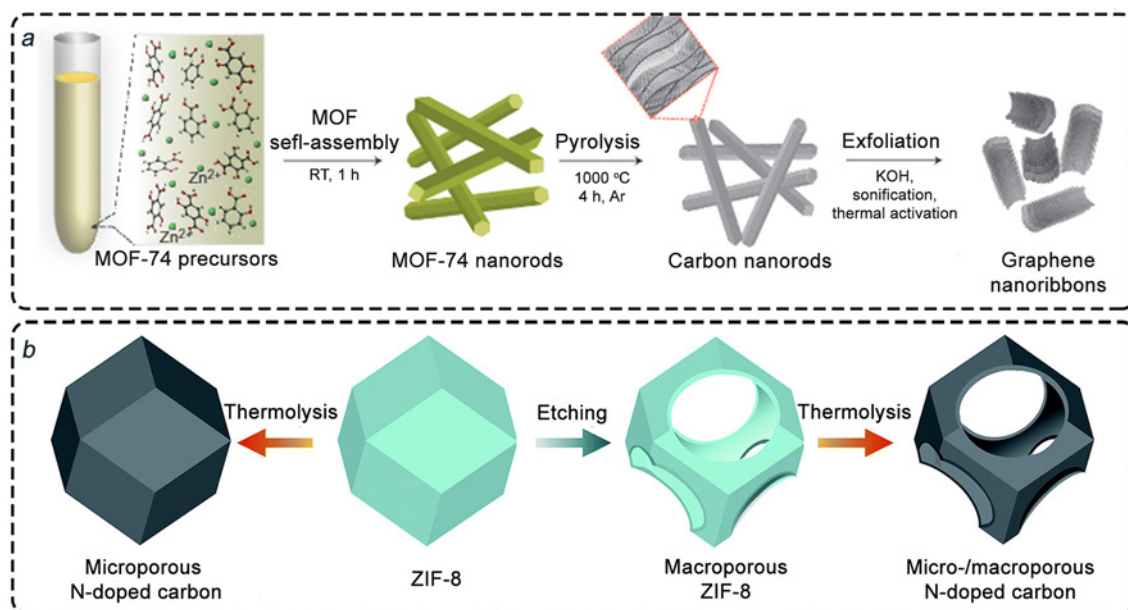
Figure 22. Self-template synthesis of porous carbon materials using MOF-74 (*a*) (Copyright Macmillan Publishers Limited 2016) [215] and ZIF-8 (*b*).[219] Copyright Royal Society of Chemistry.
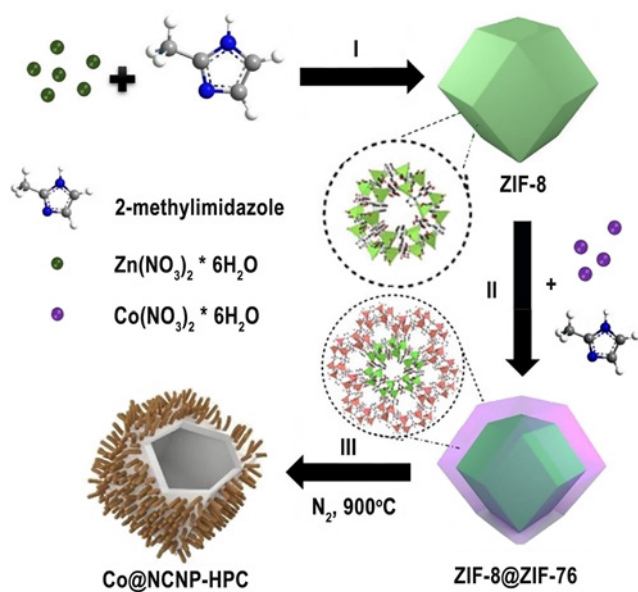

Figure 23. Schematic illustration of the formation process of Co@NCNP-HPC heterostructure (hollow porous carbon material decorated with Co-included CNTs): (I) self-assembly of ZIF-8 framework from 2-methylimidazole and $Zn(NO_3)_2$; (II) epitaxial growth of ZIF-76 on ZIF-8 surface; (III) carbonization in inert atmosphere to form Co@NCNP-HPC.[223]

be highlighted: materials obtained using hard or soft templates are characterized by ordered porous structure clearly visible in TEM images, whereas the porous structure of materials obtained using self-template or chemical activation methods is most often disordered (Fig. 24 *a*). Carbon materials obtained by self-template synthesis may have pores of various shapes and sizes depending on the precursor used. For example, the carbon material derived from magnesium citrate is characterized by narrow-necked pores with D_{av} of about 3.5 nm (Fig. 24 *b*, TC-1 curves). Materials obtained by the chemical activation method are, most often, microporous with pore sizes of less than 1 nm

and a very narrow distribution maximum (Fig. 24 *b*, Maxsorb curves) or have a hierarchical pore size distribution. The use of hard templates gives rise to cylindrical pores with a distribution maximum corresponding to the template size (Fig. 24 *b*, TC-2 curves). In some cases, formation of narrower channels is possible due to shrinkage of the carbon structure during high-temperature annealing.[190] In terms of capacitance properties, carbon materials with wider nanopores would have lower specific capacitance due to the smaller available surface area (Fig. 24 *c*), which is discussed in more detail in Section 5.2. Irrespective of the preparation method, porous carbon materials have a high degree of disorder, as evidenced by the similar intensities of peaks D and G in the Raman spectra (Fig. 24 *d*).

Details of using various strategies for the preparation of porous carbon materials by template synthesis are summarized in Table 9. Using these methods, it is possible to tune the structure of the target compound by simply varying or combining the applied templates. Nevertheless, the use of templates still has a number of drawbacks. In the case of hard templates, the drawbacks include the high cost of template removal (caused by the use of corrosive agents) and the difficulty of preparing microporous materials with high SSA values, which necessitates the application of chemical activation methods for porosity generation. The proportion of microporosity can also be increased by using combined templates (*e.g.*, hard/soft template mixtures). However, this increases the cost of the resulting material several times. In the case of soft templates, the critical drawbacks are the relatively high cost of the precursors and difficulty of scaling-up of the process for the large-scale industrial production. The use of self-templates is complicated either by relatively low content of the template in the precursor, resulting in insufficient porosity (carbonization of biomass), which requires activation, or by high cost of precursors (MOFs, ZIFs, *etc*.). On the other hand, the most recent studies of carbon materials obtained from organic salts that act as self-templates (*e.g.*, Mg, Ca, and other citrates) show that their characteristics are not inferior to those of typical samples obtained using hard templates (such as CMK-1, CMK-3, and other), with the cost of such carbon
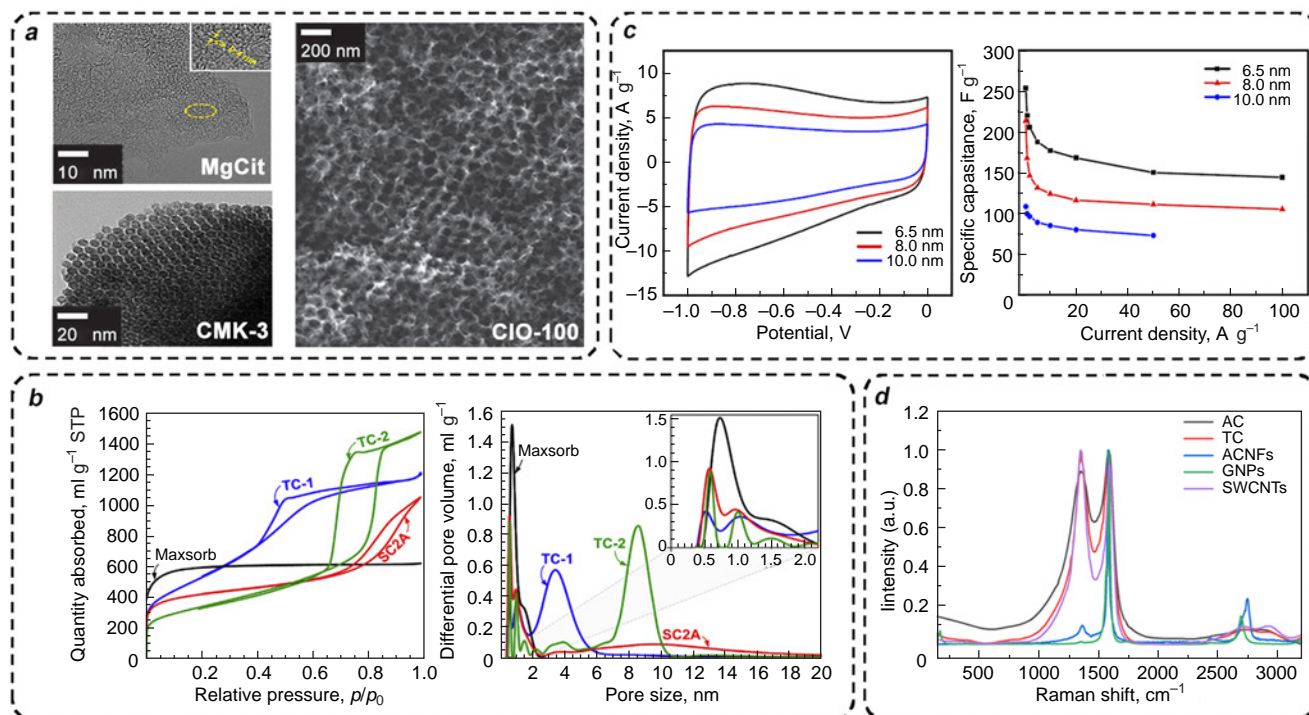
24 of 42

V.V.Pavlenko, A.Yu.Zakharov, Z.E.Ayaganov, Z.A.Mansurov
Russ. Chem. Rev., 2024, **93** (9) RCR5122

Figure 24. TEM images of the porous structure of carbon materials obtained by self-template method from magnesium citrate (MgCit) and the hard template method using MCM-48 (CMK-3) and 100-nm size silica particles (CIO-100) (*a*); adsorption isotherms and the pore size distribution for micro-mesoporous carbon black SC2A; commercial carbon Maxsorb MSP-20X; carbon obtained by self-template synthesis from magnesium citrate (TC-1); carbon obtained using 12 nm SiO_2 particles as a hard template (TC-2) (*b*); CV and GCD curves (*c*); Raman spectra of the activated carbon (AC), technical grade carbon (TC), activated carbon nanofibres (ACNFs), graphene nanoplates (GNPs), and single-walled carbon nanotubes (SWCNTs) (*d*).[43, 131, 204, 225–228]

Table 9. Characteristic features of application of various strategies of production of porous carbon materials using template synthesis.

Method	Key stages	Benefits	Drawbacks
Hard template	Ready template + precursor; pyrolysis; template removal	Simple control over the porosity; high reproducibility; scalability; ordered structure	Large number of stages and time expenditure; corrosive agents for template removal
Hard template	Surfactant + precursor self-assembly; template removal during pyrolysis	Control over the porosity; high reproducibility	Pronounced dependence on the reaction conditions; relatively high cost of the template
Combined template	Several templates + precursor; pyrolysis; template removal	Hierarchical pore size distribution	Requires several templates; high cost; large number of stages and time expenditure
Self-template	Pyrolysis of MOFs, organic salts and so on.	Hierarchical, mono- or bimodal pore size distribution; simple introduction of active sites	Large number of stages; high cost of most self-templates

precursors being many times lower than that of MOFs, ZIFs, and other standard self-templates.

Despite the considerable progress in the fabrication of carbon materials by template synthesis methods, characteristics of the resulting carbons (first of all, SSA) are still far from those of commercial carbon materials (Table 10). For example, among the commercially available carbons, note Maxsorb with SSA = 2500–3200 m^2 g^{-1}, whereas for typical CMK-3 carbons, SSA rarely exceeds 1500–1600 m^2 g^{-1}, which is closer to characteristics of Kuraray carbons, characterized by moderately high SSA values in the range of 1500–2000 m^2 g^{-1}. The cost of carbon materials obtained by template synthesis is still much higher than the cost of commercially available analogues. Although the production formulations are proprietary, analysis of porosity characteristics suggests that commercial carbon materials are produced by carbonization of natural plant raw materials or petroleum coke with subsequent chemical activation, which ensures their lower cost in comparison with the carbons obtained using template synthesis.

5. Applications

5.1. Treatment of water

Porous carbons are used as physical sorbents in conventional filtration systems and in emerging water capacitive deionization (CDI) technology [135, 158] and for the separation of non-polar organic compounds.[245]

V.V.Pavlenko, A.Yu.Zakharov, Z.E.Ayaganov, Z.A.Mansurov
Russ. Chem. Rev., 2024, **93** (9) RCR5122

25 of 42

Table 10. Porosity characteristics of most widespread commercial carbon materials.

Carbon	BET specific surface area (SSA), $m^2\,g^{-1}$	Total pore volume, $cm^3\,g^{-1}$	Micropore volume, $cm^3\,g^{-1}$	Mesopore volume, $cm^3\,g^{-1}$	Pore diameter (D_{av}), nm	Preparation principle	Ref.
Kuraray YP-80F	1917	–	0.686	0.107	1.2	Chemical activation of carbonized coconut shells	204
Kuraray YP-50F	1599	0.76	0.47	0.12	1		229, 230
YiHuan Carbon YEC-8A	1435	1.501	0.370	1.131	3.83	Unknown	229, 230
Maxsorb-III	3250	1.79	1.7	–	2.008	Various types of petroleum coke + excess KOH. Dehydration at 400 °C, chemical activation with KOH at 600–900 °C under inert atmosphere.	231–235
	3311	1.743	1.87	–	2.2		
	3140	2.01	1.79	–	2.008		
Maxsorb MSC-30	3121	1.56	1.00	0.57	1.98		
	2680	1.75	1.2	0.55	1.2–3.5		
Maxsorb MSP-20	2310	0.99	0.97	0.02	1–2		
	2510	1.14	0.98	0.23	3.08		
CMK-1	1607	0.94	0.08	0.78	0.5; 1.9	Synthesis using the MCM-48 hard template	236
CMK-2	1493	0,86	0.13	0.60	0.5; 1.2	Synthesis using the SBA-1 hard template	
CMK-3	624	–	0.18	0.43	3.42	Synthesis using the SBA-15 hard template	237
	1350	1.22	0.16	1.06	1,2; 5		238
	1222	1.17	0.07	1.05	3.7		239
CMK-5	2208	2.12	0.00	1.96	2.9; 4.1	Synthesis using the SBA-15 hard template	239
CMK-6	1373	1.17	0.04	1.06	3.2	Synthesis using the SBA-16 hard template	239
CMK-7	2141	1.72	0.00	1.6	3.0; 4.2		
CMK-8	1043	–	0.69	0.79	1.2; 6.12	Synthesis using the KIT-6 hard template	240
	1126	0.95	0.10	0.78	3.2		239
CMK-9	2113	2.08	0.00	1.94	3.0; 4.4		
TC-1	1976	1.76	0.40	1.36	0.91–3.4	Self-template synthesis with magnesium citrate at 900 °C	43
MAU-2A	800	0.78	0.40	0.30	–	Impregnation of fruit kernels and nut shells with saturated solutions of urea and thiourea at 200–250 °C, Carbonization at 600–750 °C, steam activation at 800–850 °C	241, 242
BAU-MF	608.4	0.307	0.244	0.063	0.62	Steam activation of carbonized birchwood at 800–950 °C	243
KAU	1319	0.576	0.536	0.040	0.685	Steam activation of carbonized coconut shells at 900–1000 °C	243
DAK	1430	0.447	0.133	0.440	–	Steam activation of carbonized hardwood at 850–900 °C	244

The CDI technology uses special cells consisting of two parallel electrodes and a separator through which a flow of salt water is passed. In terms of the operation principle, the CDI cell is similar to SC: as the voltage is applied, ions move towards the electrodes under the action of Coulomb forces and are concentrated in the electric double layer (EDL).[246] The material is regenerated when the voltage is switched off or reversed. Compared to commercial reverse osmosis technology, the unit cost of CDI includes much lower energy consumption $(0.13–0.59\,kW\,h\,m^{-3}$ *vs.* $0.7–2.0\,kW\,h\,m^{-3}$ for reverse osmosis).[247]

The key parameters for optimization of the system are the adsorption capacity and the adsorption rate of ions. The efficiency of using carbon materials in CDI systems depends on their porous structure, surface composition, and SSA. To attain a high adsorption capacity towards the target substances, hierarchical pore size distribution in the range similar to the size of pollutant molecules is desirable. On the one hand, this structure has a high surface area owing to micropores and, on the other hand, it has good diffusion kinetics due to meso- and macropores.[13] Fine tuning of pore diameters affects the

selectivity of CDI systems towards different ions. Gao *et al.*[248] showed that the sorption capacity towards different ions present simultaneously decreases in the series $Fe^{3+} > Cu^{2+} > Zn^{2+} > Na^{+}$, since the ion charge plays the primary role in electrical sorption processes, while the ion radius starts to play a role only if the charges are equal. Since the hydrated radius is smaller for Cu^{2+} than for Zn^{2+}, the adsorption of Cu^{2+} is more efficient.[248] Analogous results were obtained by Huang *et al.*[249] upon the co-adsorption of Cr^{3+}, Cd^{2+}, and Pb^{2+}: the adsorption capacity decreased in the series $Cr^{3+} > Pb^{2+} > Cd^{2+}$. The kinetic characteristics for Fe^{2+}, Cu^{2+}, Pb^{2+}, and Cd^{2+} cations, which confirm the above-described behaviour, were calculated by Liu *et al.*[251] and are presented in Fig. 25*a*.[133,250–254]

The chemical composition of the carbon surface is also important for sorption/desorption processes.[255] Various functional groups can form hydrogen, van der Waals or $\pi–\pi$ bonds with organic molecules, chelate heavy metals, and change the hydrophilicity of carbon electrodes (Fig. 25*b*).[133,250–254] One of the types of chemical modification of carbon that imparts a charge to the surface is doping with heteroatoms such as B, O, or N, the electronegativities of which differ from that of
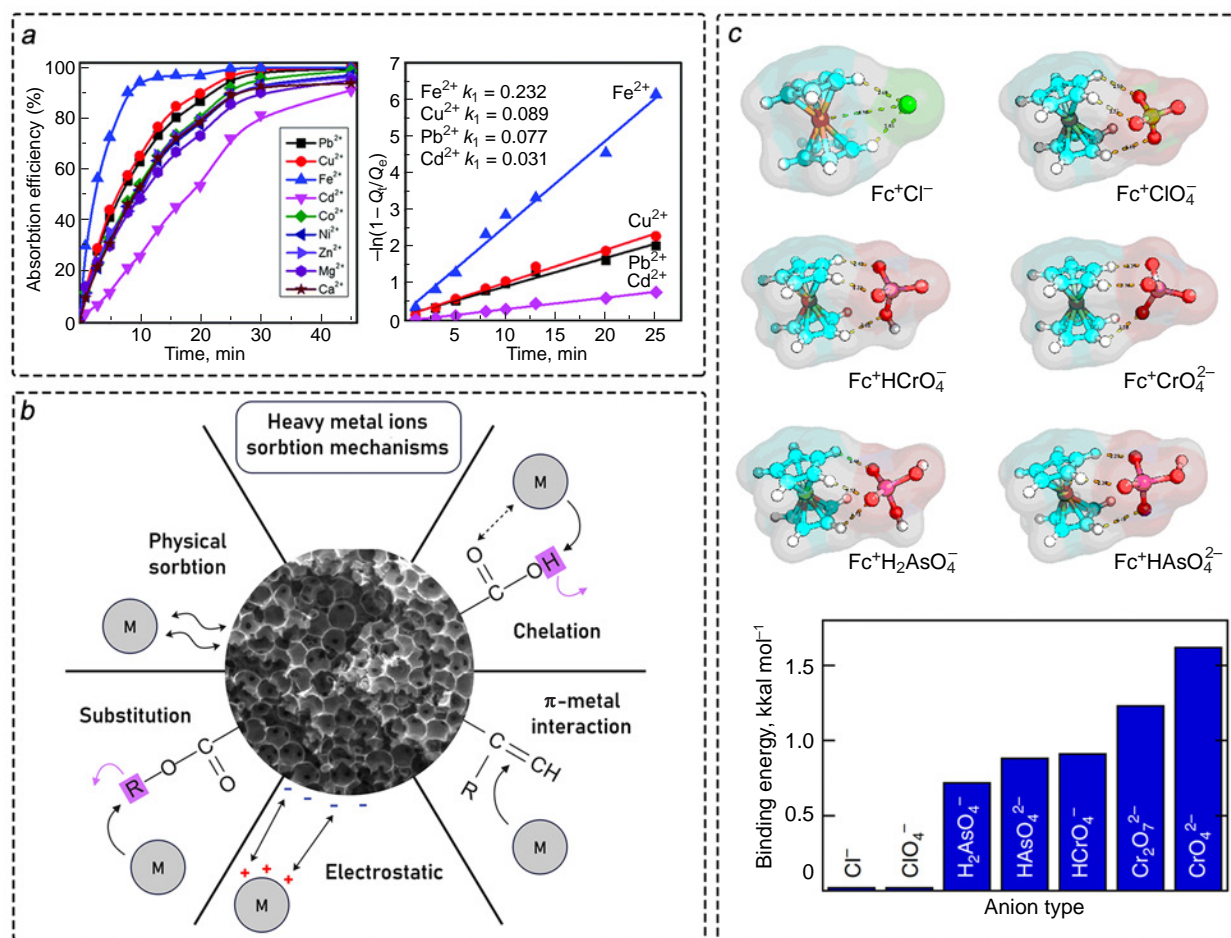
Figure 25. Efficiency of CDI cell operation and kinetic characteristics plotted *vs.* adsorption time for cations of various heavy metals (*a*); various mechanisms of cation interaction with the surface of carbon material (*b*); optimized geometries and binding energies of various anions to ferrocene functional groups (Fc$^+$) (*c*).[133,250–254]

carbon;[256] this increases the adsorption capacity and catalytic properties of porous carbon materials due to charge transfer from neighbouring carbon atoms and formation of active sites on the surface.[257,258] One more approach is the chemical modification of the carbon surface to provide either a surface charge or chelation of metal atoms for better retention. The main problem of functionalized and doped electrodes for CDI systems is their relatively low cyclability under specified conditions due to the complexity of desorption processes and to the destruction of surface active sites (functional groups and dopant atoms).

An alternative to the classical functionalization is the design of polymer–carbon composites. For example, Su *et al.*[250] described adsorption of anions containing Cr(VI) and As(V) by a composite of CNTs and polyvinylferrocene. Microscopic examination using *in situ* TEM showed good reproducibility of adsorption and high selectivity of composite electrodes to the target CrO_4^{2-} and $HAsO_4^{2-}$ anions in the presence of Cl^- and ClO_4^- anions (Fig. 25 *c*).[133,250–254]

Surface functionalization can be directed towards changing the wettability of the carbon material. For example, in order to make a carbon cloth hydrophobic, Zulfiqar *et al.*[259] functionalized the surface by soaking the material in hexane and perfluorodecyltrichlorosilane (FDTS). After modification and drying, the water contact angle with the material increased to ~145°. The modified material had a high efficiency for the recovery of toluene, hexane, heptane, and dichloromethane from water or corrosive solutions (1 M NaCl, NaOH, HCl) for at least 30 cycles.

5.2. Energy storage systems

The energy storage systems that use porous carbon materials as electrodes include SCs and storage batteries [mainly sodium- and potassium-ion batteries (SIBs and PIBs)]. Irrespective of the type of the storage system, they consist of two electrodes and a separator immersed in the electrolyte. Supercapacitors can be subdivided, depending on the energy storage mechanism, into double layer supercapacitors (EDLC) and pseudocapacitors (PsC).[11] In EDLC, energy is stored in EDL due to electrostatic adsorption/desorption of electrolyte ions at the electrolyte/electrode interface, while PsC store energy as a result of fast redox reactions of electroactive surface functional groups.[260] Supercapacitors have a high power density and cyclability; however, their energy density is relatively low compared to that in batteries or fuel cells.[261] Since the principles of energy storage in batteries (intercalation) and SCs (electrical double layer or pseudo-capacitance) are different, the approaches to selecting and optimizing the carbon materials used in these devices are also different.

Depending on the type of energy storage device in which a carbon material is used, the principles of energy storage differ. Indeed, charge and discharge processes in supercapacitors follow two mechanisms: (a) accumulation in the double EDL formed upon the electrosorption of electrolyte ions on the surface of carbon electrodes and (b) fast reversible redox reactions on the surface of active materials (pseudo-capacitive
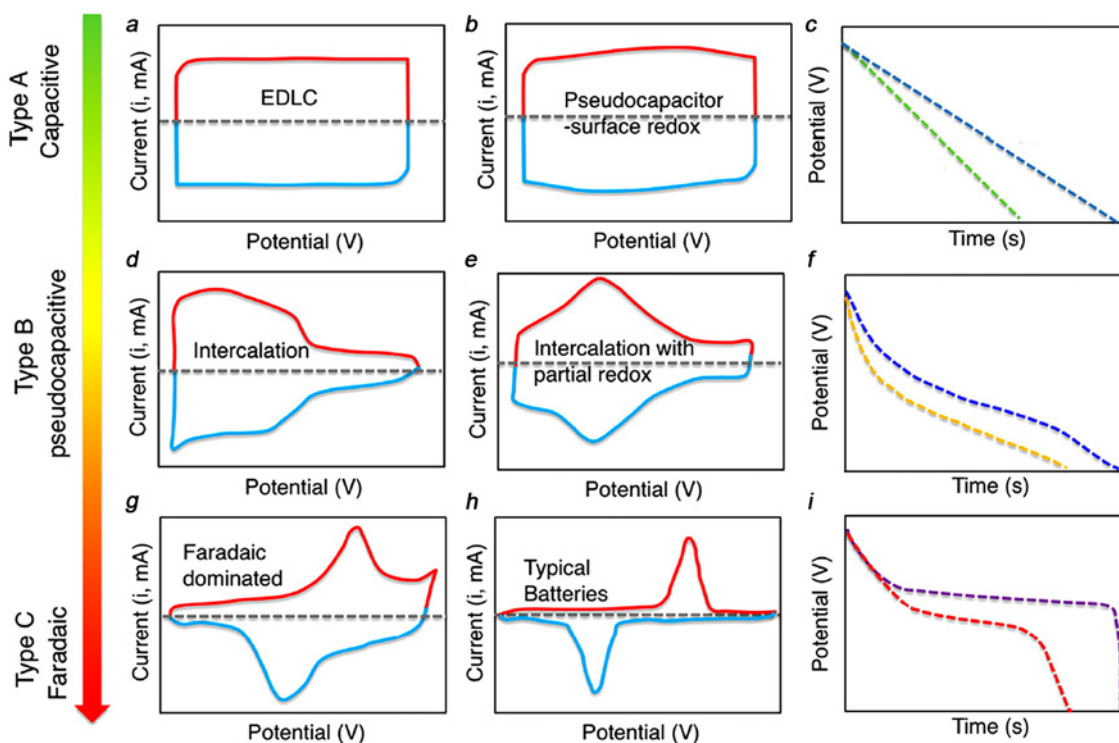
V.V.Pavlenko, A.Yu.Zakharov, Z.E.Ayaganov, Z.A.Mansurov
Russ. Chem. Rev., 2024, **93** (9) RCR5122

27 of 42

Figure 26. Typical CV and galvanostatic discharge curves for various types of energy storage devices: classical supercapacitor (type A), pseudo-capacitor (type B), and battery (type C), respectively. Typical CV profile for EDL-based capacitor (*a*), surface redox reactions (*b*), intercalation type (*d*), and intercalation type with partially reversible redox peaks (*e*). (*c*, *f*, *i*) show the corresponding galvanostatic discharge peaks.[262] Copyright American Chemical Society 2019.

behaviour). In the case of batteries, the energy storage may occur by the intercalation/filling, adsorption/intercalation, and adsorption/filling mechanisms,[9] which is reflected in the patterns of the CV and GCD curves (Fig. 26).[262]

5.2.1. Storage batteries

A typical carbon material used as an anode accumulating Li, K, or Na in storage batteries is graphite. The above ions are stored as intercalation compounds in which metal atoms are inserted into the interlayer space of the graphite-like part of the carbon material, where they are ionized giving off an electron to the graphite conduction band. The following steps of lithium intercalation into pure graphite in LIBs are distinguished: $LiC_{36} \rightarrow LiC_{24} \rightarrow LiC_{12} \rightarrow LiC_6$. As the degree of intercalation increases, the interplanar spacing in the graphite-like structure increases from 3.550 Å (graphite) to 3.815 Å (LiC_6).[263, 264] In the case of sodium and potassium, owing to their large radii, the formation of NaC_6 and KC_6 proved to be energetically unfavourable, with NaC_8 and KC_8 being the highest level (Fig. 27).[9, 265–267] Porous carbon materials can store Li, K, and Na not only as intercalation compounds, but also *via* adsorption on the surface and filling of closed pores as a result of cation diffusion between the graphene sheets. Furthermore, in the case of Li, the major amount is stored *via* intercalation, while K and Na are mainly stored in closed pores. The mechanisms of energy storage in porous carbon anodes are discussed in detail in a recent review.[268]

Nevertheless, the approaches to the formation of porous structure of carbon anodes for storage batteries are similar: high conductivity, appropriate surface chemistry, and large specific surface area and pore volume are critical parameters to achieve high capacitance and stability. The electrical conductivity of carbon materials provides effective electron transport, high SSA values ensure good contact with the electrolyte to maintain high ion flux through the interface, while large pore volume makes it possible to accommodate both cations and anions and to change the volume of the anode material during intercalation/deintercalation. In addition, a hierarchical pore size distribution is desirable, because micropores promote reversible intercalation/deintercalation processes, thus providing high capacitance, while meso- and macropores are favourable for cation transport and electrolyte mobility.[269,270] The electrical conductivity can be increased by doping the carbon structure with heteroatoms (B, N, S, O).[271] Nitrogen, which has a higher electronegativity and a larger atomic radius than carbon, is used most often among the heteroatoms.[272] Apart from the listed approaches, it is possible to manufacture composites based on porous carbon and silicon[273] or various metal oxides (*e.g.*, Fe_2O_3, Co_3O_4, TiO_2, CuO and other), which possess high intercalation capacity.[274] On the other hand, in the design of composites, the addition of nanoporous carbon can improve the conductivity and mechanical flexibility of these metallic materials. For example, the Co_3O_4/CMK-3 composite obtained by hydrothermal synthesis using porous carbon prepared with the SBA-15 hard template exhibited a high specific capacitance of 1131.3 F g^{-1} at 0.5 A g^{-1} and 91% retention of the capacitance after 3000 cycles.[275] Despite the numerous benefits of this technology, it is worth noting that the potential blockage of carbon pores by other materials can be undesirable; therefore, rational design of the porous structure is of great practical importance.

Similar concepts are applied for sodium-ion batteries; however, hard carbons are mainly used instead of graphite-like porous carbons because of the following issues: (1) amorphous carbon with distorted graphene-like layers provides larger interlayer spacings for faster Na$^+$ intercalation; (2) closed
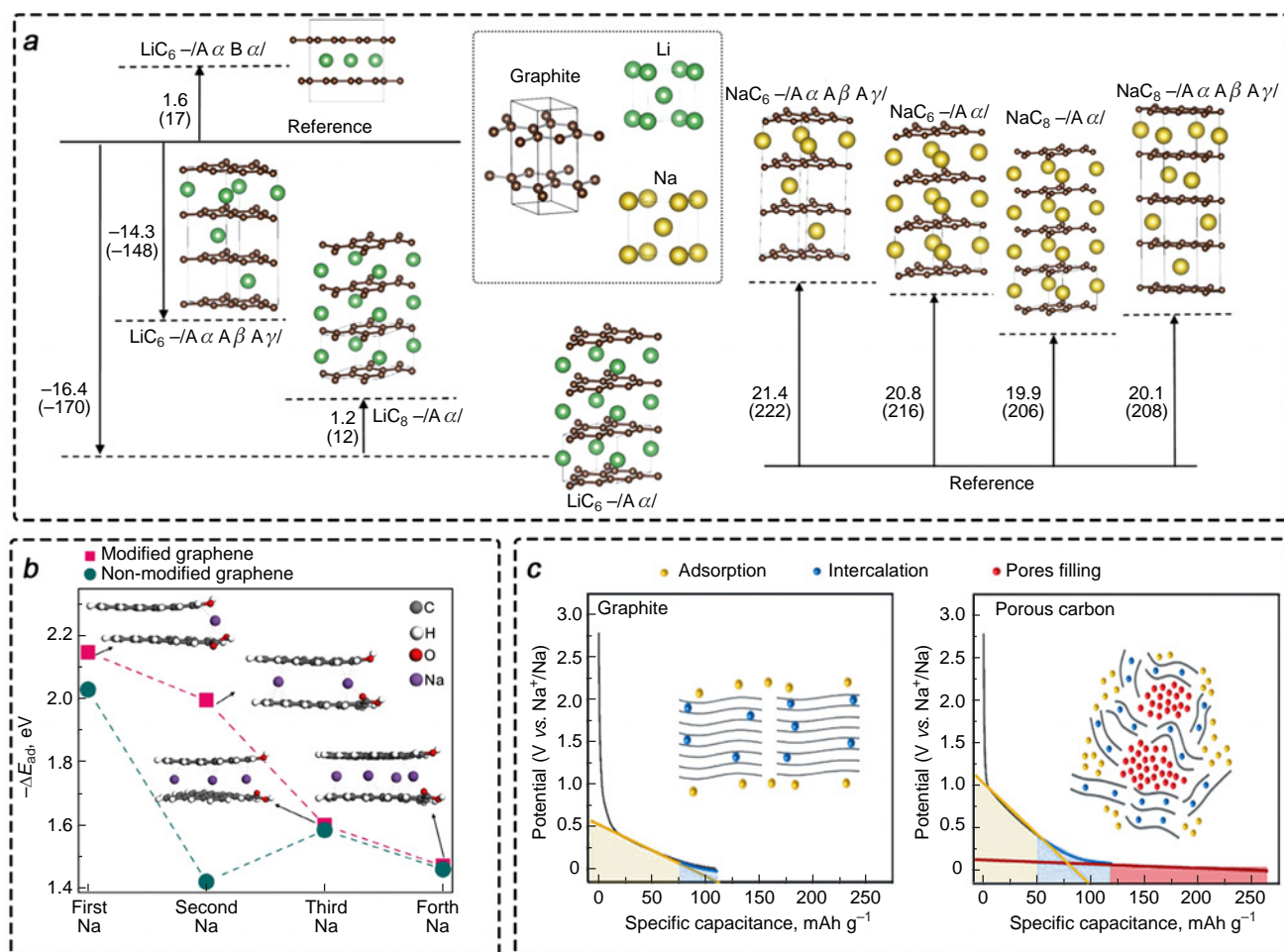
28 of 42

V.V.Pavlenko, A.Yu.Zakharov, Z.E.Ayaganov, Z.A.Mansurov
Russ. Chem. Rev., 2024, **93** (9) RCR5122

Figure 27. Enthalpies of formation of the MC_6 and MC_8 structures (M = Li, Na) relative to the reference state corresponding to graphite and the initial metal (compounds in the lowest position are most stable) (*a*); effect of introduction of functional groups (–OH and –COOH) on the adsorption energy (*b*); principles of sodium storage in graphite and porous carbon (*c*).[9, 265–267]

micropores provide sodium clusterization and increase the capacitance of the material (see Fig. 27), (3) functional groups and defects on the carbon surface serve as active sites for Na^+ adsorption, thus improving the electrochemical activity, which promotes surface-limited intercalation/deintercalation.[9, 272, 276] The most popular dopants are N, B, S, and P; nitrogen and boron are incorporated directly into graphene-like layers and generate defects and active sites on the surface, while sulfur and phosphorus are intercalated into the graphite-like structure and thus increase the interlayer spacings, which improves the Na^+ intercalation/deintercalation kinetics.[276–278] For effective utilization of closed pores to store Li, K, and Na and to maintain the productivity, it is necessary to select the optimal pore diameter and interlayer spacing. Zhou and co-workers[279–281] showed that the optimal pore diameters for the storage are 24.2 and 43.0 Å, and the optimal interlayer spacings are 3.9 and 3.7 Å for Li and K/Na, respectively.

Apart from being used as anodic materials in LIBs, SIBs, and PIBs, carbon materials can also serve as cathodes in lithium sulfur (Li–S) batteries for the storage of sulfur. The main goals of using carbon cathodes in such batteries are to suppress the migration of soluble lithium polysulfides and to provide good electrical conductivity. There are two major approaches in the development of these cathodes: storage of sulfur in the pores of a carbon material and sulfur copolymerization with other materials.[282] The former approach implies the physical retention of sulfur in the carbon porous structure to restrict the diffusion of lithium polysulfides. The second approach implies the design of a composite material in which sulfur is chemically bonded, which prevents its dissolution. In addition, the carbon material must retain its structure despite the volume expansion of sulfur during electrochemical reactions with lithium.[283] The principles of optimization and characterization of carbon structures for the use in lithium–sulfur batteries are addressed in recent reviews[284, 285] and are not considered here.

5.2.2. Supercapacitors

In EDLC, the surface area of the carbon material is in proportion with the specific capacitance of the capacitor;[286] in other words, the use of microporous carbons is expected to have a beneficial effect on the capacitance characteristics of devices. However, in practice, the use of these materials often leads to a decrease in the specific capacitance and power density due to decreasing packing density and increasing role of diffusion processes.[287] Actually, optimization of EDLC involves trade-off between the increase in the specific capacitance owing to greater contribution of the microporosity and the increase in the power density owing to the larger number of meso- and macropores, with the gain in one characteristics inevitably inducing a loss in the other one.

Supercapacitors with optimal characteristics are fabricated, most often, using carbon materials with a hierarchical pore size

V.V.Pavlenko, A.Yu.Zakharov, Z.E.Ayaganov, Z.A.Mansurov
Russ. Chem. Rev., 2024, **93** (9) RCR5122

29 of 42

distribution and the minimum diameter of micropores optimized to the size of particles present in the electrolyte, with meso- and macropores functioning as transport channels reducing diffusion resistance.[9, 11] The key challenges in the precise tuning of the structure is the need to take into account the solvation shells of electrolyte ions and the control of the chemical activation processes, which are used to prepare most carbon materials with a hierarchical pore size distribution. Pameté *et al.*[147] addressed this problem, first, by using ionic liquids as electrolytes (ionic liquids are devoid of solvation shells) and, second, by optimizing the porosity using template synthesis. For generation of hierarchical pore size distribution, the authors proposed to utilize mixtures of 'heavy' and 'light' carbons possessing internal microporosity for ion storage and external mesoporosity for the generation of channels that facilitate the diffusion.

One more way to avoid the necessity of considering solvation shells during the porosity optimization is to use solid electrolytes. The key problem involved in the design of devices with solid electrolytes is high resistance at the electrode–electrolyte interface. A variety of approaches are used to reduce the interfacial resistance: the insertion of an interlayer between the carbon material and the solid electrolyte,[288] *in situ* polymerization of the electrolyte,[289] impregnation of the porous carbon structure with a liquid electrolyte,[43] an so on. Béguin *et al.*[43] demonstrated that the introduction of the [EmIm+][FSI−] ionic liquid [EmIm+ is the 1-ethyl-3-methylimidazolium cation, FSI− is the bis(fluorosulfonyl)imide anion] into the carbon pores (D_{meso} = 3.4 nm) is accompanied by a gradual decrease in the enthalpy of first-order phase transitions. If the ratio of the volume of ionic liquid to the pore volume (V_{IL}/V_C) is lower than unity, *i.e.*, there is no excess of ionic liquid, the thermogram peak corresponding to melting disappears, which confirms strong interaction of adsorbed ions with pore walls (Fig. 28 *a–d*).

The pores are filled in the order from smaller to larger ones (Fig. 28 *e, f*), which simplifies the calculation of the ionic liquid volume needed to impregnate carbon.[43, 290] When the carbon material being impregnated has a larger diameter of mesopores (D_{meso} = 8.7 nm), the immobilized ionic liquid behaves in a different way: the observed crystallization/melting phase transitions are shifted towards lower temperatures compared to the values measured for the non-immobilized compound. The subsequent studies carried out by ^{1}H NMR spectroscopy suggested that these transitions correspond to two states of ions, which are either (i) located near the pore wall (interact with both pore wall and other molecules) or (ii) surrounded by other ions near the pore centre, thus forming the bulk state.[291] If a mesoporous carbon material is used, the mobility of all ionic species remains virtually constant until the bulk phase located at the centre of the mesopore is frozen. On further cooling, ions occurring in close contact with the pore wall retain their mobility even after the freezing transition has already taken place for the bulk molecules. Transition from one-component electrolyte (ionic liquid) to a binary mixture and then to ion gel leads to even more pronounced drop of the melting point (down to −100 °C).[292] In combination, the use of these systems in all-solid-state supercapacitors extends the temperature range of applicability of these devices. It is important to note that mesoporous carbons prove to be more favourable for low-temperature applications. It was shown in our study that microporous materials have better electrochemical performance under ambient conditions, while on going to low-temperature applications, both the specific capacitance and the energy density are higher for mesoporous materials.[269]

In the case of PsC, the surface composition of the carbon material is a more important optimization criterion. Doping with heteroatoms such as B, N, S, O, and P gives rise to various
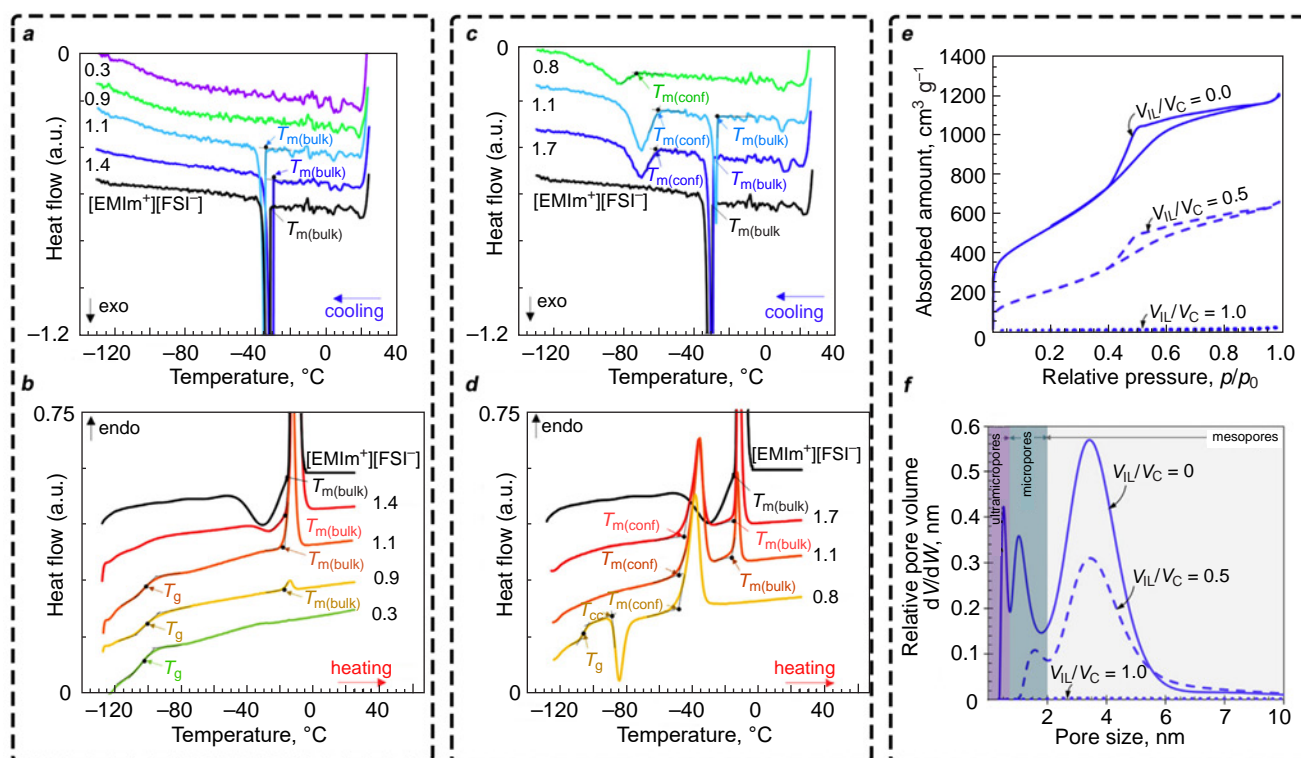
Figure 28. Differential scanning calorimetry curves of the carbon material produced using a self-template (D_{meso} = 3.4 nm) (*a, b*) and a hard template (D_{meso} = 8.7 nm) (*c, d*). Porosity characteristics of the initial (V_{IL}/V_C = 0) and [EmIm+][FSI−]-impregnated (V_{IL}/V_C = 0.5, 1.0) carbon material obtained using self-template (*e, f*). The [EmIm+][FSI−] impregnation was performed in bulk ratios (V_{IL}/V_C = 0.3, 0.9, 1.1, 1.4) and (V_{IL}/V_C = 0.8, 1.1, 1.7), respectively. V_{IL} is the ionic liquid volume, V_C is the total pore volume of the carbon material.[43]

30 of 42

V.V.Pavlenko, A.Yu.Zakharov, Z.E.Ayaganov, Z.A.Mansurov
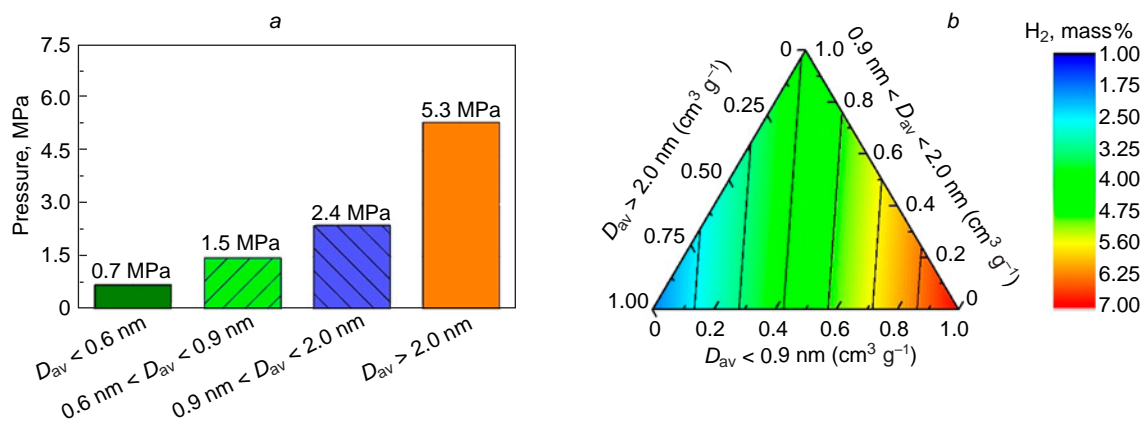*Russ. Chem. Rev.*, 2024, **93** (9) RCR5122

Figure 29. Pressure required to attain 95% of the maximum adsorption density for various pore diameters (*a*); and absolute H_2 uptake as a function of pore volume at 77 K and 4.0 MPa (*b*).[73] Published in accordance with the CC BY license.

active sites on the carbon surface, which most often leads to increasing capacitance of both EDLC and PsC and changes the hydrophilicity/hydrophobicity balance of the electrode material.[253] For example, the positively charged pyridine and pyrrole N atoms increase the electrical conductivity and facilitate the electron transport needed for PsC operation, while negatively charged pyridine and pyrrole N atoms function as active sites for pseudo-capacitive processes.[293] The use of fluorine as a dopant endows the electrode surface with hydrophobic properties, which has a beneficial effect on the characteristics of systems based on gel polymer and other non-polar electrolytes.[294] Co-doping with two or more atoms may produce a synergistic effect.

5.3. Hydrogen storage

Due to the large accessible surface area and small pore size, carbon materials are considered for the use in hydrogen storage systems. Bi *et al*.[295] performed a theoretical study of the hydrogen storage capacity of graphene with vertically arranged CNTs and fullerenes located between the sheets. The simulation was carried out for a temperature of 233 K and pressure of 100 bar. DFT calculations predicted a hydrogen gravimetric density of 12.92 mass% for volumetric uptake of 96.4 g L^{-1}. Monte Carlo simulations gave lower values (7.2 mass% and 53.8 g L^{-1}).[295] The gravimetric storage capacity values actually achieved to date rarely exceed 7 mass%.[296] The design of three-dimensional systems with interlayer spacings of about 0.7 nm optimal for the physical sorption of H_2 is required for practical applications.[297] Currently, this problem is mainly addressed using two approaches: fabrication of disordered porous frameworks and insertion of molecular columnar spacers between graphene sheets.[296] In both cases, graphene flakes or reduced graphene oxide (RGO) are used as precursors. Unlike graphene, RGO contains residual oxygen and other heteroatoms as well as structural defects. RGO is obtained from graphene oxide by ultrasonic, chemical, or thermal reduction. Klechikov *et al*.[298] used a three-dimensional structure with hierarchical pore size distribution formed from chemically activated defective RGO flakes as a material for hydrogen storage. The specific surface area and pore volume of the obtained material were 3200–3400 m² g^{-1} and 2.2 cm³ g^{-1}, respectively. The storage capacity was 7.04 mass% at 77 K and a pressure of 4 MPa; as the temperature increased to 296 K and the pressure increased to 12 MPa, while the storage capacity decreased to 1.13 mass%.[298]

The storage capacity of porous carbons, as well as graphene-like structures depends, first of all, on the accessible surface area, the size of micropores, surface chemistry, and pore size distribution.[299] The optimal pore diameter that makes it possible to use the minimum pressure for hydrogen storage (approximately 0.7 MPa at 77 K) is 0.6 nm (Fig. 29).[73] Carbons with so small pores can be obtained by means of chemical activation with KOH, which may produce carbon materials with pores of 0.5–0.7 nm in diameter.[135] Meanwhile, since the chemical etching furnishes structures with a hierarchical size distribution of pores, the actual hydrogen storage pressure is higher (about 3 MPa at 77 K), and not only micro- but also mesopores are filled. On the one hand, carbon surface functionalization with oxygen-containing groups improves hydrogen retention on the surface, but, on the other hand, the insertion of functional groups into micropores generates steric hindrance, which requires the use of carbon materials with large pore diameters for functionalization.[300]

5.4. Capture of CO_2

Carbon dioxide capture can be performed before or after combustion of hydrocarbon fuel: in the former case, CO_2 is separated from N_2, while in the latter case, either CO_2 and H_2 are separated in the synthesis gas, or CO_2 and CH_4 are separated in natural gas purification processes.[301] A standard method of CO_2 capture is absorption by aqueous solutions of amines; however, the process is complicated by amine toxicity and necessary regeneration, which is associated with additional expenditures.[302] As an alternative, various zeolite-based porous materials,[303] MOFs,[304] carbon materials,[16, 237] *etc*. are considered (Fig. 30).

Carbon dioxide capture before combustion occurs at elevated pressures of up to 20 bar. According to theoretical calculations, the most appropriate adsorbents are porous structures with a hierarchical distribution of meso- and micropores from 4 nm to less than 1 nm, which is confirmed by experimental data.[306] Currently the use of carbon molecular sieves provides high CO_2/N_2 (42 : 1) and CO_2/CH_4 (180 : 1) selectivities.[307]

When CO_2 is separated after fuel combustion, the selectivity of CO_2 capture in the presence of other products (such as N_2, H_2, H_2O, CH_4, and other) becomes the key criterion determining the efficiency. The most appropriate type of porosity in this case is microporosity with pore size less than 0.5 nm,[308] which promotes higher selectivity and specific storage capacity of the material. The closer the diameter to the size of CO_2 molecule
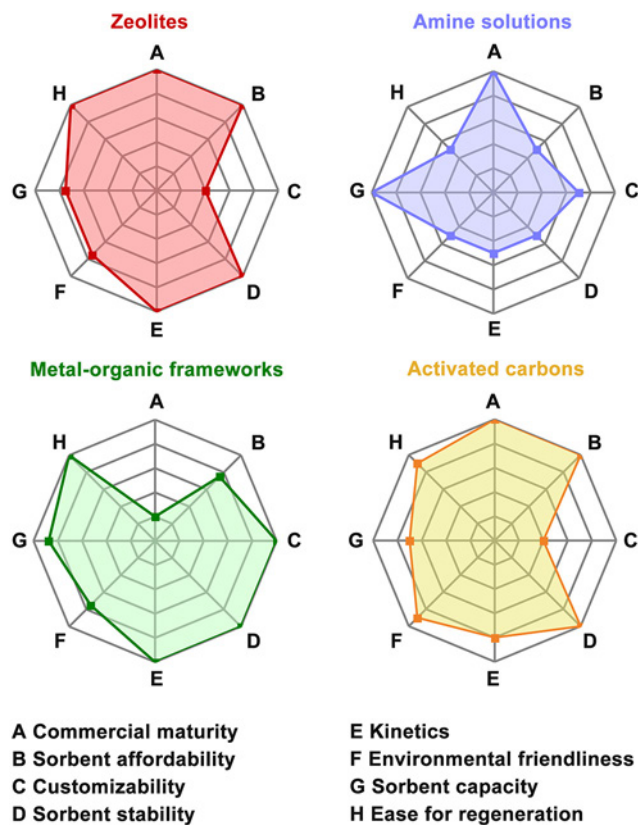
V.V.Pavlenko, A.Yu.Zakharov, Z.E.Ayaganov, Z.A.Mansurov
Russ. Chem. Rev., 2024, **93** (9) RCR5122

31 of 42

Figure 30. Radar charts of the key criteria for the selection of material for CO_2 capture.[305]

(0.33 nm), the higher the selectivity of the material, since N_2 and CH_4 are blocked due to greater diameter and lower diffusion ability.[309]

Since the CO_2 molecular is polar, unlike H_2, N_2, or CH_4, modification of carbon surface with charged functional groups (*e.g.*, $-SO_3H$ or $-NH_2$) or other active sites (N, S doping) is favourable for the selectivity of gas separation.[85] For example, carbon materials obtained by hydrothermal carbonization of glucose before functionalization had an adsorption capacity of about 0.4 mmol g^{-1}, whereas after the introduction of amine functional groups, the capacity became above 3 mmol g^{-1}.[310] It is of interest that the intermediate functionalization of porous carbon with carboxyl groups also increased the adsorption capacity towards CO_2, despite the acidity of these groups; a similar phenomenon was observed upon introduction of $-COOH$ groups into conjugated polymers[311] and MOFs.[312] In a theoretical study by Kumar *et al.*,[313] this phenomenon was attributed to interaction between the lone pair of oxygen of the carboxyl group and the CO_2 carbon atom and/or to hydrogen bonding between the $-COOH$ proton and the CO_2 oxygen. The sulfonic group $-SO_3H$ mainly retains CO_2 *via* hydrogen bonding between the acid proton of the functional group and oxygen of carbon dioxide. Although the interactions between $-SO_3H$ and CO_2 are weaker than those between $-NH_2$ and CO_2, sulfonic groups are, in some cases, more efficient than amine groups, because of free rotation around the $C-S$ bond, which makes it possible to maximize the intermolecular interactions.[314]

Typical dopants that increase the selectivity are N and S. Nitrogen doping endows the carbon surface with basic properties and retains CO_2 on the surface through Lewis acid–base interactions. In this case, the lone pair of nitrogen acts as the active site for the interaction with the electron-deficient carbon

atom of the CO_2 molecule. On the other hand, these sites may form hydrogen bonds with H_2O molecules, thus enhancing their adsorption on the surface; therefore, the use of nitrogen-doped carbon materials requires preliminary drying of flue gases. The introduction of large-size sulfur atom causes distortions of the carbon structure, and the S atom protrudes above the surface.[315] This position of the S atom and the presence of a lone pair of electrons and easily polarizable d-orbitals facilitate the interaction of the S atom with the oxygen atoms of CO_2.[316] Sulfur in thiophene structures can transfer electrons to the carbon dioxide molecule, which may result in oxidation of the surface group.[314] The effect of other functional groups and dopants on the selectivity of CO_2 adsorption is discussed in recent reviews.[134,314]

Apart from the CO_2 capture, porous carbon materials can also be used for the separation of other gases. For example, recently Du *et al.*[317] reported optimization of the porous structure for highly selective separation of n-propane and propene. They showed that the highest diffusion rate is achieved, without a decrease in the separation efficiency, when the pore size approaches the kinetic diameter of C_3H_8 (5.11 Å). As the pore size decreases to the kinetic diameter of C_3H_6, the separation efficiency is retained, but the diffusion rate decreases.

5.5. Catalysis

Carbon materials used in catalysis can be divided into two large classes: catalyst supports and materials possessing their own catalytic properties. In the development of materials of the former type, the attention is focused on tuning of the support structure towards attachment of atoms, aggregates, or nanoparticles of a catalyst (most often, metal) to the carbon surface. The commonly accepted concept implies that for successful deposition of the active component, the support must have definite sites:[318] heteroatoms that change the local electronic structure and surface defects or functional groups that hold the catalyst on the surface. Regarding the structure of the carbon material, the requirements are similar to those described above (Fig. 31): the presence of a structure with hierarchical pore size distribution, providing high density of catalytic sites in micropores and good diffusion in mesopores. When the goal is to obtain carbon materials that exhibit their own catalytic activity, the synthetic strategy should include the introduction of heteroatoms (mainly nitrogen). The main problem faced by the use of heteroatom-doped carbon materials for catalytic applications is degradation of the material caused by destruction or protonation of active sites in acid media.[84]

The main catalytic application of carbon materials is the oxygen reduction reaction, which is a key reaction in electrochemical energy storage and conversion devices, for example, fuel cells and metal air batteries.[86] The possibilities for immobilization of various enzymes on porous carbon materials and their further use as biocatalysts are also studied. Since enzymes are typically 4–20 nm in size, meso- and macro carbon materials are suitable for their immobilization.[319]

5.6. Sensors

The use of nanoporous materials as highly sensitive sensors for the detection of toxic gases,[320] heavy metals,[321] biomolecules,[322] and other species requires surface modification with functional groups, doping with heteroatoms, metals, or metal oxides.

In gas sensors, porous carbon materials act, first of all, as conducting electrodes and active site supports. Hence, the key
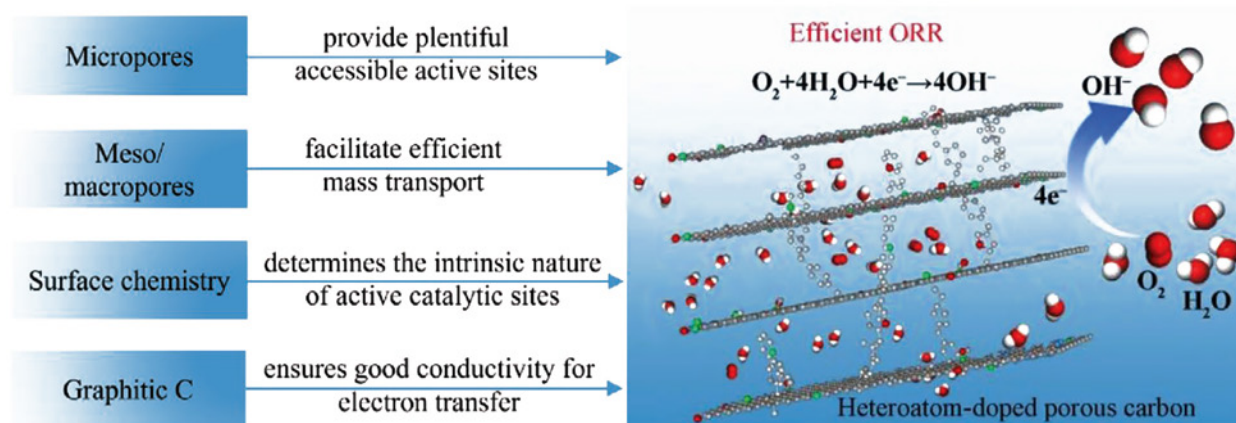
32 of 42

V.V.Pavlenko, A.Yu.Zakharov, Z.E.Ayaganov, Z.A.Mansurov
Russ. Chem. Rev., 2024, **93** (9) RCR5122

Figure 31. Relationship between the carbon structure and key characteristics influencing the catalytic efficiency in oxygen reduction reaction (ORR).[97] Copyright WILEY 2020.

requirements are electrical conductivity and the maximum surface area to provide better sensitivity. Na *et al*.[320] synthesized a porous carbon material with SSA = 1256.8 m^2 g^{-1} using a PAN and polystyrene mixture as a self-degrading soft template. Doping was performed with fluorine plasma; the resulting material contained a large number of fluorine atoms (p-type doping) and possessed pronounced hole conductivity (Fig. 32 *a*). The adsorption of ammonia is accompanied by a decrease in the effect of doping due to recombination of holes in the material with NH$_3$ electrons and disruption of electron density delocalization in the material; this altogether results in decreasing carbon conductivity (Fig. 32 *b*). A sensor based on the resulting material demonstrated high selectivity towards NH$_3$ in a mixture with water, acetone, toluene, hexane, or benzene with a linear detection range from 9 ppb to 90 ppm of NH$_3$.[320]

Heavy metals are usually detected by reverse differential pulse voltammetry. In general, sensors are fabricated by depositing a suspension of Nafion carbon material onto the prepolished surface of a glassy carbon electrode. The development of a sensor for Pb(II) based on nitrogen-doped porous carbon obtained by chemical activation of almond shells with KOH was reported by Baikeli *et al*.[323] The synthesis was carried out according to the classical two-stage procedure, and doping was performed by keeping the carbon material in a solution of urea in a Teflon reactor at 180 °C. The limit of detection for the sensor based on this material was 0.7 μg L^{-1}; the linear range was from 2.0 to 120.0 μg L^{-1}.[323] Gao *et al*.[321] reported a material based on N- and S-doped porous carbon nanofibres. The authors electrospun trithiocyanuric acid, silica nanospheres (hard template), and PAN, the resulting composite was subjected to carbonization and the hard template was etched with HF. The resulting material showed a high selectivity and sensitivity to Cd(II) ions, which could be detected in the range from 2.0 to 500 μg L^{-1}.[321]

A highly relevant task of biomolecule quantification is determination of glucose. This problem can be solved by catalytic oxidation of glucose with glucose oxidase enzyme, which is accompanied by the release of two electrons. The detection of oxidation by conductometry is a convenient and sensitive method for glucose determination; however, direct electron transfer to the analytical electrode is difficult due to the glycoprotein shell of the enzyme. A possible solution to the
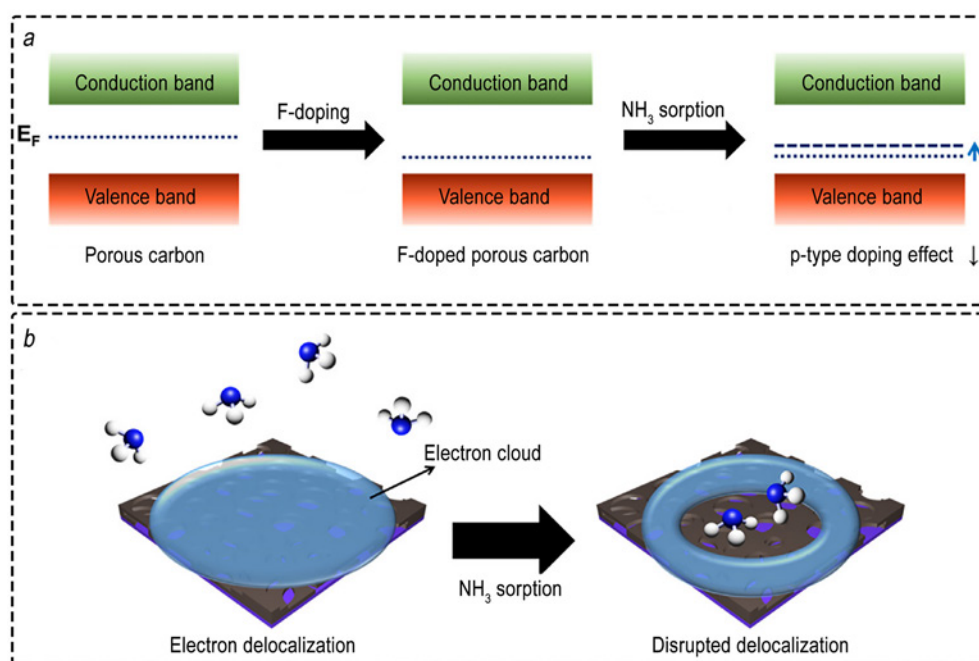

Figure 32. Schematic diagram of operation of a sensor based on a fluorine-doped porous carbon material (*a*) and disruption of the electron density delocalization in the material (*b*).[320] Copyright Elsevier 2020.

V.V.Pavlenko, A.Yu.Zakharov, Z.E.Ayaganov, Z.A.Mansurov
Russ. Chem. Rev., 2024, **93** (9) RCR5122

33 of 42

problem is enzyme immobilization in the pores of a conducting material. The design of such sensor based on porous carbon nanofibres from bacterial cellulose was reported by Liang *et al.*[324] The fine tuning of the porous structure by varying the annealing temperature allowed the authors to immobilize a considerable amount of glucose oxidase enzyme on the surface and to achieve a sensitivity of 123.3 µA mmol L^{-1} cm^{-2} and a limit of detection of 0.023 µmol L^{-1} in the range of $0.0002-0.10$ mmol L^{-1}. Chen *et al.*[322] demonstrated that the glucose sensor based on hollow graphene fibres with a porous 3D graphene coating and glucose oxidase immobilized in the pores makes it possible to measure glucose with a sensitivity of 148.02 µA mmol L^{-1} cm^{-2} in the range of $0.01-1$ mmol L^{-1}.

5.7. Microwave absorption

The microwave absorption technologies are important for both military purposes where they are used primarily to hide various objects from radar radiation (stealth technology) and civil sector in which these materials are used to shield electronic components, convert microwave radiation to thermal radiation, *etc*. An ideal absorbing material should meet two main criteria: first, the radiation should travel deep into the material as far as possible rather than be reflected from the surface, which requires a high degree of impedance matching, and, second, the radiation should be rapidly attenuated. The attenuation can be attained *via* dielectric and magnetic losses.[325] Quite a few materials can be used to absorb microwaves, including porous carbons. Li *et al.*[326] demonstrated that hollow carbon spheres have better characteristics than non-hollow ones. Apparently, this is due to the fact that in hollow spheres, the initial wave undergoes multiple scattering and/or polarization at the interface upon reflections within the sphere.[327]

Tao *et al.*[328] described a microwave absorption material based on spherical porous carbon nanoparticles obtained by the template method using a soft template made of a mixture of 3-aminophenol and formaldehyde. A 1.6-mm thick material had a considerable shielding effect: the minimum reflection loss was -18.3 dB; the 1.6 to 4 mm thick samples covered the C, X, and

Ku ranges. Chen *et al.*[329] demonstrated that filling of hollow porous carbon nanoparticles with gold and positioning of the nanoparticles on a carbon aerogel considerably improves characteristics of the material. The reflection losses for an optimized sample with a thickness from 1 to 5.0 mm virtually covered the C, X, and Ku ranges. The minimum reflection loss was -55.9 dB at a sample thickness of 1.8 mm; the maximum effective scattering area was -49 dB m^2 in the θ range from $-180°$ to $+180°$ (Fig. 33). The progress in the development of carbon aerogels for the absorption of microwaves is addressed in a number of recent reviews.[330–332]

Despite the considerable recent progress in the development of materials for the absorption of electromagnetic radiation, there are still unsolved challenges. First, although considerable progress in wave attenuation in the $2-18$ GHz range has been attained, the absorption bands are still rather narrow and seldom exceed $4-6$ GHz.[325] In addition, the development of radars that use metre and millimetre wavelengths requires the development of materials capable of attenuating this radiation. Second, the introduction of additional dopants (mainly metals) to enhance characteristics of carbon materials markedly increases the weight of the final composite, which is extremely important for the use of these materials, for example, in aircraft construction. Third, due to the high demand for materials that absorb radiation in the military-industrial complex, it is necessary to pay attention to the development of multifunctional materials stable under harsh weather conditions and possessing, for example, corrosion-protective, hydrophobic, and other properties.

5.8. Biomedicine

Porous carbon materials can be used for immobilization of proteins, vitamins, and enzymes in drug delivery systems.[333] In particular, magnetic composites made of mesoporous carbon with a bimodal pore size distribution showed great immobilization capacity for cytochrome C and lysozyme.[334] A broad range of ordered carbon materials were used to develop drug delivery systems.[335,336] For example, nanoparticles of the CMK-1 mesoporous carbon synthesized using the mesoporous MCM-48
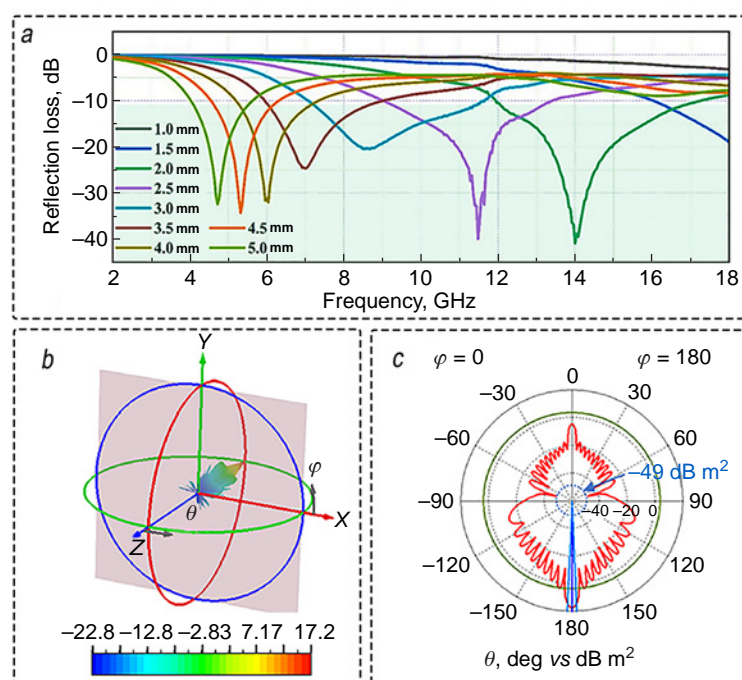

Figure 33. Characteristics of a microwave-shielding material: reflection loss for $1-5$ mm sample (*a*), simulation of the wave zone of a perfect conductor coated by a microwave-shielding material (wave propagation along the Z axis; θ is the detection angle) (*b*), bistatic effective scattering area diagram (*c*).[329] Copyright Elsevier 2022.

34 of 42

V.V.Pavlenko, A.Yu.Zakharov, Z.E.Ayaganov, Z.A.Mansurov
Russ. Chem. Rev., 2024, **93** (9) RCR5122

silica nanoparticles as a template can be used for the delivery of chemicals that cannot penetrate cell membranes to get into eukaryotic cells.[337]

Activated carbons are widely used as enterosorbents, but the lack of selectivity reduces the prospects of using porous carbon materials for this purpose.[338] However, it was shown that combined enterosorbents composed of porous carbons and palygorskite pretreated with copper ferrocyanide can selectively bind radionuclides and eliminate them from the body.[339] Carbon-based macroporous sorbents also showed promising results as a means to treat bacterial translocation in acute and chronic liver failure.[340,341] Carbon adsorbents can also be used to remove excess bilirubin at various liver diseases. The use of porous carbon nanotubes, porous graphenes, or hollow carbon spheres obtained using SBA-15 hard template provides adsorption of up to 649.5 mg g^{-1} of bilirubin.[342,343] In this case, the use of conventional activated carbons is impossible because the carbon fragments that split-off can induce the formation of clots.[338]

A promising application of carbon materials is nanopore sequencing. Currently, there are two main carbon materials potentially suitable for this application, graphene and CNTs.[344] Graphene is considered to be a more beneficial material for this application, as it can function as both a membrane and an electrode for DNA sequencing (Fig. 34$a-d$).[345] The use of bilayer graphenes further increases the resolution of the method (Fig. 34e,f).[346] Extensive possibilities for surface modification using defects, doping, and functionalization make it possible to precisely tune the relative positions of the DNA molecule and the nanopore.[347] Modern synthetic methods make it possible to fabricate CNTs with a diameter equal to the diameter of DNA molecule; however, the CNT heterogeneity along the length deteriorates the results of sequencing.[348]

Apart from the above-listed applications, SWCNTs can be used as fluorescent labels owing to their bioinertness and high radiation intensity in the range from 900 to 1600 nm,[349] which is close to the blood transparency window (900–1400 nm). Fluorescence intensity can be further enhanced by linking nanotubes to small organic dyes,[350] fluorescent proteins,[351] or quantum dots[352] *via* non-covalent interactions and Förster energy transfer. Upon surface modification with specific proteins, carboxyl groups, amino groups, *etc.*, SWCNTs can be considered as optical biosensors, which change the fluorescence maximum upon binding to particular biomolecules.[353]

6. Results and prospects of development

The synthesis of nanoporous carbon materials continues to be one of the most promising areas of materials science. The composition and porous structure play a key role in the development of catalysts and catalyst supports, promising materials for hydrogen storage, electrochemical sensors and electrode materials for SCs, batteries, CDI systems, and other modern applications. Template synthesis allows highly precise control of the porous structure geometry, which opens up broad opportunities for tailoring materials to particular applications. However, high cost of this method in comparison with conventional chemical activation methods is still a considerable limitation. The future studies aimed at the use of readily available organic salts as self-templates may reduce the cost and increase the competitiveness of template synthesis.

Functionalization of nanoporous carbon materials markedly improves their performance for catalytic and electrosorption applications. To attain the maximum efficiency, it is necessary to continue investigations of the diffusion properties, composition and structure of surface functional groups. Particular attention should be paid to the reactivity inside carbon pores, which can act as transport channels providing optimal conditions for chemical reactions.

In the field of energy storage systems, nanoporous carbon materials face a number of challenges such as low stored energy density and decrease in the efficiency at high current loads. Combination of the control of nanopore architecture with nanopore functionalization by redox-active groups can partially solve these problems, although it is accompanied by an increase in the prime cost of the products. Optimization and decrease in the cost of production technologies are the most important challenges for the practical application of these promising methods.

Study of the confinement effects in the nanopores on characteristics of encapsulated substances opens up new opportunities for the design of more efficient energy devices. For example, control of the pore diameter can substantially

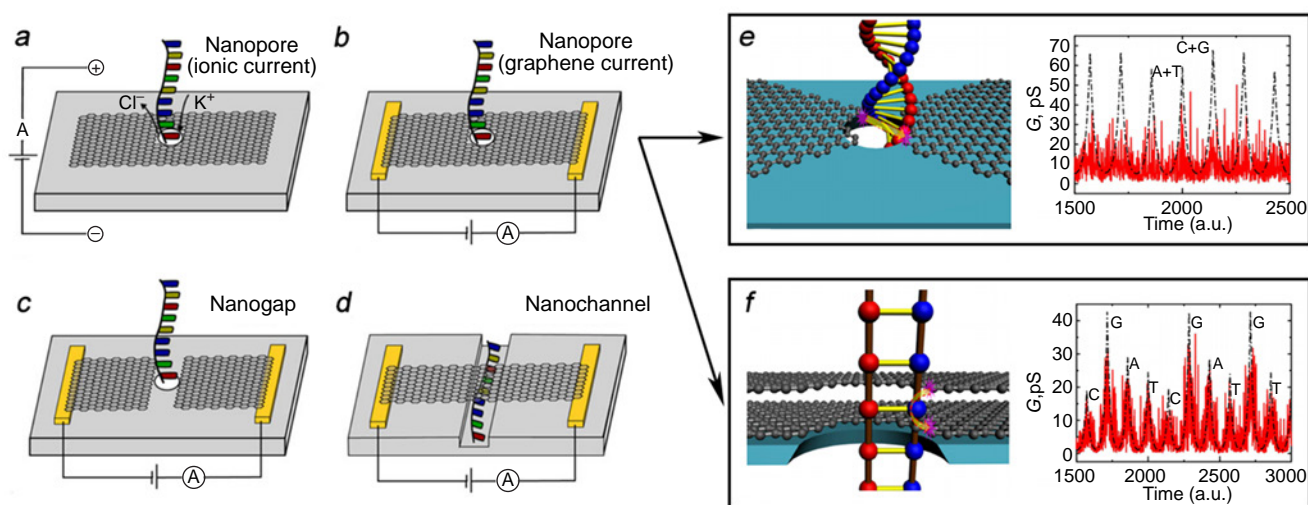

Figure 34. Schematic view of ionic current-based DNA sequencing using graphene nanopores (*a*) or DNA sequencing using the conductive properties of graphene (*b–d*): DNA translates through a nanopore in graphene (*b*), nanogap in graphene (*c*) or nanochannel (*d*). Differences in the signal resolution during sequencing graphene nanopores in one- (*e*) and bilayer (*f*) graphene.[345,346]

V.V.Pavlenko, A.Yu.Zakharov, Z.E.Ayaganov, Z.A.Mansurov
Russ. Chem. Rev., 2024, **93** (9) RCR5122

35 of 42

reduce the melting and crystallization points of imidazolium ionic liquids, making them more suitable for use as low-temperature electrolytes. Immobilization of redox species in carbon nanopores can also prevent adverse effects including ion migration and increase the energy density and service life of hybrid energy storage devices.

Nanoporous carbon materials have a huge potential for applications in various fields including environmentally clean energy production, medicine, and environmental protection. In particular, materials with unique porous structure can be used in carbon dioxide adsorption, which provides significant environmental benefits. In medicine, they may find applications as platforms for targeted drug delivery or for the fabrication of highly sensitive biosensors. The prospects for the development of these materials are also related to their use in new energy devices such as hybrid supercapacitors and sodium-ion batteries, where they can markedly improve efficiency and durability.

The current development of the synthesis and functionalization techniques would open up the way for the creation of carbon materials with unique characteristics, which would markedly expand the scope of their commercial applications. Thus, nanoporous carbon materials can become key elements in the elaboration of advanced technologies and can offer innovative solutions to the new challenges of our time.

Conflicts of interest

The authors declare that they have no conflicts of interest.

Author's contributions

V.V.Pavlenko — editing the draft, conceptualization of the work;

A.Yu.Zakharov — writing the draft;

Z.E.Ayaganov — writing the draft, drawing the Figures;

Z.A.Mansurov — conceptualization of the work, heading the research team.

7. List of abbreviations and symbols

BET — Brunauer – Emmett – Teller (theory),
CDI — capacitive deionization (of water),
CNTs — carbon nanotubes,
CV — cyclic voltammetry,
DFT — density functional theory,
EDL — electric double layer,
EDLC — electric double layer capacitor,
EDX — energy dispersive spectroscopy,
EELS — electron energy loss spectroscopy,
EIS — electrochemical impedance spectroscopy.
FDTS — perfluorodecyltrichlorosilane,
FTIR — Fourier transform infrared spectroscopy,
GCD — galvanostatic charge/discharge,

IUPAC — International Union of Pure and Applied Chemistry,
LIB — lithium-ion battery,
MOF — metal-organic framework,
NLDFT — non-local density functional theory,
ORR — oxygen reduction reaction,
PAN — polyacrylonitrile,
PIB — potassium-ion battery,
PMMA — poly(methyl methacrylate),
PsC — pseudocapacitor,
QSDFT — quenched solid density functional theory,
RGO — reduced graphene oxide,
SAXS — small-angle X-ray scattering,
SC — supercapacitor,
SEM — scanning electron microscopy,
SIB — sodium-ion battery,
SSA — specific surface area,
SWCNTs — single-walled carbon nanotubes,
TBAOH — tetrabutylammonium hydroxide,
TPAOH — tetrapropylammonium hydroxide,
TEM — transmission electron microscopy,
TEOS — tetrakis(2-hydroxyethyl)silane,
XRD — X-ray diffraction,
XPS — X-ray photoelectron spectroscopy,
ZIF — zeolitic imidazolate frameworks.

8. References

1. D.A.Giannakoudakis, T.J.Bandosz. *Detoxification of Chemical Warfare Agents*. (Cham, 2018)
2. L.-H.Zhang, Y.Shi, Y.Wang, N.R.Shiju. *Adv. Sci.*, **7**, 1902126 (2020); https://doi.org/10.1002/advs.201902126
3. E.Goikolea, R.Mysyk. In *Emerging Nanotechnologies in Rechargeable Energy Storage Systems*. (Eds L.M.Rodriguez-Martinez, N.Omar, L.M.Rodriguez-Martinez, N.Omar). (Boston, 2017). P. 131
4. J.H.Knox, K.K.Unger, H.Mueller. *J. Liquid Chromatogr.*, **6**, 1 (1983); https://doi.org/10.1080/01483918308067647
5. R.M.Barrer. *J. Chem. Soc.*, 2158 (1948); https://doi.org/10.1039/JR9480002158
6. M.E.Davis, C.Saldarriaga, C.Montes, J.Garces, C.Crowdert. *Nature*, **331**, 698 (1988); https://doi.org/10.1038/331698a0
7. T.Yanagisawa, T.Shimizu, K.Kuroda, C.Kato. *Bull. Chem. Soc. Jpn.*, **63**, 988 (1990); https://doi.org/10.1246/bcsj.63.988
8. C.T.Kresge, M.E.Leonowicz, W.J.Roth, J.C.Vartuli, J.S.Beck. *Nature*, **359**, 710 (1992); https://doi.org/10.1038/359710a0
9. E.N.Abramova, Z.V.Bobyleva, O.A.Drozhzhin, A.M.Abakumov, E.V.Antipov. *Russ. Chem. Rev.*, **93** (2), RCR5100 (2024); https://doi.org/10.59761/RCR5100
10. J.Yin, W.Zhang, N.A.Alhebshi, N.Salah, H.N.Alshareef. *Small Methods*, **4**, 1900853 (2020); https://doi.org/10.1002/smtd.201900853
11. Y.M.Volfkovich. *Russ. Chem. Rev.*, **91** (8), RCR5044 (2022); https://doi.org/10.1070/RCR5044
12. N.Yuan, A.Zhao, Z.Hu, K.Tan, J.Zhang. *Chemosphere*, **287**, 132227 (2022); https://doi.org/10.1016/j.chemosphere.2021.132227
13. Y.Li, N.Chen, Z.Li, H.Shao, L.Qu. *Dalton Trans.*, **49**, 5006 (2020); https://doi.org/10.1039/D0DT00684J
14. D.Dong, Y.Xiao. *Chem. Eng. J.*, **470**, 144441 (2023); https://doi.org/10.1016/j.cej.2023.144441
15. R.Vinodh, C.V.V.M.Gopi, V.G.R.Kummara, R.Atchudan, T.Ahmad, S.Sambasivam, M.Yi, I.M.Obaidat, H.-J.Kim. *J. Energy Storage*, **32**, 101831 (2020); https://doi.org/10.1016/j.est.2020.101831
16. G.Singh, K.S.Lakhi, S.Sil, S.V.Bhosale, I.Kim, K.Albahily, A.Vinu. *Carbon*, **148**, 164 (2019); https://doi.org/10.1016/j.carbon.2019.03.050

36 of 42

V.V.Pavlenko, A.Yu.Zakharov, Z.E.Ayaganov, Z.A.Mansurov
Russ. Chem. Rev., 2024, **93** (9) RCR5122

17. M.Sevilla, N.Díez, A.B.Fuertes. *ChemSusChem*, **14**, 94 (2021); https://doi.org/10.1002/cssc.202001838

18. Z.Heidarinejad, M.H.Dehghani, M.Heidari, G.Javedan, I.Ali, M.Sillanpää. *Environ. Chem. Lett.*, **18**, 393 (2020); https://doi.org/10.1007/s10311-019-00955-0

19. W.Zhang, R.-r.Cheng, H.-h.Bi, Y.-h.Lu, L.-b.Ma, X.-j.He. *New Carbon Mater.*, **36**, 69 (2021); https://doi.org/10.1016/S1872-5805(21)60005-7

20. N.Díez, M.Sevilla, A.B.Fuertes. *Carbon*, **178**, 451 (2021); https://doi.org/10.1016/j.carbon.2021.03.029

21. A.Bianco, H.-M.Cheng, T.Enoki, Y.Gogotsi, R.H.Hurt, N.Koratkar, T.Kyotani, M.Monthioux, C.R.Park, J.M.D.Tascon, J.Zhang. *Carbon*, **65**, 1 (2013); https://doi.org/10.1016/j.carbon.2013.08.038

22. Y.M.Manawi, Ihsanullah, A.Samara, T.Al-Ansari, M.A.Atieh. *Materials*, **11**, 822 (2018); https://doi.org/10.3390/ma11050822

23. R.B.Heimann, S.E.Evsvukov, Y.Koga. *Carbon*, **35**, 1654 (1997); https://doi.org/10.1016/S0008-6223(97)82794-7

24. R.E.Franklin, J.T.Randall. *Proc. R. Soc. Lond. A*, **209**, 196 (1951); https://doi.org/10.1098/rspa.1951.0197

25. H.F.Stoeckli, F.Kraehenbuehl. *Carbon*, **22**, 297 (1984); https://doi.org/10.1016/0008-6223(84)90174-X

26. P.J.F.Harris. *Int. Mater. Rev.*, **42**, 206 (1997); https://doi.org/10.1179/imr.1997.42.5.206

27. E.Härk, M.Ballauff. *C – J. Carbon Res.*, **6**, 82 (2020); https://doi.org/10.3390/c6040082

28. J.-G.Wang, H.Liu, X.Zhang, X.Li, X.Liu, F.Kang. *Small*, **14**, 1703950 (2018); https://doi.org/10.1002/smll.201703950

29. S.Pinjari, T.Bera, G.S.Kapur, E.Kjeang. *Int. J. Hydrogen Energy*, **48**, 1930 (2023); https://doi.org/10.1016/j.ijhydene.2022.10.080

30. M.Terrones, A.R.Botello-Méndez, J.Campos-Delgado, F.López-Urías, Y.I.Vega-Cantú, F.J.Rodríguez-Macías, A.L.Elías, E.Muñoz-Sandoval, A.G.Cano-Márquez, J.-C.Charlier, H.Terrones. *Nano Today*, **5**, 351 (2010); https://doi.org/10.1016/j.nantod.2010.06.010

31. M.Esser, R.Dronskowski. *Carbon*, **123**, 708 (2017); https://doi.org/10.1016/j.carbon.2017.08.010

32. E.A.Belenkov, V.A.Greshnyakov. *Phys. Solid State*, **55**, 1754 (2013); https://doi.org/10.1134/S1063783413080039

33. E.A.Belenkov, V.A.Greshnyakov, E.A.Belaya. *IOP Conf. Ser.: Mater. Sci. Eng.*, **447**, 012016 (2018); https://doi.org/10.1088/1757-899X/447/1/012016

34. M.Monthioux. *Carbon Trends*, **14**, 100325 (2024); https://doi.org/10.1016/j.cartre.2024.100325

35. I.V.Eremin, T.M.Bronevets. *Marochnyi Sostav Uglei i ikh Ratsionalnoe Ispolzovznie: Spravochnik. (BrandCcomposition of Coals and their Rational Use: a Reference Book)*. (Moscow, 1994)

36. X.-L.Zhou, H.Zhang, L.-M.Shao, F.Lü, P.-J.He. *Waste Biomass Valor*, **12**, 1699 (2021); https://doi.org/10.1007/s12649-020-01109-y

37. W.Spencer, G.Senanayake, M.Altarawneh, D.Ibana, A.N.Nikoloski. *Minerals Eng.*, **212**, 108712 (2024); https://doi.org/10.1016/j.mineng.2024.108712

38. M.Härmas, R.Palm, T.Thomberg, R.Härmas, M.Koppel, M.Paalo, I.Tallo, T.Romann, A.Jänes, E.Lust. *J. Appl. Electrochem.*, **50**, 15 (2020); https://doi.org/10.1007/s10800-019-01364-5

39. S.Mopoung, N.Dejang. *Sci. Rep.*, **11**, 13948 (2021); https://doi.org/10.1038/s41598-021-93249-x

40. Y.Lin, H.Xu, Y.Gao, X.Zhang. *Biomass Conv. Bioref.*, **13**, 3785 (2023); https://doi.org/10.1007/s13399-021-01407-y

41. Z.-H.Yang, J.-P.Cao, Q.-Q.Zhuang, Y.Wu, Z.Zhou, Y.-L.Wei, X.-Y.Zhao. *Fuel Proc. Technol.*, **243**, 107665 (2023); https://doi.org/10.1016/j.fuproc.2023.107665

42. A.Wang, K.Sun, R.Xu, Y.Sun, J.Jiang. *J. Clean. Produc.*, **283**, 125385 (2021); https://doi.org/10.1016/j.jclepro.2020.125385

43. F.Béguin, V.Pavlenko, P.Przygocki, M.Pawlyta, P.Ratajczak. *Carbon*, **169**, 501 (2020); https://doi.org/10.1016/j.carbon.2020.07.071

44. J.Li, R.Xiao, M.Li, H.Zhang, S.Wu, C.Xia. *Fuel Proc. Technol.*, **192**, 239 (2019); https://doi.org/10.1016/j.fuproc.2019.04.037

45. H.Park, J.Bang, S.W.Han, R.K.Bera, K.Kim, R.Ryoo. *Micropor. Mesopor. Mater.*, **318**, 111038 (2021); https://doi.org/10.1016/j.micromeso.2021.111038

46. M.O.Loeh, F.Badaczewski, M.von der Lehr, R.Ellinghaus, S.Dobrotka, J.Metz, B.M.Smarsly. *Carbon*, **129**, 552 (2018); https://doi.org/10.1016/j.carbon.2017.12.044

47. L.Peng, C.-T.Hung, S.Wang, X.Zhang, X.Zhu, Z.Zhao, C.Wang, Y.Tang, W.Li, D.Zhao. *J. Am. Chem. Soc.*, **141**, 7073 (2019); https://doi.org/10.1021/jacs.9b02091

48. R.Suresh Babu, R.Vinodh, A.L.F.de Barros, L.M.Samyn, K.Prasanna, M.A.Maier, C.H.F.Alves, H.-J.Kim. *Chem. Eng. J.*, **366**, 390 (2019); https://doi.org/10.1016/j.cej.2019.02.108

49. T.Szatkowski, K.Kopczyński, M.Motylenko, H.Borrmann, B.Mania, M.Graś, G.Lota, V.V.Bazhenov, D.Rafaja, F.Roth, J.Weise, E.Langer, M.Wysokowski, S.Żółtowska-Aksamitowska, I.Petrenko, S.L.Molodtsov, J.Hubálková, C.G.Aneziris, Y.Joseph, A.L.Stelling, H.Ehrlich, T.Jesionowski. *Nano Res.*, **11**, 4199 (2018); https://doi.org/10.1007/s12274-018-2008-x

50. Y.Pan, K.Sun, S.Liu, X.Cao, K.Wu, W.-C.Cheong, Z.Chen, Y.Wang, Y.Li, Y.Liu, D.Wang, Q.Peng, C.Chen, Y.Li. *J. Am. Chem. Soc.*, **140**, 2610 (2018); https://doi.org/10.1021/jacs.7b12420

51. K.Jayaramulu, D.P.Dubal, B.Nagar, V.Ranc, O.Tomanec, M.Petr, K.K.R.Datta, R.Zboril, P.Gómez-Romero, R.A.Fischer. *Adv. Mater.*, **30**, 1705789 (2018); https://doi.org/10.1002/adma.201705789

52. B.Qiu, M.Xing, J.Zhang. *Chem. Soc. Rev.*, **47**, 2165 (2018); https://doi.org/10.1039/C7CS00904F

53. L.Sarkisov. *Adv. Mater.*, **24**, 3130 (2012); https://doi.org/10.1002/adma.201104708

54. P.-Y.Yang, S.-P.Ju, S.-M.Huang. *Computat. Mater. Sci.*, **143**, 43 (2018); https://doi.org/10.1016/j.commatsci.2017.10.051

55. M.Cox, R.Mokaya. *Sustain. Energy Fuels*, **1**, 1414 (2017); https://doi.org/10.1039/C7SE00300E

56. N.Albeladi, L.Scott Blankenship, R.Mokaya. *Energy Environ. Sci.*, **17**, 3060 (2024); https://doi.org/10.1039/D3EE03957A

57. A.S.Ahmed, M.Alsultan, A.A.Sabah, G.F.Swiegers. *J. Compos. Sci.*, **7**, 179 (2023); https://doi.org/10.3390/jcs7050179

58. E.D.Biase, L.Sarkisov. *Carbon*, **94**, 27 (2015); https://doi.org/10.1016/j.carbon.2015.06.056

59. E.D.Biase, L.Sarkisov. *Carbon*, **64**, 262 (2013); https://doi.org/10.1016/j.carbon.2013.07.061

60. S.Brunauer, L.S.Deming, W.E.Deming, E.Teller. *J. Am. Chem. Soc.*, **62**, 1723 (1940); https://doi.org/10.1021/ja01864a025

61. D.Dollimore, P.Spooner, A.Turner. *Surface Technol.*, **4**, 121 (1976); https://doi.org/10.1016/0376-4583(76)90024-8

62. R.Bardestani, G.S.Patience, S.Kaliaguine. *Canadian J. Chem. Eng.*, **97**, 2781 (2019); https://doi.org/10.1002/cjce.23632

63. S.J.Gregg, K.S.W.Sing. *Berichte Bunsen. Phys. Chem.*, **86**, 957 (1982); https://doi.org/10.1002/bbpc.19820861019

64. K.Kaneko, N.Setoyama, T.Suzuki. In *Characterization of Porous Solids III*. Vol. 87. (Eds J.Rouquerol, F.Rodríguez-Reinoso, K.S.W.Sing, K.K.Unger, J.Rouquerol, F.Rodríguez-Reinoso, K.S.W.Sing, K.K.Unger). (Elsevier, 1994). P. 593

65. K.S.W.Sing. *Pure Appl. Chem.*, **57**, 603 (1985); https://doi.org/10.1351/pac198557040603

66. K.V.Kumar, S.Gadipelli, B.Wood, K.A.Ramisetty, A.A.Stewart, C.A.Howard, D.J.L.Brett, F.Rodriguez-Reinoso. *J. Mater. Chem. A*, **7**, 10104 (2019); https://doi.org/10.1039/C9TA00287A

V.V.Pavlenko, A.Yu.Zakharov, Z.E.Ayaganov, Z.A.Mansurov
Russ. Chem. Rev., 2024, **93** (9) RCR5122

37 of 42

67. K.Chen, T.Zhang, X.Chen, Y.He, X.Liang. *Petrol. Expl. Devel.*, **45**, 412 (2018); https://doi.org/10.1016/S1876-3804(18)30046-6

68. Z.Wang, Y.Cheng, G.Wang, G.Ni, L.Wang. *Fuel*, **309**, 122120 (2022); https://doi.org/10.1016/j.fuel.2021.122120

69. C.Schlumberger, M.Thommes. *Adv. Mater. Interfaces*, **8**, 2002181 (2021); https://doi.org/10.1002/admi.202002181

70. K.Kaneko. *J. Membr. Sci.*, **96**, 59 (1994); https://doi.org/10.1016/0376-7388(94)00126-X

71. A.Gil, P.Grange. *Colloids Surf. A: Physicochem. Eng. Aspects*, **113**, 39 (1996); https://doi.org/10.1016/0927-7757(96)81455-5

72. G.Kupgan, T.P.Liyana-Arachchi, C.M.Colina. *Langmuir*, **33**, 11138 (2017); https://doi.org/10.1021/acs.langmuir.7b01961

73. G.Sdanghi, R.L.S.Canevesi, A.Celzard, M.Thommes, V.Fierro. *C – J. Carbon Res.*, **6**, 46 (2020); https://doi.org/10.3390/c6030046

74. G.Y.Gor, M.Thommes, K.A.Cychosz, A.V.Neimark. *Carbon*, **50**, 1583 (2012); https://doi.org/10.1016/j.carbon.2011.11.037

75. J.Jagiello, J.P.Olivier. *J. Phys. Chem. C*, **113**, 19382 (2009); https://doi.org/10.1021/jp9082147

76. W.M.Hess, C.R.Herd. In *Carbon Black*: *Science and Technology*. (Ed. J.-B.Donnet). (CRC Press, 1993). Ch. 3. P. 89

77. M.Arias, E.López, A.Nuñez, D.Rubinos, B.Soto, M.T.Barral, F.Díaz-Fierros. In *Effect of Mineral-Organic-Microorganism Interactions on Soil and Freshwater Environments*. (Eds J.Berthelin, P.M.Huang, J.M.Bollag, F.Andreux). (New York: Springer, 1999). P. 361

78. E.Santoso, R.Ediati, Y.Kusumawati, H.Bahruji, D.O.Sulistiono, D.Prasetyoko. *Mater. Today Chem.*, **16**, 100233 (2020); https://doi.org/10.1016/j.mtchem.2019.100233

79. P.Yao, J.Cen, M.Fang, T.Wang, Q.Wang. *RSC Adv.*, **8**, 17558 (2018); https://doi.org/10.1039/C7RA13344H

80. P.González-García. *Renew. Sustain. Energy Rev.*, **82**, 1393 (2018); https://doi.org/10.1016/j.rser.2017.04.117

81. A.Nikitin, Y.Gogotsi. *Encyclopedia Nanosci. Nanotechnol.*, **7**, 553 (2004)

82. J.M.Stratford, A.K.Kleppe, D.S.Keeble, P.A.Chater, S.S.Meysami, C.J.Wright, J.Barker, M.-M.Titirici, P.K.Allan, C.P.Grey. *J. Am. Chem. Soc.*, **143**, 14274 (2021); https://doi.org/10.1021/jacs.1c06058

83. V.Thapliyal, M.E.Alabdulkarim, D.R.Whelan, B.Mainali, J.L.Maxwell. *Diamond Relat. Mater.*, **127**, 109180 (2022); https://doi.org/10.1016/j.diamond.2022.109180

84. X.Li, G.Liu, H.Zheng, K.Sun, L.Wan, J.Cao, S.Asif, Y.Cao, W.Si, F.Wang, A.Bokhari. *Energies*, **16**, 128 (2023); https://doi.org/10.3390/en16010128

85. X.Ma, C.Su, B.Liu, Q.Wu, K.Zhou, Z.Zeng, L.Li. *Separat. Purificat. Technol.*, **259**, 118065 (2021); https://doi.org/10.1016/j.seppur.2020.118065

86. J.Quílez-Bermejo, E.Morallón, D.Cazorla-Amorós. *Carbon*, **165**, 434 (2020); https://doi.org/10.1016/j.carbon.2020.04.068

87. J.I.Goldstein, D.E.Newbury, J.R.Michael, N.W.M.Ritchie, J.H.J.Scott, D.C.Joy. *Scanning Electron Microscopy and X-Ray Microanalysis*. (NY: New York, 2018)

88. J.L.Figueiredo, M.F.R.Pereira. *Catal. Today*, **150**, 2 (2010); https://doi.org/10.1016/j.cattod.2009.04.010

89. V.Likodimos, T.A.Steriotis, S.K.Papageorgiou, G.E.Romanos, R.R.N.Marques, R.P.Rocha, J.L.Faria, M.F.R.Pereira, J.L.Figueiredo, A.M.T.Silva, P.Falaras. *Carbon*, **69**, 311 (2014); https://doi.org/10.1016/j.carbon.2013.12.030

90. Q.Wang, Z.Xie, Y.Liang, L.Li, B.Liu, X.Li, C.Liu, X.Wu, Q.Huang. *Ionics*, **25**, 2111 (2019); https://doi.org/10.1007/s11581-018-2647-7

91. B.H.Stuart. In *Infrared Spectroscopy: Fundamentals and Applications*. (Wiley, 2004). P. 45

92. C.Deepika, P.Anjani, D.Arti, S.Dipak. *IJRAR*, **6**, 286 (2019);

93. E.Avramiotis, Z.Frontistis, I.D.Manariotis, J.Vakros, D.Mantzavinos. *Catalysts*, **11**, 850 (2021); https://doi.org/10.3390/catal11070850

94. E.Yagmur, Y.Gokce, S.Tekin, N.I.Semerci, Z.Aktas. *Fuel*, **267**, 117232 (2020); https://doi.org/10.1016/j.fuel.2020.117232

95. H.Nishihara, T.Kyotani. *Adv. Mater.*, **24**, 4473 (2012); https://doi.org/10.1002/adma.201201715

96. S.Zhang, N.Pan. *Adv. Energy Mater.*, **5**, 1401401 (2015); https://doi.org/10.1002/aenm.201401401

97. W.Tian, H.Zhang, X.Duan, H.Sun, G.Shao, S.Wang. *Adv. Function. Mater.*, **30**, 1909265 (2020); https://doi.org/10.1002/adfm.201909265

98. E.Leng, Y.Guo, J.Chen, S.Liu, J.E, Y.Xue. *Fuel*, **309**, 122102 (2022); https://doi.org/10.1016/j.fuel.2021.122102

99. J.Zhao, W.Xiuwen, J.Hu, Q.Liu, D.Shen, R.Xiao. *Polym. Degrad. Stab.*, **108**, 133 (2014); https://doi.org/10.1016/j.polymdegradstab.2014.06.006

100. L.Wang, J.Li, Y.Chen, H.Yang, J.Shao, X.Zhang, H.Yu, H.Chen. *Fuel*, **251**, 496 (2019); https://doi.org/10.1016/j.fuel.2019.04.061

101. J.Yu, D.Wang, L.Sun. *Fuel*, **290**, 120078 (2021); https://doi.org/10.1016/j.fuel.2020.120078

102. H.Tounsadi, A.Khalidi, M.Farnane, M.Abdennouri, N.Barka. *Process Safety Environ. Protect.*, **102**, 710 (2016); https://doi.org/10.1016/j.psep.2016.05.017

103. K.Y.Foo, B.H.Hameed. *Bioresource Technol.*, **116**, 522 (2012); https://doi.org/10.1016/j.biortech.2012.03.123

104. H.Marsh, F.Rodríguez-Reinoso. In *Activated Carbon*. (Eds H.Marsh, F.Rodríguez-Reinoso, H.Marsh, F.Rodríguez-Reinoso). (Oxford, 2006). P. 243

105. F.Salvador, M.J.Sánchez-Montero, C.Izquierdo. *J. Phys. Chem. C*, **111**, 14011 (2007); https://doi.org/10.1021/jp073723e

106. F.Rodríguez-Reinoso, M.Molina-Sabio, M.T.González. *Carbon*, **33**, 15 (1995); https://doi.org/10.1016/0008-6223(94)00100-E

107. d.A.M.Yuso, B.Rubio, M.T.Izquierdo. *Fuel Proc. Technol.*, **119**, 74 (2014); https://doi.org/10.1016/j.fuproc.2013.10.024

108. J.Pallarés, A.González-Cencerrado, I.Arauzo. *Biomass Bioenergy*, **115**, 64 (2018); https://doi.org/10.1016/j.biombioe.2018.04.015

109. Z.Li, D.Guo, Y.Liu, H.Wang, L.Wang. *Chem. Eng. J.*, **397**, 125418 (2020); https://doi.org/10.1016/j.cej.2020.125418

110. N.J.Foley, K.M.Thomas, P.L.Forshaw, D.Stanton, P.R.Norman. *Langmuir*, **13**, 2083 (1997); https://doi.org/10.1021/la960339s

111. T.Wigmans. *Carbon*, **27**, 13 (1989); https://doi.org/10.1016/0008-6223(89)90152-8

112. M.A.Yahya, Z.Al-Qodah, C.W.Z.Ngah. *Renew. Sustain. Energy Rev.*, **46**, 218 (2015); https://doi.org/10.1016/j.rser.2015.02.051

113. M.Dwiyaniti, A.G.E.Barruna, R.M.Naufal, I.Subiyanto, R.Setiabudy, C.Hudaya. *IOP Conf. Ser.: Mater. Sci. Eng.*, **909**, 012018 (2020); https://doi.org/10.1088/1757-899X/909/1/012018

114. A.Bhatnagar, W.Hogland, M.Marques, M.Sillanpää. *Chem. Eng. J.*, **219**, 499 (2013); https://doi.org/10.1016/j.cej.2012.12.038

115. V.V.Pavlenko, Q.Abbas, P.Przygocki, T.Kon'kova, Z.Supiyeva, N.Abeykoon, N.Prikhodko, M.Bijsenbayev, A.P.Kurbatov, Z.A.Mansurov. *Eurasian Chem. Technol. J.*, **20**, 99 (2018); https://doi.org/10.18321/ectj695

116. S.M.Yakout, G.Sharaf El-Deen. *Arabian J. Chem.*, **9**, S1155 (2016); https://doi.org/10.1016/j.arabjc.2011.12.002

117. Y.Gao, Q.Yue, B.Gao, A.Li. *Sci. Total Environ.*, **746**, 141094 (2020); https://doi.org/10.1016/j.scitotenv.2020.141094

118. A.Gundogdu, C.Duran, H.B.Senturk, M.Soylak, M.Imamoglu, Y.Onal. *J. Anal. App. Pyrolysis*, **104**, 249 (2013); https://doi.org/10.1016/j.jaap.2013.07.008

119. B.Li, J.Hu, H.Xiong, Y.Xiao. *ACS Omega*, **5**, 9398 (2020); https://doi.org/10.1021/acsomega.0c00461

38 of 42

V.V.Pavlenko, A.Yu.Zakharov, Z.E.Ayaganov, Z.A.Mansurov
Russ. Chem. Rev., 2024, **93** (9) RCR5122

120. X.He, P.Ling, J.Qiu, M.Yu, X.Zhang, C.Yu, M.Zheng.
J. Power Sources, **240**, 109 (2013);
https://doi.org/10.1016/j.jpowsour.2013.03.174

121. D.Angin. *Fuel*, **115**, 804 (2014);
https://doi.org/10.1016/j.fuel.2013.04.060

122. F.-C.Wu, P.-H.Wu, R.-L.Tseng, R.-S.Juang. *J. Environ.
Management*, **91**, 1097 (2010);
https://doi.org/10.1016/j.jenvman.2009.12.011

123. G.E.Harimisa, N.W.C.Jusoh, L.S.Tan, K.Shameli, N.A.Ghafar,
A.Masudi. *J. Phys.: Conf. Ser.*, **2259**, 012009 (2022);
https://doi.org/10.1088/1742-6596/2259/1/012009

124. Z.Xu, Y.Zhou, Z.Sun, D.Zhang, Y.Huang, S.Gu, W.Chen.
Chemosphere, **241**, 125120 (2020);
https://doi.org/10.1016/j.chemosphere.2019.125120

125. Z.Xu, Z.Sun, Y.Zhou, W.Chen, T.Zhang, Y.Huang, D.Zhang.
Colloids Surf. A: Physicochem. Eng. Asp., **582**, 123934 (2019);
https://doi.org/10.1016/j.colsurfa.2019.123934

126. X.Gong, Z.Guo, Z.Wang. *Energy Fuels*, **23**, 4547 (2009);
https://doi.org/10.1021/ef900550w

127. L.Wang, F.Sun, J.Gao, X.Pi, T.Pei, Z.Qie, G.Zhao, Y.Qin.
J. Taiwan Inst. Chem. Eng., **91**, 588 (2018);
https://doi.org/10.1016/j.jtice.2018.06.014

128. Y.Sun, Q.Yue, Y.Mao, B.Gao, Y.Gao, L.Huang. *J. Hazard.
Mater.*, **265**, 191 (2014);
https://doi.org/10.1016/j.jhazmat.2013.11.057

129. Q.Yuan, Z.Ma, J.Chen, Z.Huang, Z.Fang, P.Zhang, Z.Lin,
J.Cui. *Polymers*, **12**, 1982 (2020);
https://doi.org/10.3390/polym12091982

130. L.Wang, F.Sun, F.Hao, Z.Qu, J.Gao, M.Liu, K.Wang, G.Zhao,
Y.Qin. *Chem. Eng. J.*, **383**, 123205 (2020);
https://doi.org/10.1016/j.cej.2019.123205

131. Y.Li, J.Mei, L.Wu, Q.Xu, Z.Li. *Int. J. Hydrogen Energy*, **49**,
67 (2024); https://doi.org/10.1016/j.ijhydene.2023.10.319

132. S.Yorgun, D.Yıldız, Y.E.Şimşek. *Energy Sources, Part A:
Recovery, Utilization, Environ. Effects*, **38**, 2035 (2016);
https://doi.org/10.1080/15567036.2015.1030477

133. X.Yang, Y.Wan, Y.Zheng, F.He, Z.Yu, J.Huang, H.Wang,
Y.S.Ok, Y.Jiang, B.Gao. *Chem. Eng. J.*, **366**, 608 (2019);
https://doi.org/10.1016/j.cej.2019.02.119

134. Y.M.Volfkovich. *Russ. Chem. Rev.*, **92** (6), RCR5080 (2023);
https://doi.org/10.59761/RCR5080

135. A.P.Silva, A.Argondizo, P.T.Juchen, L.A.M.Ruotolo.
Separation Purification Technol., **271**, 118872 (2021);
https://doi.org/10.1016/j.seppur.2021.118872

136. N.Boulanger, A.V.Talyzin, S.Xiong, M.Hultberg, A.Grimm.
Colloids Surf. A: Physicochem. Eng. Aspects, **680**, 132684
(2024); https://doi.org/10.1016/j.colsurfa.2023.132684

137. Y.Liu, P.Liu, L.Li, S.Wang, Z.Pan, C.Song, T.Wang.
J. Electroanal. Chem., **903**, 115828 (2021);
https://doi.org/10.1016/j.jelechem.2021.115828

138. V.Yang, R.A.Senthil, J.Pan, A.Khan, S.Osman, L.Wang,
W.Jiang, Y.Sun. *J. Electroanal. Chem.*, **855**, 113616 (2019);
https://doi.org/10.1016/j.jelechem.2019.113616

139. Q.Sun, T.Jiang, J.Shi, G.Zhao. *Int. J. Electrochem. Sci.*, **14**, 1
(2019); https://doi.org/10.20964/2019.01.50

140. L.Wan, J.Hu, J.Liu, M.Xie, Y.Zhang, J.Chen, C.Du, Z.Tian.
J. Alloys Compd., **859**, 158390 (2021);
https://doi.org/10.1016/j.jallcom.2020.158390

141. Y.Gao, R.Sun, A.Li, G.Ji. *J. Electroanal. Chem.*, **882**, 114986
(2021); https://doi.org/10.1016/j.jelechem.2021.114986

142. L.Qin, Z.Hou, S.Lu, S.Liu, Z.Liu, E.Jiang. *Int. J. Electrochem.
Sci.*, **14**, 8907 (2019); https://doi.org/10.20964/2019.09.20

143. Y.Gao, Y.Tang, W.Liu, L.Liu, X.Zeng. *Int. J. Energy Res.*, **44**,
10946 (2020); https://doi.org/10.1002/er.5672

144. D.A.Khuong, H.N.Nguyen, T.Tsubota. *Biomass Bioenergy*,
148, 106039 (2021);
https://doi.org/10.1016/j.biombioe.2021.106039

145. C.Jiang, G.A.Yakaboylu, T.Yumak, J.W.Zondlo,
E.M.Sabolsky, J.Wang. *Renew. Energy*, **155**, 38 (2020);
https://doi.org/10.1016/j.renene.2020.03.111

146. E.A.Arkhipova, R.Y.Novotortsev, A.S.Ivanov, K.I.Maslakov,
S.V.Savilov. *J. Energy Storage*, **55**, 105699 (2022);
https://doi.org/10.1016/j.est.2022.105699

147. E.Pameté, B.Gorska, V.Pavlenko, F.Beguin. *Electrochim. Acta*,
350, 136416 (2020);
https://doi.org/10.1016/j.electacta.2020.136416

148. A.Kamiyama, K.Kubota, D.Igarashi, Y.Youn, Y.Tateyama,
H.Ando, K.Gotoh, S.Komaba. *Angew. Chem., Int. Ed.*, **60**,
5114 (2021); https://doi.org/10.1002/anie.202013951

149. Y.Guo, W.Liu, R.Wu, L.Sun, Y.Zhang, Y.Cui, S.Liu, H.Wang,
B.Shan. *ACS Appl. Mater. Interfaces*, **10**, 38376 (2018);
https://doi.org/10.1021/acsami.8b14304

150. K.Ramakrishnan, C.Nithya, R.Karvembu. *ACS Appl. Energy
Mater.*, **1**, 841 (2018); https://doi.org/10.1021/acsaem.7b00284

151. Y.Zhan, J.Bai, F.Guo, H.Zhou, R.Shu, Y.Yu, L.Qian. *J. Alloys
Compd.*, **885**, 161014 (2021);
https://doi.org/10.1016/j.jallcom.2021.161014

152. S.S.Gunasekaran, S.K.Elumalali, T.K.Kumaresan,
R.Meganathan, A.Ashok, V.Pawar, K.Vediappan,
G.Ramasamy, S.Z.Karazhanov, K.Raman, R.Subashchandra
Bose. *Mater. Lett.*, **218**, 165 (2018);
https://doi.org/10.1016/j.matlet.2018.01.172

153. Z.Supiyeva, K.Avchukir, V.Pavlenko, M.Yeleuov,
A.Taurbekov, G.Smagulova, Z.Mansurov. *Mater. Today:
Proceedings*, **25**, 33 (2020);
https://doi.org/10.1016/j.matpr.2019.11.013

154. G.Gou, F.Huang, M.Jiang, J.Li, Z.Zhou. *Renew. Energy*, **149**,
208 (2020); https://doi.org/10.1016/j.renene.2019.11.150

155. S.A.Bhat, V.Kumar, S.Kumar, A.E.Atabani, I.Anjum
Badruddin, K.-J.Chae. *Fuel*, **337**, 127125 (2023);
https://doi.org/10.1016/j.fuel.2022.127125

156. J.Niu, M.Liu, F.Xu, Z.Zhang, M.Dou, F.Wang. *Carbon*, **140**,
664 (2018); https://doi.org/10.1016/j.carbon.2018.08.036

157. X.Liu, W.Xu, D.Zheng, Z.Li, Y.Zeng, X.Lu. *J. Mater.
Chem. A*, **8**, 17938 (2020);
https://doi.org/10.1039/D0TA03463K

158. M.Eyvaz, E.Yüksel. *Desalination and Water Treatment*.
(London: IntechOpen, 2018)

159. Y.-J.Gu, W.Wen, J.-M.Wu. *J. Mater. Chem. A*, **6**, 21078
(2018); https://doi.org/10.1039/C8TA07561A

160. H.-f.Xia, B.Zhang, C.-h.Wang, L.Cao, B.Luo, X.-m.Fan,
J.-f.Zhang, X.Ou. *Carbon*, **162**, 136 (2020);
https://doi.org/10.1016/j.carbon.2020.02.033

161. Y.Han, Y.Lu, S.Shen, Y.Zhong, S.Liu, X.Xia, Y.Tong, X.Lu.
Adv. Functional Mater., **29**, 1806329 (2019);
https://doi.org/10.1002/adfm.201806329

162. N.R.Chodankar, S.-H.Ji, D.-H.Kim. *J. Electrochem. Soc.*, **165**,
A2446 (2018); https://doi.org/10.1149/2.0181811jes

163. J.Klein, F.Pfeifer, S.Schacht, C.Sinder. *Fuel Proc. Technol.*,
52, 17 (1997);
https://doi.org/10.1016/S0378-3820(97)00012-X

164. M.Bora, D.Bhattacharjya, B.K.Saikia. *Energy Fuels*, **35**, 18285
(2021); https://doi.org/10.1021/acs.energyfuels.1c02518

165. V.Shukla, D.Panchal, O.Prakash, P.Mondal, I.Hiwrale,
R.S.Dhodapkar, S.Pal. *Bioresource Technol.*, **369**, 128399
(2023); https://doi.org/10.1016/j.biortech.2022.128399

166. V.M.Zaichenko, M.I.Knyazeva, A.Yu.Krylova, K.O.Krysina,
A.B.Kulikov. *Solid Fuel Chem.*, **53**, 159 (2019);
https://doi.org/10.3103/S036152191903011X

167. X.Lv, T.Zhang, Y.Luo, Y.Zhang, Y.Wang, G.Zhang. *J. Analyt.
Appl. Pyrolysis*, **146**, 104717 (2020);
https://doi.org/10.1016/j.jaap.2019.104717

168. Z.-r.Zhang, S.-h.Luo, J.-c.Wang, M.-y.Sun, S.-x.Yan, Q.Wang,
Y.-h.Zhang, X.Liu, X.-f.Lei. *J. Energy Storage*, **56**, 105913
(2022); https://doi.org/10.1016/j.est.2022.105913

169. O.Boujibar, F.Ghamouss, A.Ghosh, O.Achak, T.Chafik.
J. Power Sources, **436**, 226882 (2019);
https://doi.org/10.1016/j.jpowsour.2019.226882

170. Y.Shen, Y.Hu, M.Wang, W.Bao, L.Chang, K.Xie. *Chin. J.
Chem. Eng.*, **35**, 70 (2021);
https://doi.org/10.1016/j.cjche.2021.04.007

V.V.Pavlenko, A.Yu.Zakharov, Z.E.Ayaganov, Z.A.Mansurov
Russ. Chem. Rev., 2024, **93** (9) RCR5122

39 of 42

171. S.Yaglikci, Y.Gokce, E.Yagmur, A.Banford, Z.Aktas. *Surfaces Interfaces*, **22**, 100899 (2021); https://doi.org/10.1016/j.surfin.2020.100899

172. H.Li, X.He, T.Wu, B.Jin, L.Yang, J.Qiu. *Fuel Proc. Technol.*, **230**, 107203 (2022); https://doi.org/10.1016/j.fuproc.2022.107203

173. F.Gao, Y.-h.Zang, Y.Wang, C.-q.Guan, J.-y.Qu, M.-b.Wu. *New Carbon Mater.*, **36**, 34 (2021); https://doi.org/10.1016/S1872-5805(21)60003-3

174. M.Bora, J.Tamuly, S.M.Benoy, S.Hazarika, D.Bhattacharjya, B.K.Saikia. *Fuel*, **329**, 125385 (2022); https://doi.org/10.1016/j.fuel.2022.125385

175. S.Ding, Y.Li, T.Zhu, Y.Guo. *J. Environ. Sci.*, **34**, 37 (2015); https://doi.org/10.1016/j.jes.2015.02.004

176. J.Jing, Z.Zhao, X.Zhang, J.Feng, W.Li. *Separations*, **9**, 174 (2022); https://doi.org/10.3390/separations9070174

177. X.Lan, X.Jiang, Y.Song, X.Jing, X.Xing. *Green Proc. Synthesis*, **8**, 837 (2019); https://doi.org/10.1515/gps-2019-0054

178. U.-S.Im, J.Kim, S.H.Lee, m.S.Lee, B.-R.Lee, D.-H.Peck, D.-H.Jung. *Mater. Lett.*, **237**, 22 (2019); https://doi.org/10.1016/j.matlet.2018.09.171

179. I.Men'shchikov, A.Shkolin, E.Khozina, A.Fomkin. *Nanomaterials*, **10**, 1379 (2020); https://doi.org/10.3390/nano10071379

180. S.W.Seo, Y.J.Choi, J.H.Kim, J.H.Cho, Y.-S.Lee, J.S.Im. *Carbon Lett.*, **29**, 385 (2019); https://doi.org/10.1007/s42823-019-00028-w

181. J.H.Kim, Y.J.Choi, J.S.Im, A.Jo, K.B.Lee, B.C.Bai. *J. Indust. Eng. Chem.*, **88**, 251 (2020); https://doi.org/10.1016/j.jiec.2020.04.022

182. A.Borhan, S.Yusup, J.W.Lim, P.L.Show. *Processes*, **7**, 855 (2019); https://doi.org/10.3390/pr7110855

183. V.Pavlenko, S.Khosravi H, S.Żółtowska, A.B.Haruna, M.Zahid, Z.Mansurov, Z.Supiyeva, A.Galal, K.I.Ozoemena, Q.Abbas, T.Jesionowski. *Mater. Sci. Eng.: R: Reports*, **149**, 100682 (2022); https://doi.org/10.1016/j.mser.2022.100682

184. M.Inagaki, H.Orikasa, T.Morishita. *RSC Adv.*, **1**, 1620 (2011); https://doi.org/10.1039/C1RA00608H

185. I.Y.Kaplin, E.S.Lokteva, E.V.Golubina, V.V.Lunin. *Molecules*, **25**, 4242 (2020); https://doi.org/10.3390/molecules25184242

186. L.Xie, Z.Jin, Z.Dai, Y.Chang, X.Jiang, H.Wang. *Carbon*, **170**, 100 (2020); https://doi.org/10.1016/j.carbon.2020.07.034

187. B.Yan, J.Zheng, F.Wang, L.Zhao, Q.Zhang, W.Xu, S.He. *Mater. Design*, **201**, 109518 (2021); https://doi.org/10.1016/j.matdes.2021.109518

188. V.Duraisamy, S.Palanivel, R.Thangamuthu, S.M.S.Kumar. *ChemistrySelect*, **3**, 11864 (2018); https://doi.org/10.1002/slct.201802539

189. A.B.Fuertes. *J. Mater. Chem.*, **13**, 3085 (2003); https://doi.org/10.1039/B307373D

190. J.Jagiello, A.Chojnacka, S.E.M.Pourhosseini, Z.Wang, F.Beguin. *Carbon*, **178**, 113 (2021); https://doi.org/10.1016/j.carbon.2021.02.098

191. A.Buasri, C.Pholprasert, N.Suwunnakee, T.Phuchainan, V.Loryuenyong. *Adv. Mater. Res*, **650**, 113 (2013); https://doi.org/10.4028/www.scientific.net/AMR.650.113

192. S.Yu, H.Wang, C.Hu, Q.Zhu, N.Qiao, B.Xu. *J. Mater. Chem. A*, **4**, 16341 (2016); https://doi.org/10.1039/C6TA07047G

193. T.Kyotani, T.Nagai, S.Inoue, A.Tomita. *Chem. Mater.*, **9**, 609 (1997); https://doi.org/10.1021/cm960430h

194. Z.Ma, T.Kyotani, Z.Liu, O.Terasaki, A.Tomita. *Chem. Mater.*, **13**, 4413 (2001); https://doi.org/10.1021/cm010730l

195. R.A.L.Sobrinho, G.R.S.Andrade, L.P.Costa, M.J.B.de Souza, A.M.G.P.de Souza, I.F.Gimenez. *J. Hazard. Mater.*, **362**, 53 (2019); https://doi.org/10.1016/j.jhazmat.2018.08.097

196. C.Wang, X.Li, X.Xi, W.Zhou, Q.Lai, H.Zhang. *Nano Energy*, **21**, 217 (2016); https://doi.org/10.1016/j.nanoen.2016.01.015

197. P.Tian, J.Zang, S.Song, S.Zhou, H.Gao, H.Xu, X.Tian, Y.Wang. *J. Power Sources*, **448**, 227443 (2020); https://doi.org/10.1016/j.jpowsour.2019.227443

198. N.Pal, A.Bhaumik. *Adv. Colloid Interface Sci.*, **189**–**190**, 21 (2013); https://doi.org/10.1016/j.cis.2012.12.002

199. M.Canal-Rodríguez, J.A.Menéndez, A.Arenillas. In *Porosity*. (Eds T.H.Ghrib, T.H.Ghrib). (Rijeka, 2017). P. 69

200. M.S.Contreras, C.A.Páez, L.Zubizarreta, A.Léonard, S.Blacher, C.G.Olivera-Fuentes, A.Arenillas, J.-P.Pirard, N.Job. *Carbon*, **48**, 3157 (2010); https://doi.org/10.1016/j.carbon.2010.04.054

201. B.Gorska, P.Ratajczak, F.Béguin. *Electrochim. Acta*, **328**, 135090 (2019); https://doi.org/10.1016/j.electacta.2019.135090

202. E.G.Calvo, E.J.Juárez-Pérez, J.A.Menéndez, A.Arenillas. *J. Colloid Interface Sci.*, **357**, 541 (2011); https://doi.org/10.1016/j.jcis.2011.02.034

203. F.Barzegar, V.Pavlenko, M.Zahid, A.Bello, X.Xia, N.Manyala, K.I.Ozoemena, Q.Abbas. *ACS Appl. Energy Mater.*, **4**, 1763 (2021); https://doi.org/10.1021/acsaem.0c02908

204. Z.Ayaganov, V.Pavlenko, S.F.B.Haque, A.Tanybayeva, J.Ferraris, A.Zakhidov, Z.Mansurov, Z.Bakenov, A.Ng. *J. Energy Storage*, **78**, 110035 (2024); https://doi.org/10.1016/j.est.2023.110035

205. J.W.Yu, Y.-M.Choi, J.Jung, N.-H.You, D.S.Lee, J.-K.Lee, M.Goh. *Synth. Met.*, **211**, 35 (2016); https://doi.org/10.1016/j.synthmet.2015.11.009

206. H.Wang, Y.Shao, S.Mei, Y.Lu, M.Zhang, J.-k.Sun, K.Matyjaszewski, M.Antonietti, J.Yuan. *Chem. Rev.*, **120**, 9363 (2020); https://doi.org/10.1021/acs.chemrev.0c00080

207. W.Li, A.Zhang, H.Gao, M.Chen, A.Liu, H.Bai, L.Li. *Chem. Commun.*, **52**, 2780 (2016); https://doi.org/10.1039/C5CC07908J

208. Z.Zhou, T.Liu, A.U.Khan, G.Liu. *Sci. Adv.*, **5**, eaau6852 (2019); https://doi.org/10.1126/sciadv.aau6852

209. W.Xin, X.Li, Y.Song. *J. Clean. Product.*, **282**, 124458 (2021); https://doi.org/10.1016/j.jclepro.2020.124458

210. R.Chen, H.Tang, P.He, W.Zhang, Y.Dai, W.Zong, F.Guo, G.He, X.Wang. *Adv. Funct. Mater.*, **33**, 2212078 (2023); https://doi.org/10.1002/adfm.202212078

211. Q.Fang, W.Zhang, X.Chen, Y.Zhang, M.Hu. *Chin. Chem. Lett.*, **31**, 303 (2020); https://doi.org/10.1016/j.cclet.2019.04.006

212. Z.Tian, Z.Weng, J.Xiao, F.Wang, C.Zhang, S.Jiang. *Int. J. Mol. Sci.*, **24**, 14156 (2023); https://doi.org/10.3390/ijms241814156

213. L.Wang, Q.Zhu, J.Zhao, Y.Guan, J.Liu, Z.An, B.Xu. *Micropor. Mesopor. Mater.*, **279**, 439 (2019); https://doi.org/10.1016/j.micromeso.2019.01.034

214. M.Kim, R.Xin, J.Earnshaw, J.Tang, J.P.Hill, A.Ashok, A.K.Nanjundan, J.Kim, C.Young, Y.Sugahara, J.Na, Y.Yamauchi. *Nat. Protoc.*, **17**, 2990 (2022); https://doi.org/10.1038/s41596-022-00718-2

215. P.Pachfule, D.Shinde, M.Majumder, Q.Xu. *Nature Chem.*, **8**, 718 (2016); https://doi.org/10.1038/nchem.2515

216. R.R.Salunkhe, Y.Kamachi, N.L.Torad, S.M.Hwang, Z.Sun, S.X.Dou, J.H.Kim, Y.Yamauchi. *J. Mater. Chem. A*, **2**, 19848 (2014); https://doi.org/10.1039/C4TA04277H

217. C.Wang, J.Kim, J.Tang, M.Kim, H.Lim, V.Malgras, J.You, Q.Xu, J.Li, Y.Yamauchi. *Chem*, **6**, 19 (2020); https://doi.org/10.1016/j.chempr.2019.09.005

218. J.Ren, Y.Huang, H.Zhu, B.Zhang, H.Zhu, S.Shen, G.Tan, F.Wu, H.He, S.Lan, X.Xia, Q.Liu. *Carbon Energy*, **2**, 176 (2020); https://doi.org/10.1002/cey2.44

219. S.Jeoung, I.T.Ju, J.H.Kim, S.H.Joo, H.R.Moon. *J. Mater. Chem. A*, **6**, 18906 (2018); https://doi.org/10.1039/C8TA05747H

220. K.Chen, Z.Sun, R.Fang, Y.Shi, H.-M.Cheng, F.Li. *Adv. Funct. Mater.*, **28**, 1707592 (2018); https://doi.org/10.1002/adfm.201707592

40 of 42

V.V.Pavlenko, A.Yu.Zakharov, Z.E.Ayaganov, Z.A.Mansurov
Russ. Chem. Rev., 2024, **93** (9) RCR5122

221. C.Liu, X.Huang, J.Wang, H.Song, Y.Yang, Y.Liu, J.Li, L.Wang, C.Yu. *Adv. Funct. Mater.*, **28**, 1705253 (2018); https://doi.org/10.1002/adfm.201705253

222. T.Feng, M.Zhang. *Chem. Commun.*, **54**, 11570 (2018); https://doi.org/10.1039/C8CC05959D

223. B.Yang, M.Shao, Y.Xu, Y.Du, H.Yang, D.Bin, B.Liu, H.Lu. *ChemElectroChem*, **9**, e202200438 (2022); https://doi.org/10.1002/celc.202200438

224. Y.Zhang, J.Wu, S.Zhang, N.Shang, X.Zhao, S.M.Alshehri, T.Ahamad, Y.Yamauchi, X.Xu, Y.Bando. *Nano Energy*, **97**, 107146 (2022); https://doi.org/10.1016/j.nanoen.2022.107146

225. X.Liu, X.Liu, B.Sun, H.Zhou, A.Fu, Y.Wang, Y.-G.Guo, P.Guo, H.Li. *Carbon*, **130**, 680 (2018); https://doi.org/10.1016/j.carbon.2018.01.046

226. A.Morelos-Gómez, P.G.Mani-González, A.E.Aliev, E.Muñoz-Sandoval, A.Herrera-Gómez, A.A.Zakhidov, H.Terrones, M.Endo, M.Terrones. *Adv. Funct. Mater.*, **24**, 2612 (2014); https://doi.org/10.1002/adfm.201303391

227. R.Sun, C.-W.Tai, M.Strømme, O.Cheung. *ACS Appl. Nano Mater.*, **2**, 778 (2019); https://doi.org/10.1021/acsanm.8b02005

228. Y.Jeong, M.Cui, J.Choi, Y.Lee, J.Kim, Y.Son, J.Khim. *Chemosphere*, **238**, 124559 (2020); https://doi.org/10.1016/j.chemosphere.2019.124559

229. A.R.Aref, S.-W.Chen, R.Rajagopalan, C.Randall. *Carbon*, **152**, 89 (2019); https://doi.org/10.1016/j.carbon.2019.05.074

230. M.N.Rafat, Z.Otgonbayar, S.-H.Yang, I.-J.Kim, W.-C.Oh. *Molecules*, **27**, 7033 (2022); https://doi.org/10.3390/molecules27207033

231. B.B.Saha, A.Chakraborty, S.Koyama, S.-H.Yoon, I.Mochida, M.Kumja, C.Yap, K.C.Ng. *Int. J. Heat Mass Transfer*, **51**, 1582 (2008); https://doi.org/10.1016/j.ijheatmasstransfer.2007.07.031

232. T.Otowa, R.Tanibata, M.Itoh. *Gas Separation Purification*, **7**, 241 (1993); https://doi.org/10.1016/0950-4214(93)80024-Q

233. K.Thu, Y.-D.Kim, A.B.Ismil, B.B.Saha, K.C.Ng. *Appl. Thermal Eng.*, **72**, 200 (2014); https://doi.org/10.1016/j.applthermaleng.2014.04.076

234. S.Choi, M.A.Alkhabbaz, Y.Wang, R.M.Othman, M.Choi. *Carbon*, **141**, 143 (2019); https://doi.org/10.1016/j.carbon.2018.09.045

235. M.H.Kim, S.O.Choi, S.T.Choo. *Carbon Lett.*, **29**, 553 (2019); https://doi.org/10.1007/s42823-019-00055-7

236. R.Janus, S.Jarczewski, J.Jagiello, P.Natkański, M.Wądrzyk, M.Lewandowski, M.Michalik, P.Kuśtrowski. *Carbon*, **217**, 118575 (2024); https://doi.org/10.1016/j.carbon.2023.118575

237. M.Vorokhta, J.Morávková, M.Dopita, A.Zhigunov, M.Šlouf, R.Pilař, P.Sazama. *Adsorption*, **27**, 1221 (2021); https://doi.org/10.1007/s10450-021-00322-y

238. K.Quiroz-Estrada, M.Esparza-Schulz, C.Felipe. *J. Compos. Sci.*, **6**, 344 (2022); https://doi.org/10.3390/jcs6110344

239. R.Janus, P.Natkański, M.Wądrzyk, M.Lewandowski, M.Michalik, P.Kuśtrowski. *Carbon*, **195**, 292 (2022); https://doi.org/10.1016/j.carbon.2022.04.025

240. R.Javad Kalbasi, S.F.Rezayi. *J. Porous Mater.*, **26**, 641 (2019); https://doi.org/10.1007/s10934-018-0666-4

241. M.S. Ryakhovskii. *Sovremennye Problemy Nauki i Obrazovaniya,* (2) 63 (2020)

242. Patent RU 2622660C1 (2017)

243. Ya.A.Klimova, E.A.Farberova, E.A.Tin'gaeva. *Vestn. Perm. Natsion. Issled. Politekhn. Univ. Khim. Tekhnol. Biotekhnol.*, (2), 63 (2020)

244. D.A.Sveshnikova, R.K.Khamizov, M.B.Ataev, A.M.Amirov, K.S.Rabadanov, A.S.Ramazanov. *Sorbtsion. Khromatograf. Protsessy*, **16** (3), 270 (2016)

245. S.Feng, W.Luo, L.Wang, S.Zhang, N.Guo, M.Xu, Z.Zhao, D.Jia, X.Wang, L.Jia. *Carbon*, **150**, 284 (2019); https://doi.org/10.1016/j.carbon.2019.05.021

246. V.Pavlenko, Z.Supiyeva. *Eurasian Chem. Technol. J.*, **22**, 277 (2020); https://doi.org/10.18321/ectj996

247. S.Burn, M.Hoang, D.Zarzo, F.Olewniak, E.Campos, B.Bolto, O.Barron. *Desalination*, **364**, 2 (2015); https://doi.org/10.1016/j.desal.2015.01.041

248. Y.Gao, L.Pan, H.Li, Y.Zhang, Z.Zhang, Y.Chen, Z.Sun. *Thin Solid Films*, **517**, 1616 (2009); https://doi.org/10.1016/j.tsf.2008.09.065

249. Z.Huang, L.Lu, Z.Cai, Z.J.Ren. *J. Hazard. Mater.*, **302**, 323 (2016); https://doi.org/10.1016/j.jhazmat.2015.09.064

250. X.Su, A.Kushima, C.Halliday, J.Zhou, J.Li, T.A.Hatton. *Nat. Commun.*, **9**, 4701 (2018); https://doi.org/10.1038/s41467-018-07159-0

251. L.Liu, X.Guo, R.Tallon, X.Huang, J.Chen. *Chem. Commun.*, **53**, 881 (2017); https://doi.org/10.1039/C6CC08515F

252. C.M.Ghimbeu, J.Górka, V.Simone, L.Simonin, S.Martinet, C.Vix-Guterl. *Nano Energy*, **44**, 327 (2018); https://doi.org/10.1016/j.nanoen.2017.12.013

253. Y.M.Volfkovich. *Russ. J. Electrochem.*, **59**, 347 (2023); https://doi.org/10.1134/S1023193523050038

254. C.-C.Hu, C.-F.Hsieh, Y.-J.Chen, C.-F.Liu. *Desalination*, **442**, 89 (2018); https://doi.org/10.1016/j.desal.2018.05.013

255. M.Sultana, M.H.Rownok, M.Sabrin, M.H.Rahaman, S.M.N.Alam. *Clean. Eng. Technol.*, **6**, 100382 (2022); https://doi.org/10.1016/j.clet.2021.100382

256. Y.Cheng, Z.Hao, C.Hao, Y.Deng, X.Li, K.Li, Y.Zhao. *RSC Adv.*, **9**, 24401 (2019); https://doi.org/10.1039/C9RA04426D

257. Y.Hou, S.Yan, G.Huang, Q.Yang, S.Huang, J.Cai. *Bioresource Technol.*, **303**, 122939 (2020); https://doi.org/10.1016/j.biortech.2020.122939

258. S.K.Singh, K.Takeyasu, J.Nakamura. *Adv. Mater.*, **31**, 1804297 (2019); https://doi.org/10.1002/adma.201804297

259. U.Zulfiqar, N.Kostoglou, A.G.Thomas, C.Rebholz, A.Matthews, D.J.Lewis. *Nanoscale*, **13**, 15311 (2021); https://doi.org/10.1039/D1NR03242A

260. P.J.Hall, M.Mirzaeian, S.I.Fletcher, F.B.Sillars, A.J.R.Rennie, G.O.Shitta-Bey, G.Wilson, A.Cruden, R.Carter. *Energy Environ. Sci.*, **3**, 1238 (2010); https://doi.org/10.1039/C0EE00004C

261. P.Simon, Y.Gogotsi. *Nat. Mater.*, **7**, 845 (2008); https://doi.org/10.1038/nmat2297

262. Y.Gogotsi, R.M.Penner. *ACS Nano*, **12**, 2081 (2018); https://doi.org/10.1021/acsnano.8b01914

263. Q.Liu, S.Li, S.Wang, X.Zhang, S.Zhou, Y.Bai, J.Zheng, X.Lu. *J. Phys. Chem. Lett.*, **9**, 5567 (2018); https://doi.org/10.1021/acs.jpclett.8b02750

264. W.-B.Li, S.-Y.Lin, M.-F.Lin, K.-I.Lin. *Condens. Matter*, **7**, 35 (2022); https://doi.org/10.3390/condmat7020035

265. Z.Wang, S.M.Selbach, T.Grande. *RSC Adv.*, **4**, 4069 (2013); https://doi.org/10.1039/C3RA47187J

266. J.Zhang, Y.Lei, L.Zhou, X.Chen, S.Huang, L.Liu, H.Liu, S.Dou, J.Xu. *Adv. Funct. Mater.*, **34**, 2314160 (2024); https://doi.org/10.1002/adfm.202314160

267. M.Yuan, B.Cao, H.Liu, C.Meng, J.Wu, S.Zhang, A.Li, X.Chen, H.Song. *Chem. Mater.*, **34**, 3489 (2022); https://doi.org/10.1021/acs.chemmater.2c00405

268. X.Chen, C.Liu, Y.Fang, X.Ai, F.Zhong, H.Yang, Y.Cao. *Carbon Energy*, **4**, 1133 (2022); https://doi.org/10.1002/cey2.196

269. V.Pavlenko, S.Kalybekkyzy, D.Knez, Q.Abbas, Z.Mansurov, Z.Bakenov, A.Ng. *Ionics*, **28**, 893 (2022); https://doi.org/10.1007/s11581-021-04354-w

270. L.-F.Zhao, Z.Hu, W.-H.Lai, Y.Tao, J.Peng, Z.-C.Miao, Y.-X.Wang, S.-L.Chou, H.-K.Liu, S.-X.Dou. *Adv. Energy Mater.*, **11**, 2002704 (2021); https://doi.org/10.1002/aenm.202002704

271. W.Ni, L.Shi. *J. Vacuum Sci. Technol. A*, **37**, 040803 (2019); https://doi.org/10.1116/1.5095413

272. Q.Lin, J.Zhang, W.Lv, J.Ma, Y.He, F.Kang, Q.-H.Yang. *Small*, **16**, 1902603 (2020); https://doi.org/10.1002/smll.201902603

V.V.Pavlenko, A.Yu.Zakharov, Z.E.Ayaganov, Z.A.Mansurov
Russ. Chem. Rev., 2024, **93** (9) RCR5122

41 of 42

273. Z.Xiao, C.Wang, L.Song, Y.Zheng, T.Long. *J. Solid State Electrochem.*, **26**, 1125 (2022); https://doi.org/10.1007/s10008-022-05141-x

274. W.Long, B.Fang, A.Ignaszak, Z.Wu, Y.-J.Wang, D.Wilkinson. *Chem. Soc. Rev.*, **46**, 7176 (2017); https://doi.org/10.1039/C6CS00639F

275. G.Zhang, Y.Chen, Y.Jiang, C.Lin, Y.Chen, H.Guo. *J. Mater. Sci. Technol.*, **34**, 1538 (2018); https://doi.org/10.1016/j.jmst.2017.12.018

276. E.Wang, M.Chen, X.Guo, S.-L.Chou, B.Zhong, S.-X.Dou. *Small Methods*, **4**, 1900163 (2020); https://doi.org/10.1002/smtd.201900163

277. Q.Li, J.Huang, L.Cao, J.He, Y.Wang, W.Wu, Y.He, J.Li. *J. Electroanalyt. Chem.*, **854**, 113554 (2019); https://doi.org/10.1016/j.jelechem.2019.113554

278. Y.Li, B.Ni, X.Li, X.Wang, D.Zhang, Q.Zhao, J.Li, T.Lu, W.Mai, L.Pan. *Nano-Micro Lett.*, **11**, 60 (2019); https://doi.org/10.1007/s40820-019-0291-z

279. W.Zhou, B.He, L.Quan, R.Li, Y.Chen, C.Fan, S.Chen, C.Xu, X.Fan, L.Xing, J.Liu. *Adv. Energy Mater.*, **13**, 2202874 (2023); https://doi.org/10.1002/aenm.202202874

280. W.Zhou, Y.Mo, P.Gao, K.Wang, J.Ke, Z.Liu, S.Chen, J.Liu. *Adv. Funct. Mater.*, **34**, 2312994 (2024); https://doi.org/10.1002/adfm.202312994

281. X.Wu, W.Zhou, C.Ye, J.Zhang, Z.Liu, C.Yang, J.Peng, J.Liu, P.Gao. *Ang. Chem. Int. Ed.*, **63**, e202317135 (2024); https://doi.org/10.1002/anie.202317135

282. M.Barghamadi, A.Kapoor, C.Wen. *J. Electrochem. Soc.*, **160**, A1256 (2013); https://doi.org/10.1149/2.096308jes

283. Z.Wei Seh, W.Li, J.J.Cha, G.Zheng, Y.Yang, M.T.McDowell, P.-C.Hsu, Y.Cui. *Nat. Commun.*, **4**, 1331 (2013); https://doi.org/10.1038/ncomms2327

284. L.Djuandhi, U.Mittal, N.Sharma, H.L.Andersen. *J. Electrochem. Soc.*, **170**, 010522 (2023); https://doi.org/10.1149/1945-7111/acb1a5

285. R.M.Obodo, I.C.Nwodo, P.C.Ani, E.Omugbe, C.Mbamara, U.C.Elejere, C.U.Eze, I.Ahmad, M.Maaza, J.N.Aniezi. *Recent Adv. Nat. Sci.*, **2**, 64 (2024); https://doi.org/10.61298/rans.2024.2.1.64

286. Z.Chen, X.Wang, B.Xue, W.Li, Z.Ding, X.Yang, J.Qiu, Z.Wang. *Carbon*, **161**, 432 (2020); https://doi.org/10.1016/j.carbon.2020.01.088

287. H.Ma, L.Wang, X.Feng, Y.Chen, J.Wu, M.Zhao, J.Zhou. *J. Mater. Sci*, **56**, 12336 (2021); https://doi.org/10.1007/s10853-021-06106-7

288. D.Li, L.Chen, T.Wang, L.-Z.Fan. *ACS Appl. Mater. Interfaces*, **10**, 7069 (2018); https://doi.org/10.1021/acsami.7b18123

289. Q.Zhao, X.Liu, S.Stalin, K.Khan, L.A.Archer. *Nat. Energy*, **4**, 365 (2019); https://doi.org/10.1038/s41560-019-0349-7

290. M.Rufete-Beneite, M.C.Román-Martínez, A.Linares-Solano. *Carbon*, **77**, 947 (2014); https://doi.org/10.1016/j.carbon.2014.06.009

291. P.Ratajczak, C.Bachetzky, Z.Wang, A.Chojnacka, N.Fulik, E.Pameté, S.E.M.Pourhosseini, E.Brunner, F.Beguin. *J. Mater. Chem. A*, **10**, 7928 (2022); https://doi.org/10.1039/D1TA10367A

292. E.Pameté, Z.Wang, F.Béguin. *ChemSusChem*, **n/a**, e202400596 (2024); https://doi.org/10.1002/cssc.202400596

293. D.Hulicova-Jurcakova, M.Seredych, G.Q.Lu, N.K.A.C.Kodiweera, P.E.Stallworth, S.Greenbaum, T.J.Bandosz. *Carbon*, **47**, 1576 (2009); https://doi.org/10.1016/j.carbon.2009.02.006

294. T.Wang, X.Zang, X.Wang, X.Gu, Q.Shao, N.Cao. *Energy Storage Mater.*, **30**, 367 (2020); https://doi.org/10.1016/j.ensm.2020.04.044

295. L.Bi, J.Yin, X.Huang, Y.Wang, Z.Yang. *Int. J. Hydrogen Energy*, **45**, 17637 (2020); https://doi.org/10.1016/j.ijhydene.2020.04.227

296. O.K.Alekseeva, I.V.Pushkareva, A.S.Pushkarev, V.N.Fateev. *Nanotechnol. Russia*, **15**, 273 (2020); https://doi.org/10.1134/S1995078020030027

297. I.A.Baburin, A.Klechikov, G.Mercier, A.Talyzin, G.Seifert. *Int. J. Hydrogen Energy*, **40**, 6594 (2015); https://doi.org/10.1016/j.ijhydene.2015.03.139

298. A.Klechikov, G.Mercier, T.Sharifi, I.A.Baburin, G.Seifert, A.V.Talyzin. *Chem. Commun.*, **51**, 15280 (2015); https://doi.org/10.1039/C5CC05474E

299. S.Schaefer, A.Jeder, G.Sdanghi, P.Gadonneix, A.Abdedayem, M.T.Izquierdo, G.Maranzana, A.Ouederni, A.Celzard, V.Fierro. *Int. J. Hydrogen Energy*, **45**, 30767 (2020); https://doi.org/10.1016/j.ijhydene.2020.08.114

300. M.Mohan, V.K.Sharma, E.A.Kumar, V.Gayathri. *Energy Storage*, **1**, e35 (2019); https://doi.org/10.1002/est2.35

301. W.Gao, S.Liang, R.Wang, Q.Jiang, Y.Zhang, Q.Zheng, B.Xie, C.Y.Toe, X.Zhu, J.Wang, L.Huang, Y.Gao, Z.Wang, C.Jo, Q.Wang, L.Wang, Y.Liu, B.Louis, J.Scott, A.-C.Roger, R.Amal, H.He, S.-E.Park. *Chem. Soc. Rev.*, **49**, 8584 (2020); https://doi.org/10.1039/D0CS00025F

302. G.T.Rochelle. *Science*, **325**, 1652 (2009); https://doi.org/10.1126/science.1176731

303. S.Kumar, R.Srivastava, J.Koh. *J. CO_2 Utiliz.*, **41**, 101251 (2020); https://doi.org/10.1016/j.jcou.2020.101251

304. E.Kavak, M.Şevik, G.Değirmenci, T.Alp Arici, R.Özdemir, M.Arici. *Crystal Growth Design*, **24**, 2415 (2024); https://doi.org/10.1021/acs.cgd.3c01311

305. D.Fu, Y.Park, M.E.Davis. *Angew. Chem., Int. Ed.*, **61**, e202112916 (2022); https://doi.org/10.1002/anie.202112916

306. W.Tian, H.Zhang, H.Sun, M.O.Tadé, S.Wang. *Chem. Eng. J.*, **347**, 432 (2018); https://doi.org/10.1016/j.cej.2018.04.139

307. D.S.Karousos, L.Lei, A.Lindbråthen, A.A.Sapalidis, E.P.Kouvelos, X.He, E.P.Favvas. *Separation Purification Technol.*, **253**, 117473 (2020); https://doi.org/10.1016/j.seppur.2020.117473

308. K.Huang, S.-H.Chai, R.T.Mayes, S.Tan, C.W.Jones, S.Dai. *Micropor. Mesopor. Mater.*, **230**, 100 (2016); https://doi.org/10.1016/j.micromeso.2016.04.041

309. H.F.Hasan, F.T.Al-Sudani, T.M.Albayati, I.K.Salih, H.N.Hharah, H.S.Majdi, N.M.C.Saady, S.Zendehboudi, A.Amari, S.A.Gheni. *Process Safety Environ.Protection*, **182**, 975 (2024); https://doi.org/10.1016/j.psep.2023.12.025

310. H.Yang, Y.Yuan, S.C.E.Tsang. *Chem. Eng. J.*, **185−186**, 374 (2012); https://doi.org/10.1016/j.cej.2012.01.083

311. J.Wang, L.Wang, Y.Wang, D.Zhang, Q.Xiao, J.Huang, Y.-N.Liu. *Chin. J. Chem. Eng.*, **42**, 91 (2022); https://doi.org/10.1016/j.cjche.2021.08.028

312. M.Ding, R.W.Flaig, H.-L.Jiang, O.M.Yaghi. *Chem. Soc. Rev.*, **48**, 2783 (2019); https://doi.org/10.1039/C8CS00829A

313. K.V.Kumar, K.Preuss, L.Lu, Z.X.Guo, M.M.Titirici. *J. Phys. Chem. C*, **119**, 22310 (2015); https://doi.org/10.1021/acs.jpcc.5b06017

314. B.Petrovic, M.Gorbounov, S.M.Soltani. *Micropor. Mesopor. Mater.*, **312**, 110751 (2021); https://doi.org/10.1016/j.micromeso.2020.110751

315. W.Kiciński, M.Szala, M.Bystrzejewski. *Carbon*, **68**, 1 (2014); https://doi.org/10.1016/j.carbon.2013.11.004

316. A.D.Igalavithana, S.W.Choi, P.D.Dissanayake, J.Shang, C.-H.Wang, X.Yang, S.Kim, D.C.W.Tsang, K.B.Lee, Y.S.Ok. *J. Hazard. Mater.*, **391**, 121147 (2020); https://doi.org/10.1016/j.jhazmat.2019.121147

317. S.Du, B.Huang, L.Zhu, Y.Wu, J.Huang, Z.Li, H.Yu, J.Xiao. *Carbon*, **215**, 118451 (2023); https://doi.org/10.1016/j.carbon.2023.118451

318. I.C.Gerber, P.Serp. *Chem. Rev.*, **120**, 1250 (2020); https://doi.org/10.1021/acs.chemrev.9b00209

319. H.Funabashi, S.Takeuchi, S.Tsujimura. *Sci. Rep.*, **7**, 45147 (2017); https://doi.org/10.1038/srep45147

320. W.Na, J.Kim, Y.K.Kim, S.G.Kim, J.Jang. *Carbon*, **165**, 185 (2020); https://doi.org/10.1016/j.carbon.2020.04.085

321. S.Gao, J.Liu, J.Luo, X.Mamat, S.Sambasivam, Y.Li, X.Hu, T.Wågberg, G.Hu. *Microchim. Acta*, **185**, 282 (2018); https://doi.org/10.1007/s00604-018-2818-2

42 of 42

V.V.Pavlenko, A.Yu.Zakharov, Z.E.Ayaganov, Z.A.Mansurov
Russ. Chem. Rev., 2024, **93** (9) RCR5122

322. L.Chen, X.Ding, J.Zeng, L.Jiao, C.Wu, Y.Wang, Q.Han, L.Qu. *Sci. Bull.*, **64**, 718 (2019); https://doi.org/10.1016/j.scib.2019.04.031

323. Y.Baikeli, X.Mamat, N.Yalikun, Y.Wang, M.Qiao, Y.Li, G.Hu. *RSC Adv.*, **9**, 23678 (2019); https://doi.org/10.1039/C9RA03925B

324. T.Liang, L.Zou, X.Guo, X.Ma, C.Zhang, Z.Zou, Y.Zhang, F.Hu, Z.Lu, K.Tang, C.M.Li. *Adv. Funct. Mater.*, **29**, 1903026 (2019); https://doi.org/10.1002/adfm.201903026

325. X.Chen, Y.Wu, W.Gu, M.Zhou, S.Tang, J.Cao, Z.Zou, G.Ji. *Carbon*, **189**, 617 (2022); https://doi.org/10.1016/j.carbon.2021.12.100

326. D.-P.Li, Y.-C.Sun, X.Wang, S.Wu, S.-C.Han, Y.Yang. *RSC Adv.*, **7**, 37983 (2017); https://doi.org/10.1039/C7RA04547F

327. B.Quan, W.Gu, J.Sheng, X.Lv, Y.Mao, L.Liu, X.Huang, Z.Tian, G.Ji. *Nano Res.*, **14**, 1495 (2021); https://doi.org/10.1007/s12274-020-3208-8

328. J.Tao, J.Zhou, Z.Yao, Z.Jiao, B.Wei, R.Tan, Z.Li. *Carbon*, **172**, 542 (2021); https://doi.org/10.1016/j.carbon.2020.10.062

329. X.Chen, Z.Wang, M.Zhou, Y.Zhao, S.Tang, G.Ji. *Chem. Eng. J.*, **452**, 139110 (2023); https://doi.org/10.1016/j.cej.2022.139110

330. D.Xu, Y.Ren, X.Guo, B.Zhao. *ACS Appl. Nano Mater.*, **5**, 14133 (2022); https://doi.org/10.1021/acsanm.2c02923

331. D.Zhi, T.Li, J.Li, H.Ren, F.Meng. *Composites Part B: Eng.*, **211**, 108642 (2021); https://doi.org/10.1016/j.compositesb.2021.108642

332. Z.Liu, B.Wang, S.Wei, W.Huang, Y.Wang, Y.Liang. *ACS Appl. Nano Mater.*, **7**, 6772 (2024); https://doi.org/10.1021/acsanm.4c00426

333. A.Vinu, K.Z.Hossian, P.Srinivasu, M.Miyahara, S.Anandan, N.Gokulakrishnan, T.Mori, K.Ariga, V.V.Balasubramanian. *J. Mater. Chem.*, **17**, 1819 (2007); https://doi.org/10.1039/B613899C

334. A.Vinu, C.Streb, V.Murugesan, M.Hartmann. *J. Phys. Chem. B*, **107**, 8297 (2003); https://doi.org/10.1021/jp035246f

335. M.Gisbert-Garzarán, J.C.Berkmann, D.Giasafaki, D.Lozano, K.Spyrou, M.Manzano, T.Steriotis, G.N.Duda, K.Schmidt-Bleek, G.Charalambopoulou, M.Vallet-Regí. *ACS Appl. Mater. Interfaces*, **12**, 14946 (2020); https://doi.org/10.1021/acsami.0c01786

336. A.Mars, A.Mejri, H.Elfil. In *Handbook of Porous Carbon Materials*. (Eds A.N.Grace, P.Sonar, P.Bhardwaj, A.Chakravorty). (Singapore, 2023). P. 885

337. T.-W.Kim, P.-W.Chung, I.I.Slowing, M.Tsunoda, E.S.Yeung, V.S.Y.Lin. *Nano Lett.*, **8**, 3724 (2008); https://doi.org/10.1021/nl801976m

338. S.Wu, P.Yue, Y.Ma, Y.Zou, W.Liang, Q.Ye. *Adv. Mater.*, **n/a**, 2305152 (2023); https://doi.org/10.1002/adma.202305152

339. S.Fatullayeva, D.Tagiyev, N.Zeynalov. *Colloid Interface Sci. Commun.*, **45**, 100545 (2021); https://doi.org/10.1016/j.colcom.2021.100545

340. P.Caraceni, J.G.Abraldes, P.Ginès, P.N.Newsome, S.K.Sarin. *J. Hepatol.*, **75**, S118 (2021); https://doi.org/10.1016/j.jhep.2021.01.024

341. P.Papamichalis, K.G.Oikonomou, A.Valsamaki, M.Xanthoudaki, P.Katsiafylloudis, E.Papapostolou, A.-L.Skoura, M.Papamichalis, M.Karvouniaris, A.Koutras, E.Vaitsi, S.Sarchosi, A.Papadogoulas, D.Papadopoulos. *World J. Clin. Cases*, **11**, 3932 (2023); https://doi.org/10.12998/wjcc.v11.i17.3932

342. C.F.Ma, Q.Gao, K.S.Xia, Z.Y.Huang, B.Han, C.G.Zhou. *Colloids Surfaces B: Biointerfaces*, **149**, 146 (2017); https://doi.org/10.1016/j.colsurfb.2016.10.015

343. Z.Juan, F.Kaixuan, W.Pingping, Z.Yue, Z.Yongke. *Results Mater.*, **9**, 100172 (2021); https://doi.org/10.1016/j.rinma.2021.100172

344. J.Xu, X.Jiang, N.Yang. *Chem. Commun.*, **59**, 4838 (2023); https://doi.org/10.1039/D2CC06517G

345. J.P.Fried, J.L.Swett, X.Bian, J.A.Mol. *MRS Commun.*, **8**, 703 (2018); https://doi.org/10.1557/mrc.2018.187

346. Y.He, M.Tsutsui, R.H.Scheicher, M.Taniguchi, T.Kawai. *arXiv*, 1206.4199 (2012); https://doi.org/10.48550/arXiv.1206.4199

347. S.J.Heerema, L.Vicarelli, S.Pud, R.N.Schouten, H.W.Zandbergen, C.Dekker. *ACS Nano*, **12**, 2623 (2018); https://doi.org/10.1021/acsnano.7b08635

348. R.Peng, X.S.Tang, D.Li. *Small*, **14**, 1800013 (2018); https://doi.org/10.1002/smll.201800013

349. R.Acharya, T.V.Patil, S.D.Dutta, J.Lee, K.Ganguly, H.Kim, A.Randhawa, K.-T.Lim. *Adv. Mater. Technol.*, 2400279 (2024); https://doi.org/10.1002/admt.202400279

350. M.Wu, X.Fu, J.Li, W.Zhao, X.Li. *Separation Purification Technol.*, **338**, 126328 (2024); https://doi.org/10.1016/j.seppur.2024.126328

351. R.E.A.Gwyther, N.P.Nekrasov, A.V.Emelianov, A.G.Nasibulin, K.Ramakrishnan, I.Bobrinetskiy, D.D.Jones. *Adv. Funct. Mater.*, **32**, 2112374 (2022); https://doi.org/10.1002/adfm.202112374

352. M.J.Molaei. *Anal. Methods*, **12**, 1266 (2020); https://doi.org/10.1039/C9AY02696G

353. L.Chio, R.L.Pinals, A.Murali, N.S.Goh, M.P.Landry. *Adv. Funct. Mater.*, **30**, 1910556 (2020); https://doi.org/10.1002/adfm.201910556